Modeling of heat transfer in porous media in the context of geothermal energy extraction

Carina Bringedal

Dissertation for the degree of philosophiae doctor (PhD)
at the University of Bergen

2015

Dissertation date: 02.10

Preface

This dissertation is submitted as a partial fulfillment of the requirements for the degree Doctor Philosophy (PhD) at the University of Bergen.

The advisory committee has consisted of Inga Berre (University of Bergen, Christian Michelsen Research), Florin Adrian Radu (University of Bergen) and Iuliu Sorin Pop (University of Bergen, Eindhoven University of Technology).

Acknowledgements

Doing a Ph.D. is like running orienteering without a map. You don't know where you are or where you're going. But you have a plan and work systematically; sometimes you make progress, other times you end up at the starting point helplessly.
Then, maybe when you were about to give up, you find what you were looking for. You realize that you have actually accomplished something. For some precious moments you feel on top of the world and that feeling make all those frustrations and tedious work worth it.
Then you continue.

This dissertation would not have seen daylight without guidance from my excellent supervisors, so my first thanks goes to Inga Berre, Florin Adrian Radu and Iuliu Sorin Pop. Their inspiring advices and small pushes along the way have been highly appreciated. I am especially grateful for all the help Inga has provided. Her constant positive attitude for this project and always cheerful point of view have been a great motivation. I was also fortunate to have an exchange semester in Eindhoven. This stay turned out to be a pleasant experience with exploring interesting research topics and gaining many new friends.

I am very thankful for my colleagues at the department of Mathematics and for everything we have experienced through and outside our studies. I have been lucky to share office with Eren and I appreciate all our discussions - both scientific and remarkably non-scientific - and all the breaks we have had.

Finally, I thank my family and friends for always offering different conversation topics and new perspectives. Last, but not least, I thank Ronny for supporting me, being patient when I suddenly drop everything to go to work, and for providing interesting analyses of my problems.

Abstract

This dissertation concerns mathematical modeling related to heat transfer in the subsurface relevant for geothermal energy extraction. Two applications are considered: First, natural convection in a homogeneous porous medium around a borehole is studied. Secondly, pore scale models for non-isothermal reactive transport with changing porosity are formulated and upscaled.

Natural convection is the heat transfer due to currents arising from density differences in the fluid. A vertical borehole heat exchanger not injecting fluid into the subsurface, may encounter convection currents in the surrounding porous medium when the porous medium is saturated with water. These convection currents can affect the heat transfer into the borehole, hence have an influence on the heat production from the borehole. To address this issue, both a theoretical framework and a numerical approach for the natural convection is considered. In the theoretical framework a linear stability analysis is applied to quantify when and how convection currents may occur spontaneously without the presence of a producing borehole heat exchanger. A high-order numerical scheme is implemented to quantify the effect on an operating borehole. The linear stability analysis is performed for an idealized setting with a homogeneous porous medium filling an annular cylinder that is heated from below and cooled from above. The analysis provides criterions for onset of convection and the associated pattern for convection currents in the linearized case. As the onset criterion and the convection pattern that appears depend on the size of the annular cylinder, maps describing the onset criterion and the convection pattern as a function of the inner and outer radius of the annulus are created.

To investigate the non-linear regime of natural convection, pseudospectral methods are applied to discretize the non-linear model equations. Pseudospectral methods are high-order numerical schemes known for their exponential convergence rate. The convergence rate for our model problem is investigated, and the scheme is used to examine the stability of the convection currents found in the linear stability analysis. The linear and non-linear regimes are found to overlap when the convection is weak, while stronger convection introduces non-linear artifacts only visible through the simulations. Further, by applying a more realistic configuration for the geothermal reservoir, pseudospectral methods are used in combination with domain decomposition to estimate the effect from natural convection on an operating borehole. By varying the flow properties and temperature conditions, some cases where the presence of convection would lower the amount of heat that is produced by the borehole are found, while other cases give a positive effect on the heat production.

When geothermal energy is produced through injecting fluid into the subsurface and producing warmer fluid, other challenges arise. The in-situ groundwater and the injected water will typically have different temperature and ion content, hence the injection shifts the geochemical system from its original state of equilibrium. We focus on mineral precipitation and dissolution reactions induced by this shift. As most minerals have temperature-dependent solubilities, chemical reactions may be triggered by both the temperature change as well as the variations in ion content. Due to the rock-fluid interactions mineral precipitation and dissolution entail, the porosity and hence the permeability of the porous medium can be changed, which again alters the production conditions for the geothermal reservoir. As the fluid flow, heat transport and reactive transport affect each other and involves processes over several time scales, this problem is highly coupled and challenging to model. This coupling is illustrated and used to motivate the need for pore scale models in order to better understand how the interactions between the physical processes behave at the pore scale. Further, upscaling through homogenization is performed on three different pore scale models, each applying different assumptions on the pore scale geometry or on the underlying physics. The upscaling process isolates the average behavior of the pore scale effects and shows how the processes are coupled at Darcy scale. One of the upscaled models is illustrated by implementing it using a finite volume scheme and is compared with some simpler models to illustrate when the upscaled model should be used and when it can be disregarded for a simpler model not honoring all the pore scale effects. Finite volume methods are conservative schemes, which are applied when consistent formulation of the transportation mechanisms is important.

Outline

This dissertation consists of two parts. The first part contains the background theory covering the papers found in the second part.

Part I is structured as follows: In Chapter 1 the two main topics covered in the dissertation; natural convection and reactive transport models, are introduced. The mathematical framework is presented in Chapter 2, which includes how flow in porous media and the governing equations for both topics are formulated. In Chapter 3 the linear stability analysis that is applied to the natural convection problem is presented. Theory for homogenization of pore scale models is considered in Chapter 4. Chapter 5 presents the numerical framework that is used in the included papers. Finally, the included papers are summarized and discussed in Chapter 6.

The included papers found in part II are:

Paper A: C. Bringedal, I. Berre, J.M. Nordbotten, D.A.S. Rees, *Linear and nonlinear convection in porous media between coaxial cylinders*, Physics of Fluids **23**, 9, http://dx.doi.org/10.1063/1.3637642, 2011.
Paper based on work from Master thesis [20].

Paper B: C. Bringedal, I. Berre, J.M. Nordbotten, *Influence of natural convection in a porous medium when producing from borehole heat exchangers*, Water Resources Research **49**, 8, http://dx.doi.org/10.1002/wrcr.20388, 2013.

Paper C: C. Bringedal, I. Berre, F.A. Radu, *An Approach for Investigation of Geochemical Rock-Fluid Interactions*, Proceedings, Thirty-Ninth Workshop on Geothermal Reservoir Engineering, Stanford University, 2014.

Paper D: C. Bringedal, I. Berre, I.S. Pop, F.A. Radu, *A model for non-isothermal flow and mineral precipitation and dissolution in a thin strip*, Journal of Computational and Applied Mathematics **289**, http://dx.doi.org/10.1016/j.cam.2014.12.009, 2015.

Paper E: C. Bringedal, I. Berre, I.S. Pop, F.A. Radu, *Upscaling of non-isothermal reactive porous media flow with changing porosity*, Transport in Porous Media, http://dx.doi.org/10.1007/s11242-015-0530-9, 2015.

Paper F: C. Bringedal, I. Berre, I.S. Pop, F.A. Radu, *Upscaling of non-isothermal reactive porous media flow under dominant Péclet number: the effect of changing porosity*, submitted.

Contents

Part I

Background

Chapter 1

Introduction

Geothermal energy is a renewable energy source and utilizes the thermal energy stored in the Earth's crust. The subsurface becomes gradually warmer with depth, which is quantified through the geothermal gradient. The heat can be produced through wells and boreholes. To produce the geothermal energy it is essential to understand the subsurface thermal transport processes. In the following chapter some background information about geothermal energy is given and the two main subjects considered in this thesis are introduced.

1.1 Geothermal energy

As the world population is growing and at the same time experiences an increase in living standards, there is a large increase in the demand for energy. Simultaneously, the world suffers from global warming due to emissions from carbon based energy resources as coal, oil and gas. To account for these challenges, alternative sources of energy can be used. The EU Renewable Energy Targets, also known as the 20-20-20 targets, sets an overall target of 20 % share of energy from renewable sources within 2020 [90]. Most of the new renewable energy needed is believed to come from wind and solar energy as well as biomass, but an additional option is geothermal energy. The two main advantages of geothermal energy compared to other renewable energy sources are low surface area requirements and the reliability when operating: Solar energy and biomass require large land areas, and the daily efficiency of wind and solar power depend highly on the weather conditions. Geothermal energy is stable as it does not depend on weather conditions and is capable of producing with same effect all year long [88].

Geothermal energy is already used to some extent: In 2010, 24 countries had an installed capacity of 10715 MW [45], while the capacity in August 2013 was 11765 MW [63]. Including projects that are under construction, the global capacity will reach 13402 MW by 2017 [45]. Most of this geothermal energy production occur at so-called hot spots, which is where the geothermal gradient is locally increased, hence high temperatures are reached at lower depths. Hot spots are normally found in regions with volcanic activity, such as in Iceland, California and the Philippines [45]. However, geothermal energy for electricity production can be produced anywhere as long as the wells are drilled deep enough, and utilizing geothermal energy for direct heating has lower requirements for the subsurface temperature. These possibilities open for

geothermal energy production at more locations, and increases the availability and the geothermal energy potential worldwide. When including regions with medium and low geothermal gradient, the recoverable potential of geothermal energy in the US alone is estimated to be 2.8×10^6 EJ [88]. However, drilling deeper increases the investment costs of the geothermal plant, and may cause a potential plant to not be economically feasible.

There are several setups for extracting geothermal energy and two of the most common types are considered in this thesis: The system normally associated with geothermal energy extraction has one or several injection and production wells. The injected fluid flows through the subsurface where it may mix with any in-situ groundwater before fluid is produced at a higher temperature. This approach is suitable for utilizing geothermal energy for electricity production when the temperature and flow conditions in the reservoir are favorable, or for direct heating. Another approach for extracting geothermal energy is drilling boreholes and let a fluid circulate inside them. This way, the fluid does not interact directly with the groundwater and the thermal energy is produced by conduction due to the temperature difference between the borehole heat exchanger and the subsurface. This method is suitable for direct heating only, typically in combination with heat pumps depending on the temperature conditions.

In order to plan a geothermal plant, recognizing how the subsurface thermal processes behave is necessary. It is essential to understand the heat transfer mechanisms in the subsurface to optimize the heat extraction and to produce commercially competitive energy. Studying how heat is transferred in the subsurface and how it interacts with any fluid flow, can give vital information about how much energy can be produced from a specific reservoir; and, how one should drill to be able to produce a required amount of energy. Mathematical and numerical modeling of the interaction between flow and heat transfer in the subsurface is important to understand how the processes could affect the energy production. In this context we go into detail in two problems; the effect of natural convection on geothermal heat production and the effect of porosity changes due to mineral dissolution and precipitation. Mathematical models describing these phenomena are formulated and new insight obtained through analysis of the model equations and computer simulations is presented.

1.2 Natural convection

Heat transfer in the subsurface is mainly due to convection and conduction [17]. While conduction is caused by molecular vibrations and always transfers energy from warmer to colder regions, convection is heat transfer due to mass transfer and transfers the energy with the fluid movement. Natural convection is when the fluid movement is a result of density differences in the fluid. As warm water is less dense than cold water, these density differences can generate flow, which is then called natural convection currents. When these currents form closed trajectories they are called convection cells. For a case where the saturated porous medium is heated from below and cooled from above, see Figure 1.1.

When determining the location of a new geothermal plant, subsurface heat properties are important and a large geothermal gradient is desirable. As the geothermal gradient locally increases at the upper part in the upflow region of convection cells,

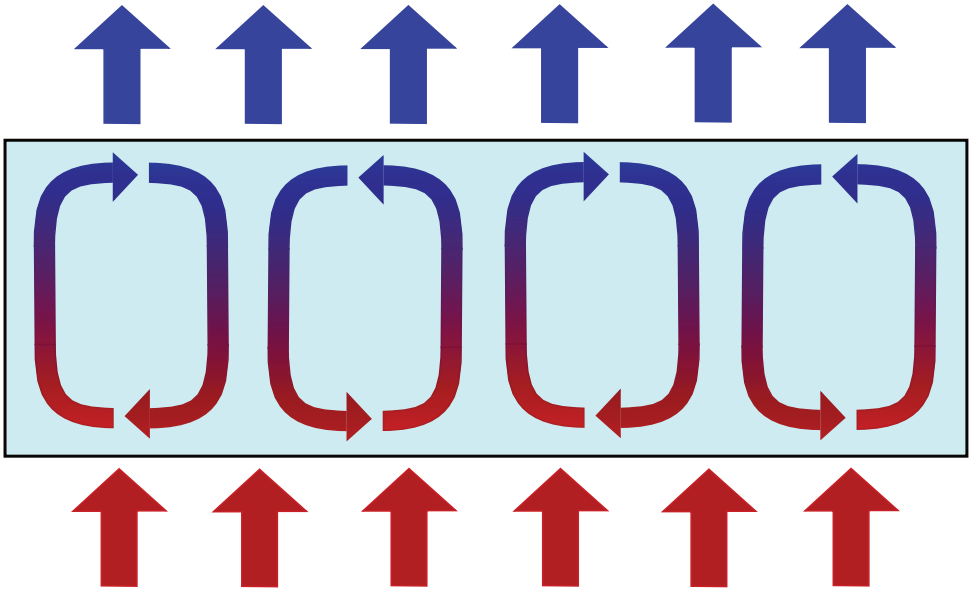

Figure 1.1: Convection cells in a porous medium. Figure from [20].

geothermal plants can be placed at locations where large, naturally occurring convection cells appear [12, 24, 29, 55, 84]. Convection cells may also occur after production initiation in the case with borehole heat exchangers. When the borehole does not inject fluid into the subsurface, there could be natural convection currents arising in the subsurface surrounding the borehole. As the borehole contains a cold fluid, the nearby ground is cooled, creating a horizontal temperature gradient which can cause density differences in the fluid and hence convection currents [91].

Convection currents can arise when there is either a horizontal or vertical temperature gradient. The onset and spatial distribution of the convection currents can be investigated through linear stability analysis and have been investigated extensively throughout the last decades [71]. The equations are linearized and solved analytically, finding criteria for when convection currents occur and how they distribute at onset. The criterion for onset of convection can be quantified through the critical Rayleigh number: When the Rayleigh number is larger than the critical, convection currents can develop. The Rayleigh number is a non-dimensional number depending on properties of the permeable rock and of the saturating fluid. Further, the linear stability analysis can show how the convections cells distribute spatially at the onset of convection. More background information on the linear stability analysis can be found in Chapter 3. To investigate the non-linear regime and to consider cases not feasible through linear stability analysis, we develop a high-order numerical scheme using pseudospectral methods. More details on the numerical solver can be found in Chapter 5.

The main contributions in this thesis related to the study of natural convection are:

1. **Performing linear stability analysis in a porous medium filling an annular cylinder.** In Paper A we consider an annular cylinder filled with a porous

medium, depicting the subsurface outside a (non-operating) borehole. To get a better understanding of how the natural convection behave, we consider two cases; either the sidewalls being perfectly heat conducting, or insulated. The critical Rayleigh number with the corresponding preferred convection mode is found. The model with insulated sidewalls has been considered before by Bau and Torrance [14], but our analysis reveals more details than previously found. Further, the non-linear model equations are implemented and the findings compared with those from the linear regime. Using the numerical scheme, the stability of the convection modes with respect to different types of perturbations is studied.

2. **Investigating the effect of natural convection on an operating borehole.** By developing the non-linear solver, a more relevant model for geothermal energy extraction is considered in Paper B. This way, we are able to investigate how the natural convection would affect the heat transfer into an operating borehole when there is no background advective flow. The considered model is idealized and tailored to isolate the effect of natural convection. Several cases where the natural convection will have a large impact on an non-injecting borehole is found.

1.3 Reactive transport and the need for pore scale models

In a geothermal system using injection and production wells, cold fluid is injected into the reservoir and mixes with the in-situ groundwater, which typically has a different ion content than the injected fluid. Before injection, the ion content of the groundwater is in equilibrium with the host rock, meaning that the groundwater is fully saturated with the minerals present in the host rock. The solubility of these minerals are normally temperature dependent, hence minerals may be triggered to dissolve or precipitate as the fluid injection starts; both due to the injection of a colder fluid and due to the changes in ion content introduced by the injected fluid.

Precipitation and dissolution of minerals as anhydrite, calcite, silica and quartz are known to cause the porosity and hence the permeability to change significantly in a (geothermal) reservoir [67, 73, 77, 86, 98, 102]. As the permeability changes, the flow conditions throughout the reservoir changes, distributing more fluid through regions where the permeability is increasing due to minerals dissolving and less through regions where minerals precipitate. As the injected fluid flows through the reservoir, its temperature and ion content change continuously as well as the flow properties of the porous medium changes. The interactions between fluid flow, chemical reactions and heat transfer challenging to model, but important to inlcude in exploiting of geothermal systems. Computer simulations have high requirements to the scheme due to the challenging physics, and mass conservative schemes are preferable.

To better understand the couplings and interactions between fluid flow, reactive transport and heat transport, a pore scale model can be considered. A pore scale model is formulated at local pore structures in the porous medium, allowing us to formulate equations valid in the fluid-filled void space and in the solid space separately. This distinction between void space and solid space enables a more accurate mathematical formulation of the relevant physical processes. Unfortunately, doing computer simulations on a pore scale model for a geothermal reservoir would require too much com-

putational power to be feasible. A typical reservoir is on kilometer-scale, while pores are typically on micrometer-scale [15]. In 3D, this would require at least 10^{27} nodes to resolve the pores, which is impossible with today's computer power. Instead, the pore scale model equations need to be upscaled to a more comprehensive scale for modeling, which is typically the Darcy scale.

Upscaling of pore scale models can be done several ways, and one common upscaling method is homogenization. The basic idea of homogenization is to find a clear separation between the relevant scales and use this separation to find which of the features in the pore scale model equations are important on the Darcy scale and which can be disregarded. This separation of scales is illustrated in Figure 1.2 where zooming in in the domain reveals a detailed pore structure. More background information on separation of scales and homogenization can be found in Chapter 4. To illustrate the behavior of the reactive transport models, we have applied a simple finite volume scheme. More details on this can be found in Chapter 5.

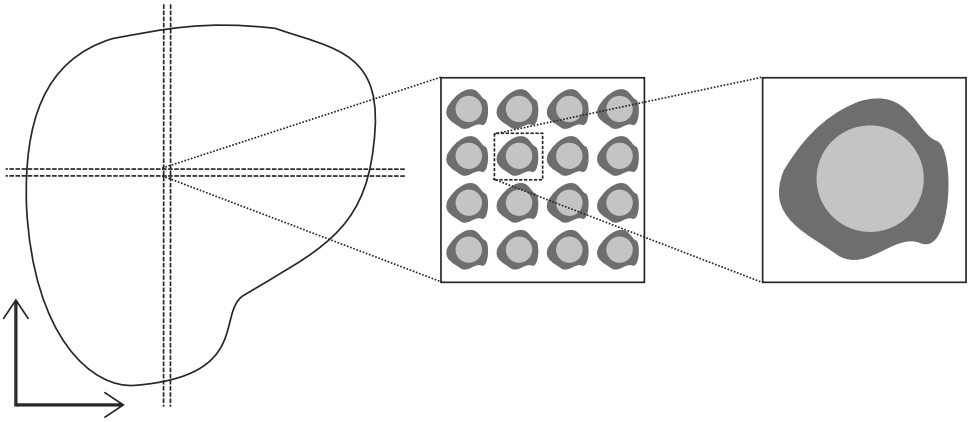

Figure 1.2: The left-most figure shows the reservoir, while the right-most figure shows the pore structure that is visible when zooming in. Figure adapted from Paper E.

The main contributions in this thesis regarding reactive transport are:

1. **Formulating a mass conservative scheme for a coupled reactive transport model at Darcy scale.** In Paper C we formulate a 2D solver using TPFA where fluid flow, heat transfer and reactive transport with changes in porosity are included. The model allows for injection and production through wells, and the wells are handled in a mass conservative way consistent with the formulation. The scheme includes a simplified geochemical model, but can illustrate the effect of changes in porosity and permeability due to the considered mineral precipitation and dissolution reactions.

2. **Formulating pore scale models taking into account fluid flow, heat transport and reactive transport and honoring the changes in pore geometry.** To better understand processes at the pore scale, we formulate several pore scale models and identify the relevant pore scale model equations. We consider two geome-

tries; a thin strip and a periodic porous medium. The thin strip model can illustrate a single channel and is easier to formulate as the presence of minerals can be handled explicitly through the varying grain width and the aperture of the strip. The chemical reactions then cause changes in the size of the grain width and is formulated through an ODE. The periodic model uses the geometry shown in Figure 1.2 and requires a level set formulation to account for the changes in porosity.

3. **Upscaling the pore scale models to Darcy scale.** Through homogenization we can upscale the pore scale models to Darcy scale, which is a more convenient scale for computer simulations. To perform the homogenization, a separation of scale must be identified: For the thin strip, the separation of scale is due to the strip being very thin compared to the length. The thin strip model is considered in Paper D and Paper F, where different assumptions on the physical processes have been assumed. In the periodic model, the separation of scale is identified through the typical length scale of the grain size and the reservoir size and is treated in Paper E. By identifying the relevant scales, we find effective variables and effective model equations through homogenization.

Chapter 2

Mathematical framework

A porous medium consists of solid rock and the void space in between the rocks, which in our case will be assumed to be fully saturated with a fluid. We separate between two scales: The pore scale which is visible when zooming in and and observing single pores with all its details, and the Darcy scale where zooming out and only consider the average behavior of the porous medium. Section 2.1 defines the governing equations relevant on the pore scale, while Section 2.2 deals with the Darcy scale. Some equations have similarities, but they are valid in different domains and scales. To emphasize the two scales, all relevant equations are defined in both settings. The different scales require different considerations. The mathematical framework is presented briefly and is based on [13, 15, 17, 47, 71, 74].

2.1 Pore scale models

The advantage of using pore scale models is the possibility of giving an accurate mathematical description of what happens at the pore scale where it is easier to isolate the relevant processes. Pore scale models requires an explicit description of the pore structure and is computationally expensive to do computer simulations on as very fine grids are required. The constitutive equations depend on few assumption, typically the continuum hypothesis and conservation laws [13]. However, utilizing pore scale models also requires information about the actual pore structure, which is often not available. Pore scale models are well used in describing flow through porous media and are considered useful when pore scale effects are important, such as in rock-fluid interactions [59, 93, 94], biofilm growth [96], drug release [81] and evolving microstructures [75]. These papers have in common that they use homogenization to derive effective models at the macroscale and this technique is covered more extensively in Chapter 4.

We consider non-isothermal reactive transport with evolving pore geometry, formulated at the pore scale. The following presentation is based on Papers D, E and F, where variations of the model are considered and the pore scale equations are upscaled to Darcy scale using certain assumptions. The reactive transport model is based on the models by van Noorden and Pop in [95] and by van Noorden in [93, 94], who consider the isothermal case. Considering pore scale models requires assumptions on the pore structure and we have investigated two different cases; either a single pore shaped as a thin strip or a more general porous medium with periodically distributed grains. In either case the mineral precipitation and dissolution are allowed to affect the porosity,

which in a pore scale setting means having a model with a free boundary. The thin strip model is shown in Figure 2.1 and the periodic model is shown in Figure 1.2 with the pore structure in Figure 2.2.

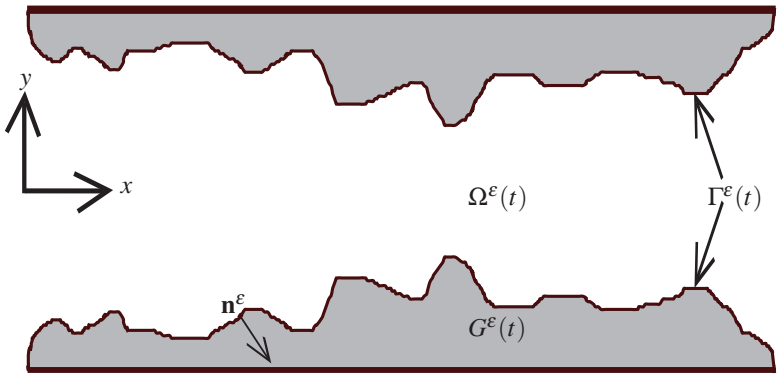

Figure 2.1: The thin strip geometry. Figure adapted from Papers D and F.

As seen in Figure 2.1 and 2.2, the pore scale models consists of the solid space, the void space and the moving boundary between them. The thin strip model is formulated within the rectangle

$$\Upsilon = \{(x,y) \in R^2 \mid 0 \le x \le L, -l/2 \le y \le l/2\},$$

where l and L are positive numbers and l is much smaller than L. These two numbers also define the microscopic and macroscopic scales, respectively. The scale difference is recognized as $\varepsilon = l/L$, where ε is a small number. In the following, dependence on the different scales is emphasized by using ε as a superscript. The mineral width $d(x,t)$ is used to characterize the domain and we assume symmetry across the horizontal axis. To avoid clogging, we assume $0 \le d(x,t) < l/2$. The void space $\Omega^\varepsilon(t)$ where fluid can flow is defined as

$$\Omega^\varepsilon(t) = \{(x,y) \in R^2 \mid 0 \le x \le L, -(l/2 - d(x,t)) \le y \le (l/2 - d(x,t))\},$$

while the grain space $G^\varepsilon(t)$ consisting of mineral is

$$G^\varepsilon(t) = \{(x,y) \in R^2 \mid 0 \le x \le L, -l/2 \le y \le -(l/2 - d(x,t)) \vee (l/2 - d(x,t)) \le y \le l/2\}.$$

The void space and grain space are separated by the moving interface $\Gamma^\varepsilon(t)$ where mineral precipitation and dissolution can occur, and is given by

$$\Gamma^\varepsilon(t) = \{(x,y) \in R^2 \mid 0 \le x \le L, y = \pm(l/2 - d(x,t))\}.$$

Assuming $d(x,t)$ is a differentiable function, the unit normal vector pointing into the grain space is expressed as

$$\mathbf{n}^\varepsilon = (\partial_x d, -1)^T / \sqrt{1 + (\partial_x d)^2}$$

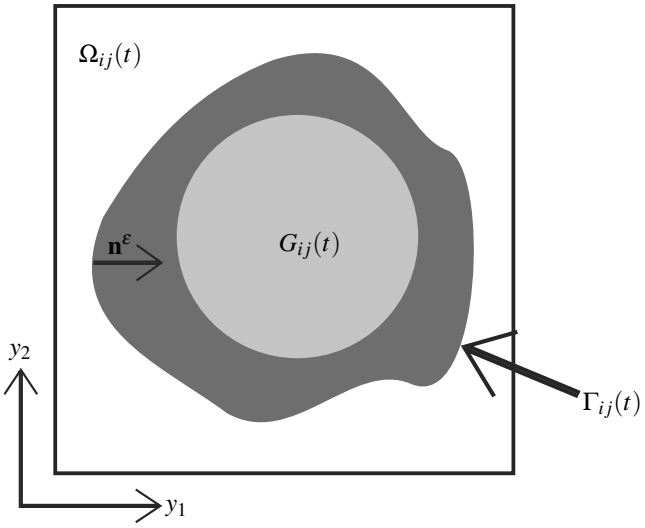

Figure 2.2: The zoomed in geometry of the periodic porous medium. Figure adapted from Paper E.

for the lower part of $\Gamma^\varepsilon(t)$.

The geometry of the periodic model is a bit more tedious to define. The porous medium is inside a two-dimensional domain Ω with external boundary Γ, seen in the left-most part of Figure 1.2. The domain is inside a square $x = (x_1, x_2) \in (0, L)^2$ for some positive number L. The domain is perforated in a periodic manner, consisting of a connected pore space $\Omega^\varepsilon(t)$, the grain space $G^\varepsilon(t)$ and the boundary between them $\Gamma^\varepsilon(t)$. The pore structure seen in Figure 2.2 can be defined using local variables $(y_1, y_2) \in (0, l)^2$, where l is much smaller than L, and this smaller region is denoted Y. As in the previous model $\varepsilon = l/L$ is a small, characteristic number and is used as a superscript to emphasize dependence on both scales. Note that x, y, L and l play different roles in this model compared to the thin strip model, but we use the same symbols to indicate the similarities: In both models x can be interpreted as a macroscopic variable with typical length L, while y is the microscopic variable having typical length l.

The region Y consists of void space $\Omega_{ij}(t)$, grain space $G_{ij}(t)$ and the moving boundary between them $\Gamma_{ij}(t)$ having unit normal $\mathbf{n}^\varepsilon$ pointing into the grain space. The grain space $G_{ij}(t)$ consists of a non-reactive part B_{ij} located in the centre of the square, seen in light grey in Figure 2.2, and is surrounded by the reactive mineral. The indices i, j denote which subdomain in the total domain Ω is considered, and the set of indices $\{i, j\}$ is such that the whole domain is covered. Assuming a periodic structure in the porous medium, $y = (y_1, y_2)$ is periodic with period l. This way, $\Omega^\varepsilon(t) = \cup\Omega_{ij}(t)$, $G^\varepsilon(t) = \cup G_{ij}(t)$, $B^\varepsilon = \cup B_{ij}$ and $\Gamma^\varepsilon(t) = \cup\Gamma_{ij}(t)$. To describe the positions of the inter-

faces Γ_{ij} the level set function $S^\varepsilon(x,t)$ [72] is defined such that

$$S^\varepsilon(x,t) = \begin{cases} < 0 & \text{if } x \in \Omega^\varepsilon(t), \\ 0 & \text{if } x \in \Gamma^\varepsilon(t), \\ > 0 & \text{if } x \in G^\varepsilon(t). \end{cases}$$

This choice of $S^\varepsilon(x,t)$ assures that the gradient of $S^\varepsilon(x,t)$ points into the grain space and will be parallel to the unit normal $\mathbf{n}^\varepsilon$, hence

$$\mathbf{n}^\varepsilon = \frac{\nabla S^\varepsilon(x,t)}{|\nabla S^\varepsilon(x,t)|}.$$

2.1.1 Describing a moving boundary

The moving boundary $\Gamma^\varepsilon(t)$ changes position due to mineral precipitation and dissolution and the development is expressed using an equation describing the rate of change. A simple mineral precipitation and dissolution reaction is considered; a mineral can dissolve into the fluid releasing two ions; or, oppositely, two ions can go together forming a mineral molecule. The two ions are assumed to have the same concentration u in the fluid. As the boundary moves it has a normal velocity v_n, which is proportional to the local difference between the dissolution and precipitation rate [54, 94]:

$$\rho_C v_n = -(f_p - f_d) \text{ on } \Gamma^\varepsilon(t), \tag{2.1}$$

where ρ_C is the molar density of the mineral and f_p and f_d are the precipitation and dissolution rates, respectively. The rates are [23, 93], for both geometries,

$$f_p(T_f,u) = k_0 e^{-\frac{E}{RT_f}} \frac{(\gamma u)^2}{K_m(T_f)} \text{ and } f_d(T_f,u,\lambda) = k_0 e^{-\frac{E}{RT_f}} w(\lambda,T_f,u), \tag{2.2}$$

where k_0 is a rate constant, T_f is fluid temperature and $K_m(T_f)$ is the solubility product of the mineral. The Arrhenius factor $exp(-E/RT_f)$ describes how reaction rates increase with higher temperatures. Here, E is the activation energy and is known through tables and R is the gas constant. The activity coefficient γ will assumed to be constant and in some cases set to be 1. The solubility product is known through tables and the reaction rates are such that the net reaction rate $(f_p - f_d)$ is positive when the fluid is supersaturated with ions and negative when the fluid is undersaturated. Our geochemical model is very simplified and includes only what is necessary to describe a moving interface. In Section 2.2.2 we consider a slightly more realistic geochemical model on the Darcy scale. The function $w(\lambda,T_f,u)$ is defined as

$$w(\lambda,T_f,u) = \begin{cases} 0 & \text{if } \lambda < 0, \\ \min(\frac{(\gamma u)^2}{K_m(T_f)}, 1) & \text{if } \lambda = 0, \\ 1 & \text{if } \lambda > 0. \end{cases}$$

The variable λ accounts for the amount of mineral that is left, hence the factor w assures that the dissolution rate is not larger than the precipitation rate when all the minerals

have dissolved. In the thin strip model, we use the grain width $d(x,t)$ in the role of λ, while in the periodic model the position x at the boundary $\Gamma^\varepsilon(t)$ is used to calculate the distance between x and B^ε, hence $dist(x,B^\varepsilon)$ replaces λ. Note that the reaction rate is discontinuous at $\lambda = 0$, which is typically handled by applying a Lipschitz approximation:

$$w(\lambda) = \begin{cases} 0 & \text{if } \lambda < 0, \\ \lambda/\delta & \text{if } 0 \le \lambda \le \delta, \\ 1 & \text{if } \lambda > \delta \end{cases}$$

for some small $\delta > 0$. This type of regularization is also common for numerical simulations. Kumar et al [58] formulates a convergent mixed finite element scheme with a discretization parameter that ensures δ approaching zero, hence ending up with the original $w(\lambda, T_f, u)$.

In the thin strip model an explicit expression for the normal velocity of $\Gamma^\varepsilon(t)$ can be found using the grain width $d(x,t)$. A point at the lower part of the interface has coordinates $\mathbf{s}(t) = (x(t), -(l/2 - d(x,t)))$ and velocity $\mathbf{s}'(t) = (x'(t), \partial_x d(x,t)x'(t) + \partial_t d(x,t))$. Hence, the normal velocity of the lower interface is

$$v_n = \mathbf{n}^\varepsilon \cdot \mathbf{s}'(t) = -\frac{\partial_t d(x,t)}{\sqrt{1 + (\partial_x d(x,t))^2}}.$$

Combining with (2.1) an equation describing how the rate of $d(x,t)$ is connected with the reaction rates is achieved:

$$\rho_C \partial_t d = (f_p(T_f,u) - f_d(T_f,u,d))\sqrt{1 + (\partial_x d)^2} \text{ on } \Gamma^\varepsilon(t).$$

In the periodic medium model the level set equation is used to describe the evolution of the changing pore structure. The level set equation is

$$\partial_t S^\varepsilon + v_n |\nabla S^\varepsilon| = 0,$$

which combined with (2.1) shows that

$$\partial_t S^\varepsilon = \frac{1}{\rho_C}(f_p(T_f,u) - f_d(T_f,u,x))|\nabla S^\varepsilon| \text{ for } x \in \Omega.$$

Note that the level set equation is defined in the entire domain and not only on the moving boundary. This is handled by defining a continuous extension of the reaction rates to Ω.

How the developing geometry is expressed depends on the model, but in both models we separate between the void space $\Omega^\varepsilon(t)$, grain space $G^\varepsilon(t)$ and the moving interface $\Gamma^\varepsilon(t)$. The normal velocity v_n of the moving boundary will be proportional to the difference between the reaction rates, as expressed in (2.1). In the following, the model equations and boundary conditions at the moving boundary are formulated for their relevant domains, keeping in mind that the evolution of the geometry is described differently.

2.1.2 Solute transport

The two ions having molar concentration u in the fluid, satisfy the convection-diffusion equation in the void space:

$$\partial_t u + \nabla \cdot (u\mathbf{q}) = \nabla \cdot (D\nabla u) \text{ for } x \in \Omega^\varepsilon(t), \tag{2.3}$$

where $\mathbf{q}$ is the fluid velocity and D is the diffusion coefficient which is assumed constant. The ions can cross the moving boundary through the precipitation and dissolution reactions. Applying a Rankine-Hugoniot condition [38] for conserving ions across a moving boundary yields

$$\mathbf{n}^\varepsilon \cdot (D\nabla u - u\mathbf{q}) = v_n(\rho_C - u) \text{ on } \Gamma^\varepsilon(t).$$

The left-hand side of the above equation is the jump of fluxes across the boundary: Ions in the fluid have a convective and diffusive flux, while the ions in the mineral molecules have zero flux. The right-hand side contains the jump of the preserved quantity: A mineral molecule consists of one of each type of the two ions, hence the difference represents the jump across the interface for each of the ions.

2.1.3 Mass conservation

Mass conservation in the void space is expressed as

$$\partial_t \rho_f + \nabla \cdot (\rho_f \mathbf{q}) = 0 \text{ for } x \in \Omega^\varepsilon(t),$$

where ρ_f is the molar density of the fluid. The fluid consists mainly of water and is assumed to not be affected by the chemical reactions, but varies with temperature. Using a linear dependence yields

$$\rho_f = \rho_0(1 - \beta_{\rho_f}(T_f - T_0)),$$

where T_f is fluid temperature, $\rho_f = \rho_0$ at some reference temperature T_0, and β_{ρ_f} is the thermal expansion coefficient. As water becomes less dense with increasing temperature, β_{ρ_f} is a positive number with the above definition. As there is a mass flux across the moving interface, the Rankine-Hugoniot condition applied to mass is

$$\mathbf{n}^\varepsilon \cdot (-\rho_f \mathbf{q}) = v_n(2\rho_C - \rho_f) \text{ on } \Gamma^\varepsilon(t). \tag{2.4}$$

The difference on the right-hand side is the jump of the mass across the moving boundary. Since a mineral molecule contains two ions, the term $2\rho_C$ appears. If $2\rho_C = \rho_f$, the normal component of the velocity is zero at the interface, meaning that the chemical reactions do not cause volume change. As the fluid density varies with temperature while the mineral density is assumed constant, this is in general not the case in our models. In [93, 94], van Noorden uses the quotient $K = (\rho_f - 2\rho_C)/\rho_f$ to describe the effect of volume changes due to chemical reactions.

2.1.4 Momentum conservation

The fluid is assumed to be newtonian, that the stress tensor is a linear function of the strain rates and that the fluid is isotropic. The model is two-dimensional so the gravity is not present, hence

$$\partial_t(\rho_f \mathbf{q}) + \nabla \cdot (\rho_f \mathbf{q}\mathbf{q}) = -\nabla p + \nabla \cdot \left(\mu(\nabla \mathbf{q} + (\nabla \mathbf{q})^T)\right) - \frac{2}{3}\nabla(\mu \nabla \cdot \mathbf{q}) \text{ for } x \in \Omega^\varepsilon(t), \tag{2.5}$$

where p is pressure and μ is fluid viscosity. Note that the dimensions of these quantities have to be in a molar manner to coincide with the molar density. Water viscosity depends on temperature, and a linear relationship is assumed:

$$\mu = \mu_0(1 - \beta_\mu(T_f - T_0)),$$

where $\mu = \mu_0$ at the reference temperature T_0. Water viscosity decreases with temperature, hence β_μ is positive. We assume no-slip conditions at the moving interface, meaning that $\mathbf{q}$ has no tangential component at $\Gamma^\varepsilon(t)$. It may however still have a normal component due to the chemical reactions, and combined with (2.4) this results in

$$\mathbf{q} = \frac{\rho_f - 2\rho_C}{\rho_f} v_n \mathbf{n}^\varepsilon \text{ on } \Gamma^\varepsilon(t).$$

2.1.5 Energy conservation

We distinguish between fluid temperature T_f and grain temperature T_g. This distinction is mainly to emphasize the different processes in the two domains. The energy is conserved in both void space and grain space. Assuming no viscous dissipation energy conservation in the void space is given by

$$\partial_t(\rho_f c_f T_f) + \nabla \cdot (\rho_f c_f T_f \mathbf{q}) = \nabla \cdot (\kappa_f \nabla T_f) \text{ for } x \in \Omega^\varepsilon(t).$$

In the grain space, energy conservation is expressed as

$$\partial_t(\rho_C c_g T_g) = \nabla \cdot (\kappa_g \nabla T_g) \text{ for } x \in G^\varepsilon(t).$$

In the above equations, c_f and c_g are specific heats, and κ_f and κ_g are heat conductivities, of fluid and grain respectively, and all are assumed constant. At the moving boundary we apply the Rankine-Hugoniot jump condition:

$$\mathbf{n}^\varepsilon \cdot (\kappa_f \nabla T_f - \rho_f c_f T_f \mathbf{q} - \kappa_g \nabla T_g) = v_n(\rho_C c_g T_g - \rho_f c_f T_f) \text{ on } \Gamma^\varepsilon(t),$$

and also require temperature continuity at the interface:

$$T_f = T_g \text{ on } \Gamma^\varepsilon(t).$$

Assuming temperature continuity at the interface corresponds to local thermal equilibrium at the pore scale. This is not the same as assuming T_f and T_g to always be equal, which would not be meaningful as the two temperatures are defined on different domains.

2.2 Darcy scale models

The Darcy scale refers to the scale where we zoom out and cannot longer observe the independent pores. Instead small volumes called representative elementary volumes (REVs) [15] are considered. An REV is so large that the average behavior is well defined, but still small enough to capture spatial variations. In an REV one cannot follow the actual route the fluid flow has through the pore structure, but only access the average mass flux flowing through a part of the domain. Darcy scale models are relevant when we are interested only in the average behavior. The advantage of using Darcy scale models is that they are computationally cheaper as they can be applied on a much coarser grid compared to the pore scale models. However, a Darcy scale model relies on several assumptions and criteria that must be met, and needs values for several "average parameters". These parameters can be found through measurements either from the reservoir or core samples, but it can be difficult to isolate specific effects, making it problematic to describe the relevant phenomena accurately. Darcy scale models are the most widely used description for flow in porous media.

As already mentioned, the porous medium consists of the solid rock and the void space between them. Some pores are isolated from the other ones and do not contribute to the fluid flow, and their contribution to the porous medium is normally neglected. The ratio of the volume of the pores, excluding the isolated pores, and the total volume within an REV, defines the effective porosity of the medium. As we are not interested in the isolated pores, we refer to this as the porosity and denotes it ϕ. Note that the porosity does not take into account any pore structure, only the volume fractions. In this sense it is an macroscopic variable as it contains only average values from the microstructure. The conservation laws are formulated as averages over the voids and grains using the porosity as weighting. Papers A, B and C deal with a Darcy scale description of the porous medium and the presentation of the model equations are based on these papers. In Paper A and Paper B we consider natural convection, while Paper C concerns reactive transport combined with heat transport.

2.2.1 Darcy's law and permeability

The permeability is considered a property of the porous medium, but is defined only through Darcy's law. Permeability describes the flow conductivity of the rock and is normally determined experimentally. Darcy's law is named after the French engineer Henry Darcy who performed experiments with water flowing through various types of sand, and found a relation between the pressure drop, sand type and the volumetric flow. The modern version of Darcy's law is written as

$$\mathbf{v} = -\frac{K}{\mu}(\nabla P + \rho_f g \mathbf{k}), \tag{2.6}$$

where $\mathbf{v}$ is the Darcy velocity, μ is the viscosity and ρ_f the density of the fluid, P is pressure, while g is the gravity acceleration and $\mathbf{k}$ is a unit vector pointing upwards. Finally, K is the permeability. The Darcy velocity $\mathbf{v}$ is the volume flux through an area and not the actual fluid velocity. If $\mathbf{q}$ is the fluid velocity through the pores, then $\mathbf{q} = \mathbf{v}/\phi$. Note that the fluid density is now defined as a mass density and similarly

with the fluid viscosity. In Papers A and B, the density is assumed to vary linearly with temperature, hence

$$\rho_f = \rho_0(1 - \beta_{\rho_f}(T_f - T_0)), \tag{2.7}$$

where T_f is fluid temperature, $\rho_f = \rho_0$ at some reference temperature T_0, and β_{ρ_f} is the thermal expansion coefficient. In Paper C density changes from varying ion concentration are also taken into account, and the density is assumed to vary linearly with temperature and ion concentrations. Also, the viscosity is assumed to vary with temperature by fitting the relevant data from [56] with a second order polynomial.

If the relation between flow and pressure drop varies with the flow direction in Darcy' law, which is often the case in layered reservoirs, the permeability is anisotropic and can be represented by a tensor $\mathbf{K}$. As only isotropic permeabilities will be considered in Papers A, B and C, K remains a scalar. However, K will be allowed to vary with space and time in the reactive transport model, giving a heterogeneous permeability. When the permeability varies due to chemical reactions, K is considered to be a function of porosity ϕ. How K varies with ϕ is not obvious; the permeability is in general increasing with larger porosity as more void space are available for flow, but the pore geometry is just as important. However, information about the pore geometry is not explicitly available at the Darcy scale as only the average quantity porosity is observed. Earlier studies for permeability-porosity relations have tried to overcome this by assuming certain pore structures and then found approximate or upscaled equations describing how the permeability can vary with porosity. One well-used model is the Kozeny-Carman equation [15, 105]

$$K(\phi) = K_0\Big(\frac{1-\phi_0}{1-\phi}\Big)^2\Big(\frac{\phi}{\phi_0}\Big)^3,$$

where $K = K_0$ for some reference porosity ϕ_0. This dependence on porosity is a simplified representation and will not necessarily describe the dependence correctly. For fractures and one-dimensional flow, a simpler cubic relationship between flow rate and hydraulic aperture is normally applied. This model is found by Witherspoon et al [103] to adequately describe the flow through a fracture.

2.2.2 Solute transport and varying porosity

In the reactive transport model in Paper C, the saturating fluid has ions dissolved in it that are transported either through advection or by random diffusion. The ion concentration of ion k is denoted c_k. Each ion type satisfies the advection-dispersion equation

$$\frac{\partial}{\partial t}(\phi c_k) + \nabla\cdot(c_k\mathbf{v}) = \nabla\cdot(\phi D\nabla c_k) + R_{c_k}(T_f, c_k, \phi), \tag{2.8}$$

where D is the diffusion coefficient and R_{c_k} is the net reaction rate for increasing concentration of ion k, possibly due to several reactions. Note that the diffusion coefficient is assumed to be constant and not depending on the ion. Also, the porosity ϕ is varying due to the mineral precipitation and dissolution reactions, and is considered as an unknown variable.

Describing the reaction rates is not straightforward and depends on the geochemical model. We consider a similar case as in [57] with calcite and anhydrite dissolving and

precipitating, and include 7 ions as well as the minerals $CaCO_3$ (calcite) and $CaSO_4$ (anhydrite). The ions are Ca^{2+}, CO_3^{2-}, SO_4^{2-}, HCO_3^-, HSO_4-, H^+ and OH^-. These ions and minerals are involved in five reactions:

$$CaCO_3(s) \leftrightarrow Ca^{2+} + CO_3^{2-} \tag{2.9a}$$
$$CaSO_4(s) \leftrightarrow Ca^{2+} + SO_4^{2-} \tag{2.9b}$$
$$H^+ + CO_3^{2-} \leftrightarrow HCO_3^- \tag{2.9c}$$
$$H^+ + SO_4^{2-} \leftrightarrow HSO_4^- \tag{2.9d}$$
$$H^+ + OH^- \leftrightarrow H_2O \tag{2.9e}$$

The first two reactions affect the porosity, while the following three are included as they highly affect the equilibrium concentrations of the involved ions. All five reactions can go both ways and will shift direction in order to reach its equilibrium state. The equilibrium can be given through thermodynamic considerations. For the first reaction (2.9a), we use the relation

$$\frac{[Ca^{2+}][CO_3^{2-}]}{[CaCO_3]} = Q_{CaCO_3},$$

where Q is called the reaction quotient and the use of brackets means the activities of the ions. Each reaction has a solubility product, which for (2.9a) is denoted $K_{CaCO_3}(T_f)$. When $Q < K$, the fluid is undersaturated with the ion pair and the reaction shifts towards dissolution of mineral. Oppositely, if $Q > K$ the fluid is supersaturated with ions and net precipitation of the mineral will take place. The solubility product as a function of temperature is known through measurements and can be found, e.g., in [76]. The activity of Ca^{2+} is given by

$$[Ca^{2+}] = \gamma_{Ca^{2+}} c_{Ca^{2+}},$$

where $\gamma_{Ca^{2+}}$ is the activity coefficient and is given by either the Debye-Hückel equation or the Davies equation depending on the ionic strength of the fluid [22]. For small ion concentrations, it is quite common to assume that activities are given by the concentration alone, which corresponds to the activity coefficients to be 1. The activities of pure water and solids are always assumed to be 1.

The reaction (2.9a) can be visioned as two separate reactions; one precipitation reaction and one dissolution reaction, where equilibrium is reached when the precipitation rate equals the dissolution rate. With this in mind, and following [57], the net reaction rate for increasing $CaCO_3$ is given by

$$R_{CaCO_3}(T_f, c_{Ca^{2+}}, c_{CO_3^{2-}}, \phi) = A(\phi) r_0 e^{-\frac{E}{RT_f}} \Big(\frac{[Ca^{2+}][CO_3^{2-}]}{K_{CaCO_3}(T_f)} - 1 \Big). \tag{2.10}$$

This way, the parenthesis is positive, resulting in net precipitation when the fluid is supersaturated with ions and negative, giving net dissolution, when the fluid is undersaturated with ions. In the above equation, A is the reactive surface and depends on porosity, while r_0 is a rate constant and $exp(-E/RT_f)$ is the Arrhenius factor as defined earlier. By tracking the amount of mineral present, one can easily rewrite the above reaction rate to assure no net dissolution when all the calcite has dissolved, as

in (2.2). The two reactions (2.9a) and (2.9b) can be described using this rate description. The three reactions (2.9c)-(2.9e) are faster such that in the typical time step we will use, they will reach equilibrium immediately. A scenario of this type is normally modeled through splitting these reactions from the rest of the system and iterate, as in [104], but for simplification an approach using rates with larger rate constants is applied. This simplification has some disadvantages, but as our purpose with this model is only to implement and illustrate the possible changes in porosity due to rock-fluid interactions, this will not cause any major problems. For each ion being described with an advection dispersion equation (2.8), the reaction rate R_{c_k} can be found by summing the contribution from each reaction rate where the ion is involved in the reaction.

The porosity varies as minerals are precipitated and dissolved. As porosity is only a volume fraction, the rate with which porosity changes is proportional to the reaction rates for the mineral reactions (2.9a) and (2.9b). Applying a volume balance equations shows that

$$\frac{\partial \phi}{\partial t} = -\nu_{CaCO_3} R_{CaCO_3} - \nu_{CaSO_4} R_{CaSO_4},$$

where ν_{CaCO_3} and ν_{CaSO_4} are the molar volumes of the two minerals.

2.2.3 Mass conservation

The general equation for mass conservation in the fluid flowing through a porous medium is

$$\frac{\partial}{\partial t}(\phi \rho_f) + \nabla \cdot (\rho_f \mathbf{v}) = 0, \tag{2.11}$$

where $\mathbf{v}$ is the Darcy velocity.

In the natural convection model in Papers A and B, we assume there are no fluid-rock interactions appearing, hence the porosity remains constant. In this model the Boussinesq approximation is applied. The Boussinesq approximation states that small density differences can be neglected, except when they appear together with the gravity acceleration, and is a common assumption when dealing with buoyancy-driven flow. The density differences are then included in the gravity term, where they should be included to achieve buoyancy-driven flow, but otherwise neglected. Hence, in the natural convection model in Papers A and B the mass conservation equation (2.11) simplifies into

$$\nabla \cdot \mathbf{v} = 0. \tag{2.12}$$

2.2.4 Energy conservation

Energy is assumed to be transported through the porous medium either through convection or conduction. Hence, any internal energy sources or sinks are neglected. However, the energy can be transported through both the solid part or the fluid part of the domain. Only conduction can occur in the solid part, while convection and conduction take place in the fluid part. Separating between fluid temperature T_f and solid temperature T_s within each REV to emphasize the different processes, we can formulate two energy conservation equations:

$$\frac{\partial}{\partial t}(\phi \rho_f c_{pf} T_f) + \nabla \cdot (\rho_f c_{pf} \mathbf{v} T_f) = \nabla \cdot (\phi k_f \nabla T_f) + h(T_s - T_f),$$

$$\frac{\partial}{\partial t}((1-\phi)\rho_s c_{ps} T_s) = \nabla \cdot ((1-\phi)k_s \nabla T_s) + h(T_f - T_s).$$

In the above equations, c_{pf} and c_{ps} are specific heat capacities and k_f and k_s are the heat conductivities, of fluid and solid respectively and are all assumed constant. Further, ρ_s is the (constant) density of the solid and h is the heat transfer coefficient between fluid and solid. Note that the two above equations are valid at Darcy scale and have the Darcy velocity appearing in the convective term. If we assume local thermal equilibrium; that is, $T_s = T_f = T$ within each REV, and sum the two equations, we obtain

$$\frac{\partial}{\partial t}((\rho c_p)_m T) + \nabla \cdot ((\rho c_p)_f \mathbf{v} T) = \nabla \cdot (k_m \nabla T),$$

where $(\rho c_p)_m = (1-\phi)(\rho c_p)_s + \phi(\rho c_p)_f$ and $k_m = (1-\phi)k_s + \phi k_f$ are the medium heat capacities and conductivities weighted over the REV. In the natural convection model, this equation can be further simplified by using that porosity is constant and rewrite using the mass conservation equation (2.12). Hence,

$$(\rho c)_m \frac{\partial T}{\partial t} + (\rho c_p)_f \mathbf{v} \cdot \nabla T = k_m \nabla^2 T. \tag{2.13}$$

Chapter 3

Linear stability analysis for natural convection

To describe natural convection in a porous medium, we apply Darcy's law (2.6), the simplified mass conservation equation (2.12) and the energy conservation equation (2.13). Even with the Boussinesq approximation for the fluid density (2.7), the system equations are non-linear due to the coupling in Darcy's law and the convective term in the energy equation. However, the model equations can still be investigated by performing a linear stability analysis. The linear stability analysis can give information about criteria for when natural convection can occur and how the convection currents will distribute at the onset of convection.

The idea behind the linear stability analysis is to linearize the model equations around a stationary solution, and find criteria for when the linear system of equations has a non-trivial solution. This criterium can be quantified, e.g., by using a homogenization approach based on pore scale perturbations [68, 69] or through the Rayleigh number, which we will focus on here. The Rayleigh number is a non-dimensional number indicating whether conduction or convection is dominating in the system. Using the Rayleigh number a critical Rayleigh number can be identified, and is such that natural convection will only occur when the Rayleigh number is larger than the critical, hence being a criterium for a non-trivial solution. While the Rayleigh number depends on flow and thermal properties of the medium and fluid, the critical Rayleigh number depends only on the geometry of the domain and the imposed boundary conditions. When a non-trivial solution exists, the linear stability analysis can also provide information about the appearance of the convection cells, which is classified through convection modes and can be presented in mode maps.

Natural convection has been investigated through linear stability analysis in several contexts. Horton, Rogers and Lapwood considered a uniform horizontal porous layer of infinite extent and found the critical Rayleigh number to be $4\pi^2$ [49, 60] when the layer was subject to impermeable and perfectly heat conducting upper and lower surfaces. Other boundary configurations can be considered as well, and an overview over critical Rayleigh numbers in an infinite porous layer with various boundary conditions can be found in Table 6.1 in [71]. In the following we look into the basic ideas behind the linear stability analysis and outline how to find criteria for onset of convection and the corresponding convection mode. To illustrate the steps of the linear stability analysis, we consider a basic Horthon-Rogers-Lapwood problem. The presentation is based on [49, 60, 71].

3.1 Non-dimensional equations and the Rayleigh number

Before the model is linearized, it is convenient to non-dimensionalize the governing equations. As we are interested in how the system behaves when relevant parameters are changed, we can avoid the possibility of unnecessary work due to two (or more) parameters giving the same effect on the system by considering non-dimensional fractions of parameters instead. This way, we can see how ratios of parameters affect the system. To nondimensionalize (2.6), (2.12) and (2.13), the following coordinate transformation is applied:

$$\mathbf{x}^* = \frac{\mathbf{x}}{h}, \qquad t^* = \frac{t\alpha_f}{\sigma h^2}, \qquad P^* = \frac{PK}{\mu\alpha_f}$$
$$\mathbf{v}^* = \frac{\mathbf{v}h}{\alpha_f}, \qquad T^* = \frac{T - T_c}{T_w - T_c},$$

where $\mathbf{x} = (x, y, z)$ denotes the spatial position. Here, h is the height of the domain, $\alpha_f = k_m/(\rho c_p)_f$ is the thermal diffusivity and $\sigma = (\rho c_p)_m/(\rho c_p)_f$ is the ratio of the volumetric heat capacities of the medium and fluid. The two temperatures T_w and T_c are reference temperatures and are the applied boundary conditions on the bottom and top of the domain, respectively. Using the star, $*$, as a superscript indicates that the variable is non-dimensional. Using this transformation, the non-dimensional versions of Darcy's law (2.6), mass conservation (2.12) and energy conservation (2.13) are now:

$$\mathbf{v}^* = -\nabla P^* + Ra T^* \mathbf{k}, \tag{3.1a}$$
$$\nabla \cdot \mathbf{v}^* = 0, \tag{3.1b}$$
$$\frac{\partial T^*}{\partial t^*} + \mathbf{v}^* \cdot \nabla T^* = \nabla^2 T^*, \tag{3.1c}$$

where $Ra = \frac{\beta_{\rho_f} \rho_f g h K (T_w - T_c)}{\mu \alpha_f}$ is the Rayleigh number. As mentioned earlier, the Rayleigh number is a measure of the strength of the convection. Using the non-dimensional form makes it easier to identify important aspects by the model equations as it is now clear what effect various parameters as permeability, temperature difference and density differences has on the system in the natural convection context. The model equations are accompanied with boundary conditions at the top and bottom of the domain. No boundary conditions are applied in the horizontal direction as the domain is an infinite layer. The top and bottom of the layer are assumed to be impermeable and perfectly heat conducting; hence,

$$T^* = 1 \text{ and } v_z^* = 0 \text{ at } z^* = 0,$$
$$T^* = 0 \text{ and } v_z^* = 0 \text{ at } z^* = 1.$$

3.2 Linearization around a stationary solution

The model equations (3.1) with the above boundary conditions have a steady-state solution. This is the solution corresponding to no fluid flow, and all heat transfer being in the form of conduction due to the temperature difference between top and bottom of the

domain. Using a linear stability analysis, we are interested in the onset of convection. Hence, the starting point will be the steady-state solution and this solution is perturbed - investigating whether convection currents will evolve or diminish. The steady state solution of (3.1) with the above boundary conditions is

$$\mathbf{v}_s^* = 0, \;\; T_s^* = 1 - z, \;\; P_s^* = Ra(z - \frac{z^2}{2}) + P_0,$$

for some reference pressure P_0. A small perturbation is introduced to the system, hence a small (non-dimensional) velocity $\hat{\mathbf{v}}$, temperature $\hat{T}$ and pressure field $\hat{P}$ are added to the above solution. The perturbed expressions are inserted in the model equation (3.1) and non-linear terms are neglected: The reason for this is that the perturbed quantities are small, hence a squared perturbed quantity will be negligible. As we are only interested at the onset of convection, the time dependence is also neglected:

$$\hat{\mathbf{v}} = -\nabla\hat{P} + Ra\hat{T}\mathbf{k}, \tag{3.2a}$$

$$\nabla \cdot \hat{\mathbf{v}} = 0, \tag{3.2b}$$

$$-\hat{v}_z = \nabla^2\hat{T}. \tag{3.2c}$$

These equations can be rewritten into a single fourth order equation for $\hat{T}$. Combining (3.2), we obtain

$$\nabla^4\hat{T} + Ra\nabla_1^2\hat{T} = 0, \tag{3.3}$$

where $\nabla_1^2 = \nabla^2 - \frac{\partial^2}{\partial z^2}$. The perturbed quantities fulfill homogeneous versions of the above boundary conditions, and rewritten into boundary conditions in $\hat{T}$ only, results in

$$\hat{T} = 0 \text{ and } \nabla^2\hat{T} = 0 \text{ at } z^* = 0, 1. \tag{3.4}$$

Assuming separation of variables, the solution is given as

$$\hat{T}(x^*, y^*, z^*) = \sin(lx^*)\sin(my^*)Z(z^*),$$

for some positive numbers l and m. Inserting this expression into (3.3) results in an equation for Z only:

$$(\frac{d^2}{dz^*} - a^2)^2 Z = a^2 RaZ,$$

where $a = (m^2 + l^2)^{1/2}$ is called the wavenumber. Requiring fulfillment of the boundary conditions (3.4), yields

$$\hat{T}(x^*, y^*, z^*) = \sin(lx^*)\sin(my^*)\sin(j\pi z^*), \tag{3.5}$$

where

$$Ra = \frac{(j^2\pi^2 + a^2)^2}{a^2} \tag{3.6}$$

and j is a positive integer.

3.3 The critical Rayleigh number

With each solution (3.5), there is a corresponding Rayleigh number associated with the choices of a and j through the relation (3.6). We seek the wavenumber a and the integer j minimizing the Rayleigh number. This will be the smallest Rayleigh number for which convection is possible, hence it is the critical Rayleigh number. The minimum still giving a non-trivial solution is reached when $j = 1$ and $a = \pi$; hence,

$$Ra_c = 4\pi^2.$$

The critical Rayleigh numbers acts as a criterion for whether natural convection currents can develop. When $Ra < Ra_c$, only conduction is present, but convection currents can occur when the Rayleigh number is above $4\pi^2$.

The critical Rayleigh number is a result of the geometry and boundary conditions that were applied. Later works applying linear stability analysis on natural convection have included other geometries such as boxes [16, 99] and cylinders [44, 100, 106]. When finite domains as boxes and cylinders are investigated, the boundary conditions at the vertical boundaries must also be accounted for, giving a large variety in potential configurations, and also new shapes of the solution $\hat{T}$. Typically, the solution method for finding $\hat{T}$ and the critical Rayleigh number is changed to account for the vertical boundary conditions, but the steps concerning perturbation of a steady-state solution are the same as described above. Beck [16] considered an impermeable three-dimensional box with insulated sidewalls which is heated from below and cooled from above. For various box sizes he found critical Rayleigh numbers. The presence of vertical walls impedes convection to develop, resulting in the critical Rayleigh number being either equal to or larger than $4\pi^2$. Wang [99] used a similar configuration as Beck, but where the bottom is heated by a constant flux, giving lower values for the critical Rayleigh number. Wang also considered a cylinder where the top was permeable, while the bottom was either held at a constant temperature or at a constant heat flux [100]. A vertical porous cylinder which is heated from below and cooled from above has also been considered by Haugen and Tyvand [44], who investigated the case when the sidewalls were heat conducting, and by Zebib [106], who considered insulated sidewalls. Several other configurations have been considered as well, and we refer to Chapter 6 in Nield and Bejan's book [71] which provides an extensive overview over the studied cases. Paper A in this dissertation is also mentioned.

In Paper A we apply linear stability analysis to a porous medium filling the domain between two coaxial cylinders where the top and bottom are kept at constant temperatures. The domain can be seen in Figure 3.1. All external walls are impermeable, and the sidewalls are either perfectly heat conducting or insulated. This case is similar to the work of Haugen and Tyvand [44] and Zebib [106], but replacing the cylinder with an annular cylinder. The internal cylinder introduces an extra obstacle for the natural convection to overcome and can represent the presence of a borehole. The case with an annular cylinder with insulated sidewalls has also been considered by Bau and Torrance [14].

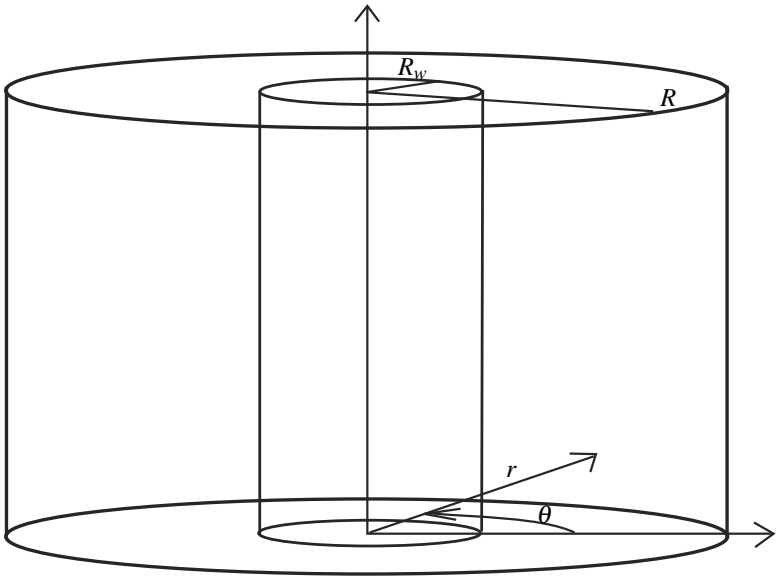

Figure 3.1: Annular cylinder with inner radius R_w and outer radius R. Figure adapted from Paper A and [20].

3.4 Convection modes

The linear stability analysis may identify the number of convection cells at the onset of convection through the minimizing wavenumber. The number of convection cells and how they distribute at the onset of convection is called the convection mode. As seen from the perturbed temperature profile (3.5) of the Horton-Rogers-Lapwood problem, the solution consists of convection cells with length $2\pi/l$ and width $2\pi/m$, hence l and m determines the shape of the convection pattern. However, in the Horton-Rogers-Lapwood problem, the convection mode determination is degenerate as the wavenumber is given by $a^2 = l^2 + m^2$ and any combination of l and m fulfilling $l^2 + m^2 = \pi^2$ corresponds to the convection mode at onset of convection. Hence, linear theory is not sufficient to determine the convection for this setting, but can be performed for other geometries.

Mode maps giving the convection mode as a function of the size of the domain have been found by Beck [16], Wang [99, 100], Zebib [106], and Haugen and Tyvand [44] for their configurations. Bau and Torrance [14] who also considered an annular cylinder with insulated sidewalls, found mode maps. However, as shown in Paper A, we find a mode map with greater detail than Bau and Torrance.

Chapter 4

Homogenization of pore scale models

The model equations defined in Section 2.1 constitute the processes relevant at the pore scale. These model equations take into account the changing geometry of the porous medium and allows for detailed treatment of the pore structure. The development of the pore structure is important when modeling chemical reactions with mineral precipitation and dissolution as the flow conditions can change significantly in a geothermal reservoir, but doing simulations using a pore scale model would require a very fine grid as a typical pore size could be micrometers, while the reservoir scale is typically kilometers [15]. Also, even if we would have been able to explicitly include the pore scale effects in the simulations, we are maybe only interested in finding the average behavior of the system. Hence, a system of equations at Darcy scale would be more comprehensive.

To incorporate pore scale effects into Darcy scale models, upscaling from pore scale to Darcy scale can be applied: Then model equations at the Darcy scale including the pore scale effects through upscaled effective parameters are achieved. Hence, the average effects of the pore scale processes are still included. Upscaling of pore scale models shows clearer how the pore scale mechanisms affect the average behavior at Darcy scale. The alternative - using a Darcy scale method based on measurements at reservoir scale, obstructs isolating the pore scale effects and might result in inaccurate parameters. Through upscaling, the values of effective parameters can be determined using values known from pore scale measurements.

There exists a variety of upscaling techniques applicable for porous media, both analytical and numerical. The assumptions and applicabilities of the techniques vary, and we refer to e.g. [30, 37] for a review of various methods. Which method to apply depends on the starting and ending scale, which features that are present in the model, and what the goal of the upscaling is. We focus here on homogenization as upscaling method, which is an analytical technique deriving effective model problems based on the pore scale model equations. Upscaling techniques such as spatial averaging and Green's function approaches are capable of doing the same, but using different assumptions [30]. The basis behind homogenization is the notion of separation of scales and using asymptotic expansions to capture the macroscale behavior of the microscale equations.

Pore scale models and upscaling through homogenization can be used for a much wider group of problems than reactive transport in the subsurface and are, e.g., used in biological applications as well. Weller et al [101] analyzed various growth problems

of a thrombus in a blood vessel: As the thrombus grows, the model contains a free boundary and the authors show existence of a smooth solution. Using a periodic porous medium approach, Marciniak-Czochra and Ptashnyk [62] upscaled the behavior of cell receptors to derive an effective macroscopic formulation. Several models with mineral precipitation and dissolution at pore scale have been considered, as in [92, 97] where geochemical reactions on a fixed boundary is analyzed. Models with a fixed geometry are applicable when size of the mineral layer does not change much in width due to the chemical reactions. Pore scale models with a free boundary but no fluid flow is studied in [95]. Later, van Noorden included fluid flow and performed upscaling from pore scale to Darcy scale of a thin strip [94] and van Noorden extended the analysis to consider upscaling in a periodic porous medium [93]. Ray et al [81] considered a similar model as in [93], describing drug release from collagen matrices. Kumar et al [59] performed upscaling of a model including solute transport with Taylor dispersion in a thin strip with changing aperture due to mineral precipitation and dissolution, while Allaire et al [11] considered a similar problem in a periodic porous medium, but with a fixed geometry. Allaire and Habibi [8] upscaled various forms of heat transfer in a fixed periodic porous medium.

The following presentation of homogenization as upscaling technique is based on [27, 46, 47]. For illustration, we consider first a simple diffusion problem, but keeping the pore scale model equations from Section 2.1 in mind.

4.1 Scale separation

The first step in a homogenization process is isolating a separation of scales through some small number ε. This could be an highly oscillating diffusion coefficient varying with period ε or a medium with holes of size ε. The two geometries presented in Section 2.1 included a thin strip with height l and length L, and a perforated medium contained in $(0,L)^2$ where the typical perforated structure was contained within $(0,l)^2$. As the microscopic length scale l is much smaller than the macroscopic length scale L, the quotient $\varepsilon = l/L$ can be used as the indicator of the separation of scales. As already introduced in Section 2.1 we separate between the macroscopic variable x and the microscopic variable y.

To illustrate the scale separation a simple 1D diffusion equation is presented, which is the same illustrative example used in [47]. We consider the boundary value problem

$$\begin{aligned} \frac{d}{dx}\big(a^\varepsilon(x)\frac{d}{dx}u^\varepsilon(x)\big) = 0 \text{ for } 0 < x < 1,\\ u^\varepsilon(x) = 0 \text{ at } x = 0,\\ u^\varepsilon(x) = 1 \text{ at } x = 1, \end{aligned}$$

where $a^\varepsilon(x)$ is a highly oscillatory diffusion coefficient and can be written as $a^\varepsilon(x) = a(\frac{x}{\varepsilon})$ where $a(y)$ is a periodic function with period 1. The possibility of rewriting $a^\varepsilon(x)$ this ways, defines the separation of scales: The model equation is formulated using the macroscopic variable x, but the problem depends on variations on a much smaller scale, which is better captured using the microscopic variable y instead, and ε gives the scaling between x and y. Even though this problem can be solved explicitly, we are

interested in the average solution, which in this case would be when $a^\varepsilon(x)$ is replaced with a constant a^*. Solving the original problem leads to

$$u^\varepsilon(x) = x + \frac{\int_0^{\frac{x}{\varepsilon}} (\frac{1}{a(y)} - 1)dy}{\int_0^{\frac{1}{\varepsilon}} \frac{1}{a(y)} dy},$$

while the solution of the average problem, denoted $u(x)$, is

$$u(x) = x.$$

Hence, the original solution can be written as

$$u^\varepsilon(x) = u(x) + \varepsilon u_1(\frac{x}{\varepsilon}),$$

where $u_1(y)$ is a 1-periodic function given by

$$u_1(y) = \frac{\int_0^y \frac{d\bar{y}}{a(\bar{y})}}{\int_0^1 \frac{d\bar{y}}{a(\bar{y})}} - y.$$

Normally, the explicit solution of the original problem is not known, but this simple 1D-problem illustrates the separation of scale. The solution to the average problem $u(x)$ is found, and we see that the solution of the original problem contains this average solution in addition to a correction term containing the microscopic behavior. When ε is small, the correction term is also small, and

$$\lim_{\varepsilon \to 0} u^\varepsilon(x) = u(x).$$

Hence, for small values of ε the average solution is expected to mimic the original solution well.

A similar scale separation can be made in the two geometries defined in Section 2.1. In the periodic model we separated between the macroscopic variable x and the microscopic variable y capturing the behavior in the pore structure, and ε was found in the scaling between the two variables. The thin strip model has a slightly different separation of scale; here y is not a scaled version of x, but in another spatial direction. As the strip is thin and long, we can still identify a difference in length scales and a value for ε.

The model equations defined in Section 2.1 can be clearer investigated if written using non-dimensional variables. Non-dimensionalizing the model equations shows at which scale various terms depend on and will clarify the further analysis. In Papers D, E and F we use slightly different ways of non-dimensionalizing the equations and present here from the version in Paper E. As our purpose is to illustrate the procedure, we only non-dimensionalize the solute transport equation (2.3) and the momentum equation (2.5) here. We introduce t_{ref}, $x_{ref} = L$, $y_{ref} = l$, u_{ref}, q_{ref}, $p_{ref} = L^4 u_{ref}/t_{ref}^2 l^2$, $\mu_{ref} = l^2 p_{ref}/L q_{ref}$, and let $\varepsilon = l/L$. Non-dimensional variables are denoted with a hat and are defined as

$$\hat{t} = t/t_{ref}, \qquad \hat{x} = x/x_{ref}, \qquad \hat{y} = y/y_{ref}, \qquad \hat{u}^\varepsilon = u/u_{ref},$$
$$\hat{\mathbf{q}}^\varepsilon = \mathbf{q}/q_{ref}, \qquad \hat{p}^\varepsilon = p/p_{ref}, \qquad \hat{\rho}_f = \rho_f/u_{ref}, \qquad \hat{\mu} = \mu/\mu_{ref}.$$

We emphasize dependence on the small variable ε by denoting our main variables with ε as a superscript. To proceed we introduce some relevant reference times: The reference time for fluid flow is $T_F = L/q_{ref}$ which will also act as reference time for observations; t_{ref}. This is because we are interested in the typical time for any injected fluid flowing through the reservoir. For solute diffusion the reference time is $T_D = L^2/D$. The Péclet number, which is a measure of the relative strength between advection and diffusion, is defined as

$$Pe_D = \frac{T_D}{T_F} = O(\varepsilon^{-\beta}).$$

In Paper F we have a convection dominated problem, hence β will be positive, giving large Péclet number and we assume $\beta = 1$. In Papers D and E we assume convection and diffusion to be at the same time scale, hence $\beta = 0$ in these papers. Following Paper E, the non-dimensional solute diffusion parameter is

$$\hat{D} = \frac{D}{Lq_{ref}},$$

where $\hat{D}$ is assumed independent of ε. Since we will only use non-dimensional variables in the following, we skip the hat. The non-dimensional convection-diffusion equation (2.3) becomes

$$\partial_t u^\varepsilon + \nabla \cdot (\mathbf{q}^\varepsilon u^\varepsilon) = D\nabla^2 u^\varepsilon \text{ in } \Omega^\varepsilon(t), \tag{4.1}$$

while the momentum balance equation (2.5) is now written

$$\begin{aligned}\varepsilon^2 \Big(\partial_t(\rho_f \mathbf{q}^\varepsilon) + \nabla \cdot (\rho_f \mathbf{q}^\varepsilon \mathbf{q}^\varepsilon) \Big) &= -\nabla p^\varepsilon \\ &+ \varepsilon^2 \left(\nabla \cdot \Big(\mu(\nabla \mathbf{q}^\varepsilon + (\nabla \mathbf{q}^\varepsilon)^T) \Big) - \frac{2}{3} \nabla(\mu \nabla \cdot \mathbf{q}^\varepsilon) \right) \text{ in } \Omega^\varepsilon(t),\end{aligned} \tag{4.2}$$

All the model equations have been non-dimensionalized and we refer to Papers D, E and F for a complete overview. Equations (4.1) and (4.2) illustrate how the non-dimensionalization can emphasize the scale dependence. We see that all the terms but the pressure gradient is multiplied with ε^2 in (4.2), indicating that pressure differences have an important role in the momentum equation as all other terms are much smaller. In Paper F, the diffusive term in (4.1) is multiplied with a factor ε due to the assumption of dominating convection, while diffusion and convection have the same relative strength in Papers D and E. Our goal is to find an average problem mimicking the behavior of the pore scale problem, using the assumption that ε is small.

4.2 Homogenization ansatz

The steps towards finding upscaled model equations start with the homogenization ansatz and using formal asymptotic expansions. We assume that the unknowns $u^\varepsilon(x)$ and $\mathbf{q}^\varepsilon(x)$ can be written in the form of two-scale asymptotic expansions such that

$$u^\varepsilon(x) = u_0(x,y) + \varepsilon u_1(x,y) + \varepsilon^2 u_2(x,y) + \ldots, \tag{4.3a}$$

$$\mathbf{q}^\varepsilon(x) = \mathbf{q}_0(x,y) + \varepsilon \mathbf{q}_1(x,y) + \varepsilon^2 \mathbf{q}_2(x,y) + \ldots, \tag{4.3b}$$

and similarly for the other variables. We can call u_0 the macroscopic part of u^ε and we see that

$$u_0 = \lim_{\varepsilon \to 0} u^\varepsilon,$$

while u_1 can be thought of as the first order correction as

$$u_1 = \lim_{\varepsilon \to 0} \frac{1}{\varepsilon}(u^\varepsilon - u_0),$$

and similarly with u_2. Due to the inclusion of explicit dependence of y in the series expansion terms, it follows from the chain rule that the nabla-operator is $\nabla = \nabla_x + \frac{1}{\varepsilon}\nabla_y$. The $\frac{1}{\varepsilon}$-factor is due to the difference in scaling of y.

Note that introducing the asymptotic expansion is an *assumption*. Assuming that the series representation is valid, we seek model equations that capture the main features when ε is small. The procedure is to insert the asymptotic expansions (4.3) into the model equations (4.1) and (4.2), and isolate the terms that are dominating since ε is small. Through this procedure one can show that u_0 will be a function of x only, meaning that the dominating part of the solution does not depend on the microscale variable y - as expected. By detecting terms that are of same order with respect to ε, new model equations using u_0 (and sometimes also including u_1) as a variable can be formulated. The new system of model equations is known as the homogenized problem.

The thin strip case is slightly different as the y-dependence comes from the transversal direction in the strip and is not a product from scaling. The homogenization of the periodic porous medium relies on the periodicity of y, while no periodicity is necessary in the thin strip setting. However, as the strip is thin there is still a separation of length scales and similar asymptotic expansions. The ∇-operator is in the thin strip case given as $\nabla = \frac{\partial}{\partial x}\mathbf{i} + \frac{1}{\varepsilon}\frac{\partial}{\partial y}\mathbf{j}$, hence the procedure with finding dominating terms in the thin strip case is surprisingly similar as with the periodic porous medium, and is presented in Papers D and F.

4.3 Two-scale convergence

The disadvantage of the above described procedure is that it relies on the assumption of the validity of asymptotic expansions and if u_0 is in fact the limit of u^ε as ε approaches zero. Nguetseng [70] introduced the notion of two-scale convergence to address this challenge, which was later developed further by Allaire [6]. The concept of two-scale convergence is applicable for the periodic porous medium and is defined in the following way:

Definition 1. *A sequence of functions $u^\varepsilon \in L^2(\Omega^\varepsilon)$ is said to converge two-scale to a limit $u_0 \in L^2(\Omega \times Y)$ if*

$$\lim_{\varepsilon \to 0} \int_{\Omega^\varepsilon} u^\varepsilon(x)\phi(x, \frac{x}{\varepsilon})dx = \int_\Omega \int_Y u_0(x,y)\phi(x,y)dxdy$$

for all $\phi \in \mathcal{D}(\Omega; C^\infty_{per}(Y))$, where $C^\infty_{per}(Y)$ is the space of infinite differentiable periodic functions.

The definition is accompanied by two theorems providing the two-scale convergence and strong convergence for linear elliptic problems [6]:

Theorem 1. *Let u^ε be a bounded sequence in $L^2(\Omega)$. There exists a subsequence, also denoted u^ε, and a function $u_0(x,y) \in L^2(\Omega \times Y)$, where Y is the unit cube, such that*

$$\lim_{\varepsilon \to 0} \int_\Omega u^\varepsilon(x)\phi(x,\frac{x}{\varepsilon})dx = \int_\Omega \int_Y u_0(x,y)\phi(x,y)dxdy$$

for any smooth function $\phi(x,y)$ which is Y-periodic in y.

Theorem 2. *Let u^ε be a sequence that two-scale converges to $u_0(x,y)$. Then, u^ε weakly converges in $L^2(\Omega)$ to $u(x) = \int_Y u_0(x,y)dy$, and we have*

$$\lim_{\varepsilon \to 0} ||u^\varepsilon||_{L^2(\Omega)} = ||u_0||_{L^2(\Omega \times Y)},$$

and if $u_0(x,y)$ is smooth, then

$$\lim_{\varepsilon \to 0} ||u^\varepsilon(x) - u_0(x,\frac{x}{\varepsilon})||_{L^2(\Omega)} = 0.$$

The first theorem proves the existence of the first term in the ansatz (4.3). Note that the theorems are formulated in Ω, but as proven in [2], as long as Ω^ε is connected, the convergence can be proven for an extended function $\bar{u}^\varepsilon$ defined in the whole domain. To prove the two-scale convergence for a specific model equation, one needs to show boundedness in the relevant norm for u^ε. In a perforated domain, this is not straightforward as one needs to extend u^ε onto Ω in a continuous manner. How to define this extension depends on the boundary conditions imposed on the perforations. Taking into account the perforations changing with time complicates the procedure. Our model equations in Section 2.1 are non-linear, hence proving the two-scale convergence would be challenging, although convergence results for some non-linear problems exists [6, 32, 48]. We note that Peter [75] proved two-scale convergence and Meier [64] also proved existence and uniqueness for a (quasi)linear coupled reaction-diffusion process with a prescribed reaction rate by transforming the developing domain into a fixed reference domain. Using a prescribed velocity field, Allaire et al [7, 9, 10] have shown two-scale convergence for a reactive transport problem with a free boundary under various assumptions. The results were also confirmed by numerical computations.

The framework of two-scale convergence is a powerful tool to prove the existence and uniqueness of the macroscopic solution in the limit as ε approaches zero. However, applying it to the coupled model equations considered in Section 2.1 has not been done due to the complexity of the procedure for this model problem and is beyond the scope of this thesis. Hence, in Papers D, E and F, the assumption of asymptotic expansions remains an assumption.

4.4 Verifications and limitations

When the two-scale convergence is not proven, the validity of the homogenization procedure relies on the assumption of the homogenization ansatz (4.3). This is not necessarily a problem, and a quite common simplification in many homogenization papers.

The two papers by van Noorden [93, 94], which corresponds to the isothermal versions of Papers D and E, do not include any two-scale convergence, but has compared the upscaled model with the original pore scale model equations in some special cases. As one expects the upscaled model to mimic the average behavior of the original model equations when ε is close to zero, numerical calculations of both the pore scale model and the upscaled model can be done to check if there actually is a correspondence for small values of ε. This way, it is still possible to substantiate the validity of the upscaling procedure.

Kumar et al [59] compared the upscaled Taylor dispersion model in a thin strip with the original pore scale equations and found correspondence as ε decreased. Kumar et al also compared the upscaled model equations with simplified versions of the model equations and found the simplified versions to also correspond well when using a small value of ε (that is, $\varepsilon = 0.0001$). The upscaled model was the one that corresponded best with the average solution of the pore scale equations, especially for slightly larger values of ε.

Implementing the pore scale model equations with a free boundary requires extra care. Kumar et al [59] and van Noorden [93, 94] used an ALE (Arbitrary Lagrangian-Eulerian) formulation [33] to deform the grid in the void space as the geometry developed. Implementing a level set formulation to track the moving interface is also possible and we refer to, e.g., [51] for an example of such an implementation in 3D.

Chapter 5

Numerical framework

Solving the coupled non-linear model equations arising from natural convection or reactive transport, requires numerical methods. Numerical methods allow us to discretize the equations and find approximate solutions that are converging to the exact solution. There exists a large variety of numerical methods, each having advantages and deficiencies. Which numerical method to apply depends on properties of the model equations and which features are needed in the approximate solution. In our research two classes of methods have been applied: Pseudospectral methods and finite volume methods. Pseudospectral methods have the advantage of high accuracy and easy implementation, while extra care is needed for complex domains. Finite volume methods allow flexible gridding and has the advantage of being conservative, meaning that properties such as mass and energy will be conserved in the discretization. However, the convergence rate is low. In the natural convection model high accuracy is needed to capture the convection accurately. As a relatively simple domain is considered, pseudospectral methods are applicable. For the reactive transport model, conserving mass and energy through the fluid flow is important due to the intricate flow evolution caused by the changing porosity. Hence, finite volume methods are applied for this model.

5.1 Pseudospectral methods

The presentation of pseudospectral methods is based on the books of Trefethen [89] and Boyd [19]. Pseudospectral methods are a branch within spectral methods, which are based on approximating the unknown solution $u(x)$ by a sum of $N+1$ basis functions $\psi_i(x)$ that span the space where the approximate solution exists:

$$u(x) \approx u_N(x) = \sum_{i=0}^{N} a_i \psi_i(x),$$

where $\{a_i\}_{i=0}^{N}$ is a set of unknown weights. We seek the approximate solution of the differential equation

$$Lu(x) = f(x),$$

where L is a differential operator and f is a known function. The approach of pseudospectral methods is to minimize the residual

$$R(x; a_0, a_1, \ldots, a_N) = Lu_N - f$$

by requiring it to be zero in a set of $N+1$ collocation points $\{x_j\}_{j=0}^{N}$. As basis functions one uses polynomials of order $N+1$ or trigonometric functions. The basis functions are chosen such that they have the value 1 in one collocation point and 0 in the others; that is,

$$\psi_i(x_j) = \delta_{ij}. \tag{5.1}$$

This way, the unknown weights a_i are the function values of the approximated solution u_N in the collocation points x_i. If the differential operator L is linear, the differential equation can be reformulated into the linear matrix equation

$$\mathbf{Ax} = \mathbf{b},$$

where $\mathbf{x}$ is the vector containing the unknown function values $u_N(x_i)$, $\mathbf{A}$ is the $(N+1)\times(N+1)$ matrix with entries $A_{ij} = L\psi_j(x_i)$, and $\mathbf{b}$ is a vector with components $f(x_i)$. The matrix $\mathbf{A}$ will in general be a full matrix. Each line in the matrix equation represents an equation for the function value in a specific node.

5.1.1 Choice of collocation points

How to choose the collocation points, and hence the basis functions, is an essential aspect of pseudospectral methods as a bad choice could lead to low or no convergence. If the solution is expected to have some periodicity, the Fourier nodes with accompanying Fourier basis should be chosen. If the solution does not have any periodicity and exists in a finite interval, Chebyshev nodes and Chebyshev polynomials as basis function will produce the best results. For solutions on infinite or semi-infinite intervals, other choices such as Laguerre, rational Chebyshev or Hermite functions can be used as basis functions. In the natural convection model a finite domain with periodicity in the azimuthal direction is considered. As only Chebyshev and Fourier basis function will be relevant for our model, we focus on them in the following presentation.

For the radial and vertical direction, a rewritten version of Chebyshev polynomials is applied as basis functions. The set of collocation nodes will be a Gauss-Lobatto-Chebyshev (GLC) grid, which consists of the critical points of the Nth order Chebyshev polynomial $T_N(x)$ and the endpoints -1 and 1. This set of points can easily be rescaled and shifted to any finite interval. The $(N+1)$ GLC points are given by

$$x_i = \cos\left(\frac{\pi i}{N}\right) \text{ for } i = 0,\ldots,N,$$

while the basis functions satisfying the desired kronecker-delta property (5.1) are

$$\psi_i(x) = \frac{(-1)^{i+1}}{c_i N^2}\frac{(1-x^2)}{x-x_i}\frac{dT_N(x)}{dx} \text{ for } i = 0,\ldots,N, \tag{5.2}$$

where c_i is 2 when i is 0 or N and otherwise 1. The grid points are clustered near the edges of the interval, which assures minimizing any Runge's phenomenom [18].

In the azimuthal direction the critical points of $\cos(\frac{Nx}{2})$ are used as grid points:

$$x_i = \frac{2\pi i}{N} \text{ for } i = 1,\ldots,N.$$

Note that only N points are needed in the azimuthal direction instead of $N+1$. Due to the periodicity requirement the point $i=0$ would be the same point as $i=N$ and is therefore neglected. The required basis functions fulfilling (5.1) are

$$\psi_i(x) = \frac{1}{2N}\sin\big(N(x-x_i)\big)\cot\big(\frac{1}{2}(x-x_i)\big) \text{ for } i=1,\ldots,N. \tag{5.3}$$

Also note that the grid points are equidistant, which is normally associated with causing Runge's phenomenon. As the basis functions are trigonometric functions and not polynomials, this is not a risk in this case.

5.1.2 Differentiation matrices

The discretization of the differential operator L can be constructed from differentiation matrices. The differentiation matrix for single derivation will have entries $\frac{d}{dx}\psi_j(x_i)$, and similarly will a differentiation matrix for double derivation has entries $\frac{d^2}{dx^2}\psi_j(x_i)$. As the basis functions are known from (5.2) and (5.3), we can calculate the differentiation matrices. The following formulas are derived by Gottlieb et al in [42].

The first order differentiation matrix for Chebyshev nodes has entries

$$A_{ij} = \begin{cases} (1+2N^2)/6 & \text{if } i=j=0, \\ -(1+2N^2)/6 & \text{if } i=j=N, \\ -x_j/(2-2x_j^2) & \text{if } i=j; 0<j<N, \\ (-1)^{i+j}c_i/(c_j(x_i-x_j)) & \text{if } i\neq j. \end{cases}$$

Higher order differentiation matrices with this choice of Chebyshev basis function are given as

$$\mathbf{A}_k = (\mathbf{A}_1)^k,$$

where $\mathbf{A}_k$ is kth order differentiation matrix and k is a positive integer.

The first order differentiation matrix for Fourier nodes has entries

$$A_{ij} = \begin{cases} 0 & \text{if } i=j, \\ \frac{1}{2}(-1)^{i-1}\cot(\frac{1}{2}(x_i-x_j)) & \text{if } i\neq j, \end{cases}$$

while the second order differentiation matrix is given by

$$A_{ij} = \begin{cases} -(1+2N^2)/6 & \text{if } i=j, \\ \frac{1}{2}(-1)^{i-1+1}\csc^2(\frac{1}{2}(x_i-x_j)) & \text{if } i\neq j. \end{cases}$$

The differential operator is discretized by combining the necessary differentiation matrices. We can note that in the designing and assembling of the discretization, the Chebyshev and Fourier basis functions are not explicitly used, but they are part of the underlying derivation in the distribution of nodes and setup of differentiation matrices. Boyd shows in Section 4.4 in [19] that discretization using series expansions explicitly or through collocation points and differentiation matrices are equivalent and share the same convergence properties. Using the differentiation matrices, boundary conditions are incorporated through the collocation nodes located at the boundary: The equation

line corresponding to the boundary node is replaced with an equation representing the applied boundary condition. As our system of equations is non-linear due to the convective term, the resulting discretization of L will be non-linear and is solved iteratively using Newton's method, which is described in Section 5.4.

5.1.3 Convergence rates

Pseudospectral methods are known for their exponential convergence rate, which is due to the convergence properties of series expansions of orthogonal functions. As Fourier and Chebyshev series create the basis for the pseudospectral methods, the convergence properties of pseudospectral methods are the same as with these series expansions. We present two short proofs showing why the Fourier series and the Chebyshev series have such fast convergence. The proofs are given thoroughly by Gottlieb and Orszag in Section 3 in [43].

Fourier series

The complex Fourier series $g(x)$ of a periodic function $f(x)$ defined on the interval $[0, 2\pi]$ is given by

$$g(x) = \sum_{j=-\infty}^{\infty} a_j e^{ijx},$$

where i refers to the imaginary unit $\sqrt{-1}$. The series coefficients a_j are given by

$$a_j = \frac{1}{2\pi} \int_0^{2\pi} f(x) e^{-ijx} dx.$$

Defining the truncated series

$$g_N(x) = \sum_{j=-N}^{N} a_j e^{ijx},$$

we seek the convergence rate of $|f(x) - g_N(x)|$ as N increases. If $f(x)$ has continuous derivatives up to order $k-1$ for some positive integer k, and if $f^{(k)}(x)$ exists and is integrable, then integration by parts yields

$$a_j = \frac{1}{2\pi (ij)^k} \int_0^{2\pi} f^{(k)}(x) e^{-ijx} dx.$$

The Riemann-Lebesgue lemma implies that $|a_j| \ll 1/j^k$ as $j \to \pm\infty$, which assures that

$$|f(x) - g_N(x)| = O(\frac{1}{N^k}) \text{ as } N \to \infty.$$

This is called algebraic convergence of order k. If $f(x)$ is infinitely differentiable and periodic, then

$$|f(x) - g_N(x)| = O(\frac{1}{N^k}) \; \forall \; k \geq 0 \text{ as } N \to \infty.$$

This is called exponential or spectral convergence and means that $g_N(x)$ converges to $f(x)$ more rapidly than any finite power of $1/N$ as $N \to \infty$.

Chebyshev series

Chebyshev series have the same convergence properties as Fourier series as they can be interpreted as a rewritten form of the Fourier cosine series. The Chebyshev series for a function $f(x)$ defined on the interval $[-1,1]$ is

$$g(x) = \sum_{j=0}^{\infty} a_j T_j(x),$$

where $T_j(x)$ is the Chebyshev polynomial of order j. Then $G(\theta) = g(\cos\theta)$ is the Fourier cosine series of $F(\theta) = f(\cos\theta)$ for $\theta \in [0,\pi]$. This follows directly from the cosines property of Chebyshev polynomials as $T_j(\cos\theta) = \cos(j\theta)$ and the mapping $x = \cos\theta$. This mapping also ensures the periodicity requirement needed for the Fourier series. The series coefficients a_j in the above expansion are given by

$$a_j = \frac{2}{\pi d_j}\int_0^{2\pi} f(\cos\theta)\cos(j\theta)d\theta = \frac{2}{\pi d_j}\int_{-1}^{1} f(x)T_j(x)(1-x^2)^{-1/2}dx,$$

where $d_0 = 2$ and otherwise 1. Since a Chebyshev series can be mapped into a Fourier cosine series, Chebyshev series will have the same convergence properties. Hence, if $f(x)$ is infinitely differentiable, the truncated series expansion $g_N(x)$ converges to $f(x)$ at exponential/spectral rate as $N \to \infty$.

It is important to note that if $f'(x)$ is known to only be, e.g., piecewise continuous and differentiable, we cannot expect convergence faster than $O(1/N^2)$.

5.1.4 Domain decomposition

As the nodes have to be chosen in specific ways in order for pseudospectral methods to converge (fast), this puts restrictions on which domains that can be considered. Using cartesian coordinates, cuboids would be ideal, while in cylindrical coordinates cylinders or annular cylinders are preferable. To overcome this limitation when dealing with slightly more complex domains, we can decompose the domain into several parts such that a pseudospectral grid can be applied to each part. In Paper B we consider a three-layer porous medium with the borehole interacting with the middle layer. A cross-section of the domain is shown in Figure 5.1. The top and bottom layers act as heat reservoirs for the middle layer, which is connected with the borehole. The circulating fluid inside the outer part of the borehole and the interaction between the borehole and the reservoir is included explicitly.

As different model equations are applied in the layers of the porous medium, the porous medium is divided into three domains according to the layering. The borehole is introduced as one domain. Each domain is discretized using scaled and shifted Chebyshev nodes in radial and vertical direction and Fourier nodes in azimuthal direction. Where the domains meet, precautions must be made and we require continuity in relevant variables and in their fluxes across the internal boundaries. For the energy equations, this means that we demand temperature continuity across all internal boundaries as well as continuity in heat flux. As the heat conductivity varies between the layers and the borehole, this results in a discontinuous temperature gradient. The discontinuous temperature gradient entails that we cannot expect high convergence rates.

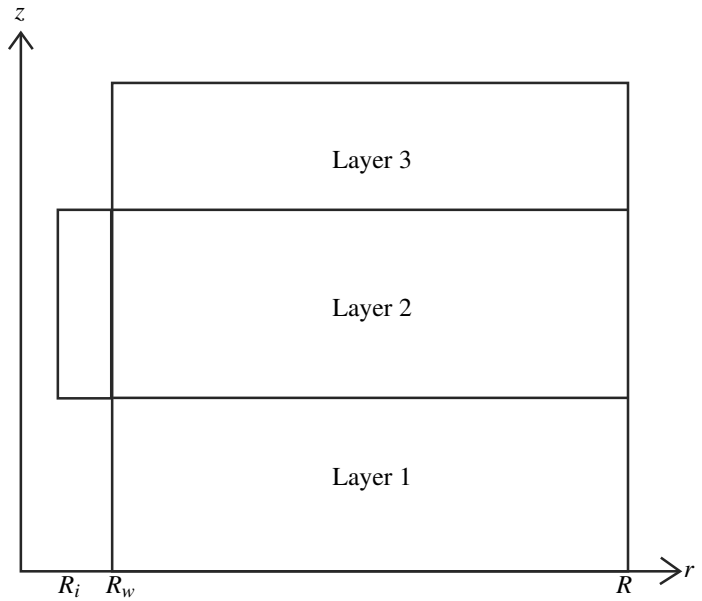

Figure 5.1: Cross-section of the annular cylinder with inner radius R_w and outer radius R. The outer part of the borehole pipe has inner radius R_i and interacts with the middle layer of the porous medium. Figure adapted from Paper B.

Pseudospectral is however still a good choice for discretizing as the truncation error from pseudospectral methods is in general smaller than from comparable methods.

5.2 Finite volume methods

The following presentation of finite volume methods is based on the book by Eymard et al [36]. As mentioned in the introduction, the advantage of using finite volume methods to discretize model equations, is due to the methods being conservative. The methods rely on dividing the computational domain into subsets called control volumes. When discretizing equations expressing conservation of some quantity; e.g., mass, energy or ions, the conservation equations are integrated over the control volume. Applying the divergence theorem leads to each control volume expressing that the accumulation of the quantity within the volume equals the fluxes over the boundary. The fluxes over the boundary are then discretized.

The finite volume methods work on arbitrary geometries and on unstructured meshes, but simplifies when used on cartesian grids. Several versions of the methods exists, depending on how to approximate the fluxes. As we have only applied two point flux approximation (TPFA), we will present this version of the method, but mention here that versions using multi point flux approximation (MPFA) exist [1, 61]. The below presentation utilizes a two-dimensional uniform cartesian grid.

5.2.1 Conservative schemes

The two-dimensional domain Ω is divided into subsets denoted V_{ij}, where the indices $\{i, j\}$ are such that the whole domain is covered. The grid is rectangular and uniform with nodes in the cell centers. We consider the discretization of the general conservation equation

$$\frac{\partial}{\partial t}u(x,t) + \nabla \cdot \mathbf{F}(x,t) = f(x,t),$$

where u is the quantity to be conserved, $\mathbf{F}$ denotes the flux of u, and f is a source/sink term, e.g., coming from a chemical reaction. Comparing with the model equations given in Section 2.2 (and also in Section 2.1, of course), we see a relationship with the above conservation law.

The above equation is integrated over the control volume V_{ij}. Applying the divergence theorem for the flux term yields

$$\int_{V_{ij}} \frac{\partial}{\partial t} u dx + \int_{\partial V_{ij}} \mathbf{F} \cdot \mathbf{n} ds = \int_{V_{ij}} f dx, \tag{5.4}$$

where ∂V_{ij} is the positively oriented boundary of V_{ij} and $\mathbf{n}$ is the unit normal of ∂V_{ij} pointing outwards. As the grid is rectangular, the four edges of the boundary can be denoted $\sigma_{i\pm 1/2, j\pm 1/2}$. For each edge, a two point flux approximation is applied, hence using the cell centers on each side of the edge to approximate the value on the edge. For the vertical edge $\sigma_{i+1/2,j}$ located on the right-hand side of V_{ij}, this means

$$\int_{\sigma_{i+1/2,j}} \mathbf{F} \cdot \mathbf{n} ds = \int_{\sigma_{i+1/2,j}} \{F_{i+1,j}, F_{i,j}\} ds.$$

How to express the flux using $F_{i+1,j}$ and $F_{i,j}$ will be explained below, but we note for now that the equation (5.4) expresses the conservation: The first term is the accumulation of u inside the control volume, while the second term is the flux of u leaving the volume over the edges. The term on the right-hand side expresses how much is produced/annihilated inside the control volume. To express the flux over the edge, and to have a conservative scheme, we require consistency. Hence, what leaves one control volume through one edge must equal what enters the neighboring control volume through the same edge. This means,

$$\int_{\sigma_{i+1/2,j}} \{F_{i+1,j}, F_{i,j}\} ds = -\int_{\sigma_{i+1/2,j}} \{F_{i,j}, F_{i+1,j}\} ds,$$

where the right-hand side is what enters the control volume $V_{i+1,j}$ through its left edge. A large variety of meshes and schemes exists, but they all require this consistency in fluxes to be conservative. To indicate how the fluxes are discretized we consider a small example using $\mathbf{F} = \mathbf{v}u - D\nabla u$, which corresponds to an convection-diffusion equation. When the flow velocity $\mathbf{v}$ is known at the control volume edges, the flux across $\sigma_{i+1/2,j}$ can be approximated by

$$\int_{\sigma_{i+1/2,j}} \{F_{i+1,j}, F_{i,j}\} ds = L_{i+1/2,j} v_{i+1/2,j} u_{i+1/2,j} - L_{i+1/2,j} D \frac{u_{i+1,j} - u_{i,j}}{h_x},$$

where $L_{i+1/2,j}$ is the length of edge $\sigma_{i+1/2,j}$, $v_{i+1/2,j}$ is the horizontal component of $\mathbf{v}$ at the edge and h_x is the distance between the cell centers in control volumes $V_{i+1,j}$ and $V_{i,j}$. If D is not constant, it should be replaced with its harmonic mean between the two cells. For the convective term upstream approximation is applied, meaning that

$$u_{i+1/2,j} = \begin{cases} u_{i,j} & \text{if } v_{i+1/2,j} \geq 0, \\ u_{i+1,j} & \text{if } v_{i+1/2,j} < 0. \end{cases}$$

5.2.2 Convergence rate

Eymard et al [36] provide several conditions for existence and convergence on some domains, meshes and flux discretizations for various types of model equations, as well as providing error estimates. For a linear elliptic equation on a two-dimensional unit square and Dirichlet boundary conditions, discretized with a uniform rectangular grid, it is straight-forward to show that the finite volume discretization provides an error that approaches zero as $O(h^2)$ in the $L^2(\Omega)$-norm as the grid size h approaches zero (Proposition 3.1, [36]).

For more general meshes and schemes, the requirement is that the mesh should be admissible, meaning that the union of all control volumes should cover the domain Ω, have common edges and not be overlapping. Then, existence and convergence of a linear elliptic model equation can still be shown. Hence, finite volume methods is a robust method as it handles more general domains and meshes. Error estimates in the form $O(h)$, where h is now a measure of the maximum diameter of the control volumes, can be shown (Theorem 3.3, [36]).

Showing convergence rates for non-linear coupled system of equations is not straightforward. In general, one can show existence of a unique solution and convergence under some requirements and we refer to Eymard et al [36] for further reading. A convergence of $O(h^2)$ is expected for uniform, rectangular grids on linear problems, but the model equations in Section 2.2 are non-linear. However, finite volume methods are preferred due to the conservation properties as they provide consistent formulations. Convergence of the discretized scheme can still be indicated by comparing numerical solutions on increasingly finer grids.

5.3 Time discretization

Up to now we have discussed spatial discretization, and we assume now that our model equations are discretized in space such that time discretization of the general system of equations

$$\frac{d}{dt}\mathbf{u} = \mathbf{S}(\mathbf{u}), \tag{5.5}$$

can be considered. Here $\mathbf{S}$ is some vector function obtained through the spatial discretization and $\mathbf{u}$ is a vector containing the values of u at the prescribed grid. Due to the non-linearities in the model equations, $\mathbf{S}$ will in general be non-linear. To perform time integration, the time variable t is divided into time steps denoted t^n. In general, the time step length $\Delta t^{n+1} = t^{n+1} - t^n$ can vary, for instance in combination with an error estimate creating an adaptive time stepping.

We separate between explicit and implicit time stepping and present them through forward Euler and backward Euler. Forward Euler is an explicit time stepping scheme and discretizes the above equation through

$$\frac{\mathbf{u}^{n+1}-\mathbf{u}^n}{\Delta t^{n+1}} = \mathbf{S}(\mathbf{u}^n),$$

where $\mathbf{u}^n$ contains the values of $\mathbf{u}$ at present time step t^n and are hence known, while $\mathbf{u}^{n+1}$ contains the values of $\mathbf{u}$ at the next time step and are unknown. The above equation can easily be solved for $\mathbf{u}^{n+1}$, giving an explicit expression for the solution at the next time step. Backward Euler uses the unknown $\mathbf{u}^{n+1}$ on the right-hand side, hence

$$\frac{\mathbf{u}^{n+1}-\mathbf{u}^n}{\Delta t^{n+1}} = \mathbf{S}(\mathbf{u}^{n+1}).$$

This means that an expression for $\mathbf{u}^{n+1}$ cannot in general be obtained due to the non-linearities in $\mathbf{S}$. Hence, $\mathbf{u}^{n+1}$ is known implicitly through the above relation, and iterative schemes are needed to find $\mathbf{u}^{n+1}$.

The stability of these two methods can be estimated through A-stability [53]. When $\mathbf{S}$ is differentiable, the Jacobian matrix $\mathbf{J}$ exists and has components $\frac{\partial S_i}{\partial u_j}$. The forward Euler method is A-stable if

$$\rho(\mathbf{I}+\Delta t^{n+1}\mathbf{J}) < 1,$$

while the backward Euler method is A-stable when

$$\rho((\mathbf{I}-\Delta t^{n+1}\mathbf{J})^{-1}) < 1.$$

The notation $\rho(\mathbf{B})$ means the spectral radius of the matrix $\mathbf{B}$ and is given as the maximum eigenvalue. In general, backward Euler will have a larger stability region than forward Euler. The backward Euler method is normally applied for stiff model problems, but has the disadvantage of introducing more smearing and each time step requires more computational effort. Forward Euler is faster, but typically introduces extra constraints on the time step.

In Papers A and B the model equations were time discretized using MATLAB's built-in ODE15s [83]. ODE15s has adaptive time stepping based on backward differentiation formulas, hence it is an implicit scheme and suitable for stiff problems. In Paper C, the model equations were decoupled and time stepped using a combination of backward Euler and forward Euler. Paper F utilizes forward Euler.

5.4 Newton's method

When the resulting discretized system of equations is non-linear, iterative methods are needed to solve it. We consider the non-linear vector equation

$$\mathbf{G}(\mathbf{x}) = \mathbf{0},$$

where $\mathbf{G}$ is an n-dimensional differentiable vector function and $\mathbf{x}$ is the n-dimensional unknown. To solve this system of equations, Newton's method is applied. Newton's method relies on the iteration

$$\mathbf{x}^{k+1} = \mathbf{x}^k - \mathbf{J}^{-1}(\mathbf{x}^k)\mathbf{G}(\mathbf{x}^k),$$

where $\mathbf{J}$ is the Jacobian matrix of $\mathbf{G}$. The starting point $\mathbf{x}^0$ of the iteration has to be close enough to the correct solution, otherwise the iteration might not converge, or converge to the wrong solution. When used in combination with time stepping, $\mathbf{x}^0$ is typically chosen to be the known values at the previous time step. Since $\mathbf{x}^0$ has to be close to the solution; that is, the unknown values at the next time step, this can result in additional constraints on the time step length. Newton's method has quadratic convergence when it converges [53]. Radu and Pop [79, 80] applied Newton's method for reactive transport using the mass conservative mixed finite element method and could show the quadratic convergence. Although the proof is performed for mixed finite elements, a corresponding proof for finite volumes on the same model equations would be similar.

Chapter 6

Summary and outlook

The research results are contained in six papers that are included in Part II, and we present here a summary and discussion of the papers. Papers A and B involve natural convection, where Paper A focuses more on the theoretical background for natural convection, while Paper B relates the convection to a geothermal setting. Papers C, D, E and F concern reactive transport. Paper C can be read as a motivation for the following pore scale models that are formulated and upscaled in Papers D, E and F. Part I of this thesis ends with some conclusive remarks and outlook.

6.1 Summary of papers

Paper A: *Linear and nonlinear convection in porous media between coaxial cylinders*

In this paper we investigate the convection in a porous medium filling an annulus. First the linear case is investigated and a linear stability analysis is performed on the model equations to find criteria for the onset of convection and the expected convection pattern at onset. Two different cases are considered: one where the sidewalls are insulated and one where the sidewalls are perfectly heat conducting. The setting is motivated mainly by the papers of Zebib [106], who considered an insulated cylinder; of Haugen and Tyvand [44], who analyzed an heat conducting cylinder; and of Bau and Torrance [14], who among other things investigated an annulus with insulated sidewalls. Hence, the linear stability analysis on the annulus with insulated sidewalls had already been considered, but our research reveals more detailed mode maps, and we include some other sizes of the annular cylinder. The case with an annular cylinder and heat conducting sidewalls have not been analyzed before.

The linear stability analysis results in critical Rayleigh numbers and mode maps as a function of the inner and outer radius of the annulus for both cases. Comparing our findings with Zebib [106] and Haugen and Tyvand [44] for small values of the inner cylinder, reveals that our critical Rayleigh numbers converge to the findings of Zebib and Haugen and Tyvand. Using Taylor series expansions, we can also show convergence in terms of the inner radius approaching zero. A recent paper by Kang et al [52] uses linear stability analysis to investigate the Coriolis effect in a viscoelastic fluid saturating a porous medium filling a rotating annulus. By introducing the non-dimensional Taylor number, which quantifies the importance of centrifugal forces, they find critical Rayleigh numbers with corresponding mode maps. They show that as the

Taylor number approaches zero, their findings reduce to the same results as in Paper A.

Using pseudospectral methods we implement the non-linear model equations using an annulus as domain and apply the same type of boundary conditions as in the stability analysis. This way, the non-linear time dependent regime can be investigated to see whether the linear and non-linear regimes show large deviations at the onset of convection. By varying the Rayleigh number, good correspondence between the linear and non-linear regimes are found for low Rayleigh numbers: When the Rayleigh number is lower than the critical, the simulations reveal no convection, while increasing the Rayleigh number to be slightly larger than the critical gives convection and the convection mode is the one predicted by the linear stability analysis. This result is important in two ways: Firstly, it shows that the linear stability analysis is capable of predicting the correct critical Rayleigh numbers and convection modes. Hence, the error made in the linearization of the model equations is not large. Secondly, this means that since the non-linear regime will give the same convection mode as the linear analysis, one can use the linear results as a benchmark for numerical implementations.

Using the implementation of the non-linear regime of the convection problem can be further investigated. By increasing the Rayleigh number even further, some convection modes are found to not be stable with respect to perturbation, and some convection modes not predicted by the linear analysis appear. This shows that the non-linear regime deviates from the linear as the Rayleigh number increases: Larger Rayleigh numbers corresponds to stronger convection, hence the perturbed quantities, herein the perturbed velocity, are not small anymore, causing the error made in the linearization of the convective term to grow. Some overlapping stability regimes are found: For a given size of the domain and Rayleigh number slightly larger than the critical, two stable convective modes are found.

The linear stability analysis proves to be an important tool for analyzing natural convection problems in a porous medium. The analysis can give information about when convection appears and how the convection currents will distribute. However, the linear analysis has some drawbacks: It is clear that the non-linear regime deviates from the linear for larger Rayleigh numbers, which is as expected. Also, to perform the linear stability analysis, one relies on solving the linearized system of equations together with the boundary conditions. This is possible using separation of variables, but the assumption of separating the variables puts some restriction on possible solutions. Even so, using more advanced or realistic boundary conditions impedes finding an analytical solution, causing the linear analysis to be unsuccessful. In this case, one has to rely on numerical methods to investigate the natural convection, which was our motivation behind Paper B.

Paper B: *Influence of natural convection in a porous medium when producing from borehole heat exchangers*

In this paper we develop the pseudospectral solver from Paper A to cover a case more realistic for geothermal energy extraction in order to say something about the effect of natural convection on a borehole heat exchanger (BHE). Borehole heat exchangers use a closed loop of pipes to extract heat and are utilized for direct heating of buildings [35]. A domain containing a three-layer porous medium and the borehole is considered.

The borehole contains a fluid that is circulated inside the borehole; where cold fluid is pumped down in an outer pipe and warmer fluid up the inner pipe. Only the outer pipe in the domain is included as this is where the heat exchange with the subsurface occurs. The geothermal reservoir is included as a three-layer medium where the middle layer is permeable and saturated with fluid. The top and bottom layers are not saturated with fluid and act as heat reservoirs and receivers for the middle layer.

The simulations are initialized with a stationary conductive heat transfer with no fluid flow. Advective groundwater flow is known to have a large impact on borehole heat exchangers when present [26, 31, 35], but to isolate the effect of natural convection, any background advective flow is neglected. Throughout the simulations the borehole is continuously filled with cold fluid which then receive heat from the warmer subsurface. The amount of heat produced by the borehole is calculated. The heat flow across the borehole wall triggers a horizontal temperature difference in the subsurface, which is known to cause convection when the porous medium is permeable [91]. By varying the Rayleigh number we can control how strong the natural convection is and hence investigate the effect on the heat production. A similar problem was studied by Zhao et al [107]: They used experiments and simulations to study the heat transfer around a BHE in saturated soil. Natural convection was studied, although from a different perspective than in our work. They concluded that borehole temperature, initial ground temperature and flow rate in the porous medium affect the heat transfer into the BHE.

For the spatial discretization the pseudospectral solver from Paper A is developed. However, the domain in the present paper is more complex, creating some challenges. The porous medium contains three layers where physical quantities as the heat conductivity vary between the layers, and where different model equations in the layers as there is no fluid in the top and bottom layers. Also, the BHE is included explicitly, although in a simplified version. The presence of the borehole also causes the domain to no longer be cylindrical, which is challenging for the discretization with pseudospectral methods. These difficulties are handled by combining pseudospectral with domain decomposition, treating the borehole and each layer of the porous medium as separate domains. The domains are glued together by requiring continuity of variables and fluxes across the interfaces. Due to the discontinuity in model parameters, we cannot expect the solver to give more than second order convergence. However, despite only having second order convergence, the errors in the simulations are found to still be small.

By varying the initial temperature conditions and the Rayleigh number and calculating the amount of heat produced in the production period, the effect of natural convection is estimated. We find that in the cases with large variations in the initial subsurface temperature and a borehole temperature close to the coldest subsurface temperature, the natural convection will have a negative effect on the heat production. The cooling of the subsurface near the well causes the colder, upperlying groundwater to flows towards the borehole, while the warmer groundwater lying deeper in the reservoir flows away. Hence, less heat is produced by the borehole. However, using colder fluid in the borehole will provide a positive effect on the convection: The convection currents still distribute such that the upperlying fluid flows towards the borehole, but due to the large temperature difference between subsurface and borehole, the effect of more mixing in the fluid becomes more important. This draws us to the conclusion that the

effect of natural convection depends on the difference between borehole temperature and subsurface temperature variations.

Our investigation on the effect of natural convection has some weaknesses. Although a more complicated porous media model is considered and the borehole is explicitly included, the model is still a very simplified one and does not contain features as permeability heterogeneities and isotropy, effect of temperature dependent viscosity, more details on the heat transfer inside the borehole, to mention some. Despite the shortcomings, the goal of the model was to isolate and describe the natural convection induced by a BHE, which the model is adequate for. The simulations show how the effect of convection could be in an idealized, but relevant, scenario, and clearly shows that natural convection could have a large impact on the production from BHEs.

Paper C: *An Approach for Investigation of Geochemical Rock-Fluid Interactions*

Paper C introduces a Darcy-scale model for coupled fluid flow, heat transport and solute transport with chemical reactions. Motivated by the interaction between fluid flow and mineral precipitation and dissolution in a geothermal reservoir, we formulate a coupled model where dissolution and precipitation of calcite and anhydrite can cause porosity changes. Our goal is to investigate how the porosity changes lead to variations in permeability and hence affect the fluid flow. As the minerals have solubilities depending on temperature, this dependence introduces more couplings.

We consider a simplified setup as the goal is only to illustrate the approach and highlight the couplings, hence the geochemical model is not complete as it only contains 7 active ions. This is a simplifications as the activities, which are needed for solubility calculations, can be affected by ions not participating in the reactions. A simple dependence of how the permeability varies with porosity is chosen. As discussed in Section 2.2.1, the permeability depends on the in-situ pore structure, which normally is not known in a geothermal reservoir, hence we are left with simplified models as the Kozeny-Carman relation. The Kozeny-Carman relation for permeability is applied, and assumptions on how the reactive surface affects the reaction rates given in Section 2.2.2 is made. Our setup is loosely inspired by Kühn et al [57] who considered porosity changes due to calcite and anhydrite precipitation and dissolution in a geothermal reservoir in Stralsund, Germany.

To describe how the interaction between flow and permeability changes can be, discretizing the model equations in a consistent way is important. Hence we choose finite volumes as discretization method. Finite volumes are conservative and utilize expressions for the fluxes of the conserved variables, which is an advantage as the fluid flow is complex to model in this case. Other codes modeling this type of coupled problem exist; Cheng and Yeh [25] developed the finite element method code 3DHYDROGEOCHEM, while Clauser [28] introduced SHEMAT and Xu et al [104, 105] made TOUGHREACT applying finite differences. However, finite elements and finite differences are in general not conservative.

The domain is two-dimensional with one injection well and one production well. The injection well injects fluid at a constant rate at a temperature lower than the initial temperature in the reservoir as in the case with heat production from a geothermal reservoir. To incorporate the two wells consistently with the conservative schemes a

discretization method similar as one presented in [36] is applied for the wells. In this discretization the wells are introduced as internal boundaries in the control volume they are located in, using the unknown flux from the well as a variable.

Despite the simplifications in the geochemical model and the permeability dependence, our findings in how the permeability changes due to the chemical reaction is in good correspondence with the findings of Kühn et al [57]. This preliminary study was meant as a starting point for further development in geochemical modeling to account for rock-fluid interactions, and to possibly incorporate this type of interactions in MRST [61], which is a open source code based on finite volumes on unstructured grids and can include fractures [85]. However, this study also made us aware of the need to understand couplings between flow, heat transport and reactive transport at the pore scale [15, 34]. As how the permeability in Darcy's law evolves due to the chemical reactions is of high importance in this type of models, we decided to prioritize better understanding of the pore scale processes. Hence, the continued focus turned out to be on upscaling of pore scale models, which is treated in Papers D, E and F.

Paper D: *A model for non-isothermal flow and mineral precipitation and dissolution in a thin strip*

In this paper we follow the ideas from Paper C to better incorporate pore scale effects in the model equations. The strategy is to start with a pore scale model and upscale through formal homogenization to Darcy scale, and hence obtain a better understanding of how the coupled fluid flow, heat flow and reactive transport interact at Darcy scale. As formulating a pore scale model requires an explicit presentation of the pore scale geometry, we start with a simple thin strip, representing a single pore channel.

The pore scale model consists of the void space, which is filled with fluid, the grain space consisting of minerals and the boundary between them. The possible changes in geometry are included by letting the boundary between void and grain space to move, hence causing the void and grain space to develop dynamically with time. For the thin strip case, this development is expressed through the grain width $d(x,t)$. The conservation equations for mass, solute and heat are expressed in their respective spaces and with a Rankine-Hugoniot jump condition across the moving boundary, as described in Section 2.1. The model is inspired by van Noorden [94] who considered a pore scale model of a thin strip with changing aperture, but without temperature dependence. Including a moving boundary is challenging, and there are more research available for the pore scale models in the fixed geometry case, such as [92, 97].

Although the pore scale model of a thin strip is a simplified presentation of pore geometry, the upscaling process can still give important information about the coupling between the various processes at Darcy scale. Also, if the thin strip is interpreted as a fracture, the upscaled equations could be included in a fracture network model [3, 39]. These types of models are typically applied for highly fractured granite reservoirs when the matrix has low permeability outside the fractures.

The present work is similar to the paper by van Noorden [94], but including the temperature dependence entails several new elements and complications to the model and the upscaling of it. Including the energy conservation equation in the void space is not an impeding element as this model equation is very similar as the ion conserva-

tion equation. However, as the variations in the grain temperature must be included, there is now a model equation also in the grain space, unlike the model by van Noorden that consists of model equations only in the void space. The presence of a model equation in the grain space affects the choice of boundary conditions for energy at the moving boundary. Upscaling the two coupled energy conservation equations requires new strategies for how to handle such a system. Further, as the fluid density is varying, the mass conservation equation is different and has to be considered in another way than by van Noorden, who upscaled the simplified mass conservation equation by incorporating it into the momentum equation.

The upscaling process results in five unknowns; ion concentration, transmissivity, pressure, temperature and grain width, and five coupled equations to describe them. The five equations express ion conservation, mass conservation, fluid flow, energy conservation and how the grain width depends on the reaction rates; all one-dimensional. Note that even though the pore scale model contains two energy conservation equations and two temperature variables, this system reduces as the lowest order asymptotic expansion term of the fluid and grain temperatures turn out to be equal and the two conservation equations combine into one. The fluid flow equation can be interpreted as Darcy's law with a cubic relationship between the volume flux and the aperture, as known from flow through fractures [103]. The three conservation equations follow the same system with weighting the conserved quantity over void space and the grain space, using $(1-2d_0)$ (the width of the void space) and $2d_0$ (the total width of the grain space) as weights. This weighting is similar to porosity-weighting if the void space aperture is interpreted as the porosity ϕ and the grain part as $(1-\phi)$. As the grain width $d_0(x,t)$ changes with time according to the mineral precipitation and dissolution rates, the chemical reactions and varying aperture are incorporated into the upscaled model equations. The upscaled equations are all one-dimensional, only keeping the direction along the strip, while the transversal direction has been averaged away in the upscaling procedure. This shows, as expected, that the most important features of the model equations are what happens along the thin strip. The upscaled model contains a discontinuous reaction rate and Agosti et al [4, 5] showed well-posedness for a similar model and introduced a numerical strategy for implementation of such a reaction rate.

The resulting effective model shows how fluid flow, reactive transport and heat transfer are coupled when taking into account the changes in geometry. This type of pore scale model with a free boundary has not been considered in an upscaling process earlier. A simple geometry has been used, but is still relevant for flow through a single channel, possibly part of a pore or fracture network. A natural extension of this work would hence be considering a more complex geometry, which is investigated in Paper E.

For completeness, we mention that a more detailed version of the paper with extensive explanation of the upscaling process can be found in the technical report [21].

Paper E: *Upscaling of non-isothermal reactive porous media flow with changing porosity*

One limitation of the model in Paper D is the simplified geometry, as the choice of

thin strip introduces a constraint in how applicable and descriptive the upscaled model can be. Hence, in Paper E we consider a more general geometry with solid grains distributed periodically in the medium. These grains consist of some non-reactive solid in the center and are covered by a layer of some mineral that can dissolve or precipitate. The assumption of periodic distribution of the grains is made in order to perform the homogenization and derive Darcy-scale equations.

We consider the same pore scale model equations for ion conservation, mass conservation, momentum conservation and energy conservation as in Paper D, but apply a level set formulation to describe the free boundary. The Rankine-Hugoniot boundary conditions at the free boundary are the same as in Paper D, but the unit normal vector at the free boundary is defined through the gradient of the level set function. The model formulation is similar to van Noorden [93], who considered a pore scale model with the same periodic structure of the porous medium and included the free boundary with the level set formulation. The model of van Noorden considered reactive transport at isothermal conditions. As in Paper D, we incorporate temperature variations by including two energy conservation equations and letting fluid density and viscosity as well as the reaction rates and solubility product depend on temperature.

Using the level set formulation to describe the developing geometry gives a flexible formulation of the model geometry as it is not necessary to assume certain shapes or use explicit functions to describe the shape of the boundary, neither initially nor at later times. Instead, the boundary is given implicitly as where the level set function $S^\varepsilon(x,t)$ is equal to zero. This implicit formulation causes some challenges in the upscaling, but is handled through parametrization representations and Taylor expanding the level set function. As the considered pore geometry is given in a general way, some cautionary steps must be made before the upscaling procedure starts. Similar precautions are also done by van Noorden [93]. As in the thin strip model in Paper D, including the energy conservation in the grain space introduces difficulties and requires special care in the upscaling procedure. We prove an extension of a lemma from [93] to deal with the energy conservation equations. As the mass conservation equation is more complex due to varying fluid density, this equation must be dealt with independently as in Paper D.

The upscaling process results in five unknowns; ion concentration, transmissivity, pressure, temperature and the level set function, and five coupled equations to desbrice them. The five equations express ion conservation, mass conservation, fluid flow, energy conservation and how the level set function develops with the reaction rates, all valid at the Darcy scale. The equations are still two-dimensional, but only the level set function contains explicit dependence on the microscale variable. As in Paper D, the upscaled equations contain terms with porosity-weighted averages of the conserved quantities. The porosity is defined through the level set function, which varies with the reaction rates. The volume flux is given by Darcy's law, where the permeability is defined through a tensor with components arising from a cell problem on the microscale. Hence, to find the permeability one still needs to take the microscale into account, but the two scales are decoupled: For each macroscopic point (that is, for each REV), one needs to solve the microscale cell problem and use the calculated permeability to solve the macroscopic flow problem. From a computational point of view, this decoupling is important as it is no longer necessary to solve the full problem on a fine grid. Redeker and Eck [82] proposed a fast adaptive solution strategy for a model with two-scale

dependence through a similar separation of the micro- and macroscale as formulated here.

The upscaled solute diffusion and heat conduction also introduce tensors with components coming from cell problems. The purpose of the tensors is to account for the permeability, diffusion and conduction potentially being anisotropic due to the shape of the grains. If the grains in Figure 2.2 are, e.g., elliptic, the fluxes in the direction of the semi-major axis are expected to be larger than in the transversal direction. The well-used geothermal simulator TOUGHREACT [105] utilizes only scalar diffusion, conduction and permeability, which could be a limitation. Simulations on upscaled models formulated through cell problems have been implemented: We mention that Frank et al [40, 41] performed some interesting simulations using mixed finite elements for a Stokes-Nernst-Planck-Poissson system using various shapes of the grains and considered circular grains in the case of varying porosity, and other models incorporating changing geometry and depence on cell problems have been implemented as well [81, 93].

As with Paper D, the resulting effective model shows how fluid flow, reactive transport and heat transfer are coupled in the presence of rock-fluid interactions. Through the level set formulation a more general porous medium than the channel can be considered, but the upscaling process relies on the assumption of periodicity in the grain distribution. The upscaling results are only formal as no two-scale convergence is proved. The upscaled model still provide important information about how the various processes are coupled and how the flow and diffusion are affected by the interaction between the processes.

Paper F: *Upscaling of non-isothermal reactive porous media flow under dominant Péclet number: the effect of changing porosity*

In this paper we return to homogenization of a thin strip, but include dominant convection by applying a large Péclet number in the model equations. The formulation of the geometry and the model equations is the same as in Paper D, except that the Péclet number is assumed to be of order $1/\varepsilon$. This means that the convection is dominating, as the solute diffusion and heat conduction in the dimensionless model is now multiplied with a factor ε, indicating these processes being less important. This change in model equations is made as geothermal problems typically are convection dominated due to the large injection rates of fluid into the subsurface. Model equations honoring the dominating convection is expected to give a better description of the transport processes after upscaling to Darcy scale.

Homogenization procedures for a thin strip including dominant convection has been, among others, considered earlier by Kumar et al [59], by Mikelić et al [65] and by Mikelić and Rosier [66]. The two latter assume a prescribed velocity and only upscale the ion conservation equation, while Kumar et al also consider the interaction effects between flow and changing aperture of the strip. Kumar et al [59] consider an isothermal model where the fluid density is constant and they also assume that the chemical reaction does not include any volume change, hence simplifying the boundary condition for the flow rate at the internal boundary. As in Papers D and E, including temperature variations introduces new challenges through dealing with the energy con-

servation in the grains and the more complicated mass conservation equation, but also through the model equations being more coupled. Also, due to the dominating convection the upscaling procedure is more laborious; both for the energy equations and for the other model equations.

A straight-forward upscaling approach as in Paper D, would lead to an hyperbolic model. This is because the diffusive and conductive terms are multiplied with a factor ε, hence these terms are one order smaller than in Paper D. A hyperbolic model would maybe not be a good enough description of the Darcy scale processes, hence an alternative approach is to keep terms of the second lowest order as well [59]. Keeping terms of $O(\varepsilon)$ in the upscaling process means that the diffusion is honored, while still preserving the dominating convection. This will introduce Taylor dispersion in the Darcy-scale equations [87].

While we in Paper D (and Paper E) found Darcy scale equations using only the lowest order approximations in the asymptotic expansions, the first order correction terms are now kept. In a thin strip, the lowest order approximations are independent of the transversal variable y, but this is general not the case with the first order correction terms. As we seek Darcy scale equations that are one-dimensional, effective variables that take into account the vertical average of the first order correction terms are introduced. This procedure requires some extra care in the non-linear convective terms, which in the upscaling process gives rise to the dispersive terms. As the transversal direction is averaged over, the resulting model equations are one-dimensional.

In Paper D we showed that the lowest order expansions of the fluid and grain temperatures were equal, hence the Darcy-scale model equations only contained one temperature variable. As first order correction terms are included and the vertical averages of these are in general not equal, the Darcy-scale model must include two temperature variables, and also one extra equation to describe the energy conservation properly. Hence, the upscaled system of equations contains six unknowns and six coupled equations, all containing some corrective terms compared to the model found in Paper D. Darcy's law contains non-linear terms due to the viscosity depending on temperature: The extra term can be interpreted as a Forchheimer-term [50], which is expected to appear when inertial effects are important. The mass conservation equation and ion conservation equation both include dispersion terms and correction terms due to the varying aperture. The equation connecting the grain width with reaction rates include these correction terms and also derivatives of the reaction rates.

As already mentioned, fluid and grain temperature at the Darcy scale are in general not equal anymore, hence the energy conservation equation must be accompanied by an extra equation describing how the two temperatures deviate. Note that the more common modeling choice is to consider one conservation equation for energy in the grain, and one equation for fluid, and coupling these with some transfer term [78]. Hence, our description can be considered as an alternative, but still valid formulation. The two equations describing the temperature development contain correction terms due to the changing geometry, and the energy conservation equation has a Taylor dispersion term arising from the fluid convection.

As the six resulting model equations are quite complex, we implement the system of equations along with three simplified versions of the model to test two scenarios. In the first scenario, the upscaled Péclet model is compared with one model containing diffusion but no dispersion, and one hyperbolic model. In the other scenario, we

compare the Péclet model with a model using a fixed aperture of the thin strip, but otherwise including dispersive terms. For both scenarios, the idea is to investigate when simpler versions of the upscaled model will give effectively the same results, and when the models deviate, hence giving some notion of when the upscaled Péclet model can be replaced with a simplified version. Applying finite volumes to discretize the model equations (which is in fact equivalent to finite differences due to the cell-centered equispaced grid) and forward Euler in time, we vary the input parameters and the external boundary conditions to investigate any potential differences between the models. In the first scenario, the models produce quite different results for larger values of ε; that is, in the range $0.05 - 0.01$. Decreasing ε will provide the models to produce more similar results; this is reasonable as the Péclet model, and also the diffusion model, reduce to the hyperbolic model as ε approaches zero. In the second scenario the variable and the fixed geometry models deviate for small values of the (dimensionless) mineral density ρ; that is, in the range $1 - 5$. Increasing the mineral density means that the precipitated mineral layer will have a smaller volume, hence the changes in aperture of the strip will be smaller. Using a value of ρ around 10 gives small differences between the two models.

Through the upscaling of the pore scale equations, we can show how fluid flow, reactive transport and heat transfer are coupled when taking into account the changes in geometry. Including the dominating convection, which is typical for geothermal plants using large injection rates, shows how the Taylor dispersion occur. As we keep track of lower order terms, several new terms compared to Paper D appear in the upscaled model. These terms are second order effects from the varying aperture and from the temperature dependent viscosity and density. By implementing the upscaled equations and comparing the findings with simpler models, we can indicate when the second order terms are important and when they can be neglected. Comparing the upscaled model with one assuming a fixed geometry, shows when the varying aperture is important to include and when it can be neglected.

6.2 Conclusion and outlook

This thesis concerns mathematical modeling regarding heat transfer processes in the context of geothermal energy extraction. The studied issues have involved natural convection, which may have an affect on the heat production for non-injecting borehole heat exchangers, and the coupling between heat transfer and reactive transport with porosity changes, which is relevant for energy production systems utilizing injection and production wells. To analyze these issues we have applied linear stability analysis, numerical simulations and upscaling procedures.

By investigating the theoretical framework for onset of natural convection in a porous medium filling an annulus by a linear stability analysis, we have gained better understanding of how the natural convection currents behave in an idealized setting. The findings of this theoretical analysis was used as a benchmark for a high-order numerical simulator, which was then applied to investigate the non-linear regime of natural convection. The simulator was later developed to consider a configuration more

realistic for geothermal energy production of a non-injecting borehole and the effect of natural convection on a producing borehole was quantified for some cases. This investigation have shown that natural convection may have either a positive or negative effect on the heat production, depending on the flow properties of the subsurface and on the temperature difference between the borehole and the subsurface.

As the natural convection may have an effect on the production from borehole heat exchangers, continued analysis of this problem setting is a topic that deserves future attention. The model we applied was idealized and did not include features as temperature dependent viscosity and heterogeneities in the porous medium, and the borehole was incorporated in a simplified manner. Also, we assumed there was no background advective groundwater flow present. Extending the simulator to include the presence of such components would have been useful to better understand the interaction with natural convection and heat production better. Especially, considering a case with a borehole and surrounding porous medium from a real-life scenario would be interesting and could also contribute to validate our findings through field experiments.

Considering a geothermal system including injection and production wells introduces new challenges through potential porosity changes due to mineral precipitation and dissolution. The presence and effect of these chemical reactions have already been described through numerous field studies and numerical studies, and the work presented in this thesis contributes to the modeling of the interaction between heat transfer, solute transport and permeability changes due to porosity changes. As pore scale effects are highly important in this setting, we have performed upscaling through homogenization from pore scale to Darcy scale in three different scenarios to investigate the coupling and effective behavior of the relevant physical processes. Two of the models concerned a single pore channel; either with convection dominating the diffusion or with convection and diffusion being at the same time scale, while the third model investigated convection and diffusion at the same order in a periodic porous medium. Our findings quantifies the average behavior of the pore scale effects under the different assumptions.

To continue the analysis of the reactive transport model and the pore scale effects, it would be interesting to include the findings from the upscaled system of equations in an existing simulator. The thin strip model can be useful when incorporated in a pore (or fracture) network model, and in this context including mechanical effects would be an appropriate extension as opening of fractures through pressure stimulation is a highly relevant topic in geothermal energy extraction for low-permeable rocks. The upscaled model with a periodic porous medium is more applicable when concerning flow through porous media. We have not attempted to implement the periodic model, but doing so would give more insight to the coupling of the physical processes and the importance of the pore scale effects. For the periodic porous medium we have only considered the case when convection and diffusion is at the same time scale and a possible extension would be to consider when convection is dominant also for this geometry. However, including dominant convection and second order effects in the thin strip case required intricate calculations for the second order terms, which are not expected to be easier in the periodic porous medium. The results from the upscaling procedure have not been validated through two-scale convergence proofs or numerical simulations. Implementing the pore scale equations and comparing with the upscaled equations would substantiate the validity of the upscaled models.

Bibliography

[1] AAVATSMARK, I. An introduction to multipoint flux approximations for quadrilateral grids. *Computational Geosciences 6*, 3-4 (2002), 405–432.

[2] ACERBI, E., CHIADÒPIAT, V., DAL MASO, G., AND PERCIVALE, D. An extension theorem from connected sets, and homogenization in general periodic domains. *Nonlinear Analysis: Theory, Methods & Applications 18*, 5 (1992), 481–496.

[3] ADLER, P. M., AND THOVERT, J.-F. *Fractures and fracture networks*, vol. 15. Springer Science & Business Media, 1999.

[4] AGOSTI, A., FORMAGGIA, L., GIOVANARDI, B., AND SCOTTI, A. MOX-Report No. 08/2015, Numerical simulation of geochemical compaction with discontinuous reactions. Tech. rep., MOX, Politecnico di Milano, 2015.

[5] AGOSTI, A., FORMAGGIA, L., AND SCOTTI, A. Analysis of a model for precipitation and dissolution coupled with a Darcy flux. *Journal of Mathematical Analysis and Applications* (2015), doi: http://dx.doi.org/10.1016/j.jmaa.2015.06.003.

[6] ALLAIRE, G. Homogenization and two-scale convergence. *SIAM Journal on Mathematical Analysis 23*, 6 (1992), 1482–1518.

[7] ALLAIRE, G., BRIZZI, R., MIKELIĆ, A., AND PIATNITSKI, A. Two-scale expansion with drift approach to the Taylor dispersion for reactive transport through porous media. *Chemical Engineering Science 65*, 7 (2010), 2292–2300.

[8] ALLAIRE, G., AND HABIBI, Z. Homogenization of a conductive, convective, and radiative heat transfer problem in a heterogeneous domain. *SIAM Journal on Mathematical Analysis 45*, 3 (2013), 1136–1178.

[9] ALLAIRE, G., AND HUTRIDURGA, H. Homogenization of reactive flows in porous media and competition between bulk and surface diffusion. *IMA Journal of Applied Mathematics 77*, 6 (2012), 788–815.

[10] ALLAIRE, G., AND HUTRIDURGA, H. Upscaling nonlinear adsorption in periodic porous media - homogenization approach. *arXiv preprint arXiv:1412.8301* (2014).

[11] ALLAIRE, G., MIKELIC, A., AND PIATNITSKI, A. Homogenization approach to the dispersion theory for reactive transport through porous media. *SIAM Journal on Mathematical Analysis 42*, 1 (2010), 125–144.

[12] BÄCHLER, D., KOHL, T., AND RYBACH, L. Impact of graben-parallel faults on hydrothermal convection–Rhine Graben case study. *Physics and Chemistry of the Earth, Parts A/B/C 28*, 9-11 (2003), 431–441.

[13] BATCHELOR, G. K. *An introduction to fluid dynamics*. Cambridge university press, 2000.

[14] BAU, H. H., AND TORRANCE, K. E. Onset of convection in a permeable medium between vertical coaxial cylinders. *Physics of Fluids 24*, 3 (1981), 382–385.

[15] BEAR, J. *Dynamics of fluids in porous media*. Dover Publications, 1988.

[16] BECK, J. L. Convection in a box of porous material saturated with fluid. *Physics of Fluids 15*, 8 (1972), 1377–1383.

[17] BEJAN, A., AND KRAUS, A. D. *Heat Transfer handbook*. John Wiley and Sons, 2003.

[18] BERRUT, J.-P., AND TREFETHEN, L. N. Barycentric Lagrange interpolation. *Siam Review 46*, 3 (2004), 501–517.

[19] BOYD, J. P. *Chebyshev and Fourier spectral methods*. Dover Pubns, 2001.

[20] BRINGEDAL, C. Linear and nonlinear convection in porous media between coaxial cylinders. Master thesis, University of Bergen, 2011.

[21] BRINGEDAL, C., BERRE, I., RADU, F. A., AND POP, I. S. Pore scale model for non-isothermal flow and mineral precipitation and dissolution in a thin strip. CASA Report 14-24, 2014.

[22] BUNDSCHUH, J., AND ZILBERBRAND, M. *Geochemical Modeling of Groundwater, Vadose and Geothermal Systems*. CRC Press, 2011.

[23] CHANG, R., AND GOLDSBY, K. A. *General Chemistry, The Essential Concepts*. McGraw-Hill, 2014.

[24] CHAPMAN, D. S., AND RYBACH, L. Heat flow anomalies and their interpretation. *Journal of geodynamics 4*, 1-4 (1985), 3–37.

[25] CHENG, H.-P., AND YEH, G.-T. Development and demonstrative application of a 3-D numerical model of subsurface flow, heat transfer, and reactive chemical transport: 3DHYDROGEOCHEM. *Journal of contaminant hydrology 34*, 1 (1998), 47–83.

[26] CHIASSON, A. D., REES, S. J., AND SPITLER, J. D. A preliminary assessment of the effects of groundwater flow on closed-loop ground source heat pump systems. Tech. rep., Oklahoma State Univ., Stillwater, OK (US), 2000.

[27] CIORANESCU, D., AND DONATO, P. *An introduction to homogenization*, vol. 8. Oxford University Press Oxford, 1999.

[28] CLAUSER, C. *Numerical simulation of reactive flow in hot aquifers: SHEMAT and processing SHEMAT*. Springer Science & Business Media, 2003.

[29] CLAUSER, C., AND VILLINGER, H. Analysis of conductive and convective heat transfer in a sedimentary basin, demonstrated for the Rheingraben. *Geophysical Journal International 100*, 3 (1990), 393–414.

[30] CUSHMAN, J. H., BENNETHUM, L. S., AND HU, B. X. A primer on upscaling tools for porous media. *Advances in Water Resources 25*, 8 (2002), 1043–1067.

[31] DIAO, N., LI, Q., AND FANG, Z. Heat transfer in ground heat exchangers with groundwater advection. *International Journal of Thermal Sciences 43*, 12 (2004), 1203–1211.

[32] DONATO, P., AND MOSCARIELLO, G. On the homogenization of some nonlinear problems in perforated domains. *Rendiconti del Seminario Matematico della Università di Padova 84* (1990), 91–108.

[33] DONEA, J., HUERTA, J.-P., AND RODRIGUEZ-FERRAN, A. Arbitrary Lagrangian-Eulerian methods. In *Encyclopedia of Computational Mechanics, Volume 1: Fundamentals*, E. Stein, R. de Borst, and T. J. R. Hughes, Eds. John Wiley and Sons, New York, 2004, pp. 413–437.

[34] EMMANUEL, S., AND AGUE, J. J. Modeling the impact of nano-pores on mineralization in sedimentary rocks. *Water Resources Research 45*, 4 (2009).

[35] ESKILSON, P. *Thermal analysis of heat extraction boreholes*. PhD thesis, Lund University, 1987.

[36] EYMARD, R., GALLOUËT, T., AND HERBIN, R. Finite volume methods. *Handbook of numerical analysis 7* (2000), 713–1018.

[37] FARMER, C. L. Upscaling: a review. *International Journal for Numerical Methods in Fluids 40*, 1-2 (2002), 63–78.

[38] FASANO, A. *Mathematical models of some diffusive processes with free boundaries*. Universidad Austral. Departamento de Matemática, 2005.

[39] FORMAGGIA, L., FUMAGALLI, A., SCOTTI, A., AND RUFFO, P. A reduced model for Darcy's problem in networks of fractures. *ESAIM: Mathematical Modelling and Numerical Analysis 48*, 04 (2014), 1089–1116.

[40] FRANK, F. *Numerical Studies of Models for Elektrokinetic Flow and Charged Solute Transport in Periodic Porous Media*. PhD thesis, Friedrich-Alexander-Universität Erlangen-Nürnberg (FAU), 2013.

[41] FRANK, F., RAY, N., AND KNABNER, P. Numerical investigation of homogenized Stokes–Nernst–Planck–Poisson systems. *Computing and visualization in science 14*, 8 (2011), 385–400.

[42] GOTTLIEB, D., HUSSAINI, M. Y., AND ORSZAG, S. A. Introduction: Theory and applications of spectral methods. In *Spectral Methods for Partial Differential Equations*, R. G. Voigt, D. Gottlieb, and M. Y. Hussaini, Eds. SIAM, 1984.

[43] GOTTLIEB, D., AND ORSZAG, S. A. *Numerical analysis of spectral methods: theory and applications*. Society for Industrial Mathematics, 1977.

[44] HAUGEN, K. B., AND TYVAND, P. A. Onset of thermal convection in a vertical porous cylinder with conducting wall. *Physics of Fluids 15*, 9 (2003), 2661–2667.

[45] HOLM, A., BLODGETT, L., JENNEJOHN, D., AND GAWELL, K. Geothermal energy: International market update. *Geothermal energy association 7* (2010).

[46] HOLMES, M. H. *Introduction to perturbation methods*, vol. 20. Springer Science & Business Media, 2012.

[47] HORNUNG, U. *Homogenization and porous media*, vol. 6. Springer Science & Business Media, 1997.

[48] HORNUNG, U., JÄGER, W., AND MIKELIC, A. *Reactive transport through an array of cells with semi-permeable membranes*. Universität Heidelberg. Interdisziplinäres Zentrum für Wissenschaftliches Rechnen [IWR], 1992.

[49] HORTON, C. W., AND ROGERS, F. T. Convection currents in a porous medium. *Journal of Applied Physics 16*, 6 (1945), 367–370.

[50] IRMAY, S. On the theoretical derivation of Darcy and Forchheimer formulas. *Eos, Transactions American Geophysical Union 39*, 4 (1958), 702–707.

[51] JAVIERRE, E., VUIK, C., VERMOLEN, F. J., AND SEGAL, A. A level set method for three dimensional vector Stefan problems: dissolution of stoichiometric particles in multi-component alloys. *Journal of Computational Physics 224*, 1 (2007), 222–240.

[52] KANG, J., NIU, J., FU, C., AND TAN, W. Coriolis effect on thermal convective instability of viscoelastic fluids in a rotating porous cylindrical annulus. *Transport in porous media 98*, 2 (2013), 349–362.

[53] KINCAID, D. R., AND CHENEY, E. W. *Numerical analysis: mathematics of scientific computing*, vol. 2. American Mathematical Soc., 2002.

[54] KNABNER, P., VAN DUIJN, C. J., AND HENGST, S. An analysis of crystal dissolution fronts in flows through porous media. Part 1: Compatible boundary conditions. *Advances in water resources 18*, 3 (1995), 171–185.

[55] KOHL, T., BÄCHLER, D., AND RYBACH, L. Steps towards a comprehensive thermo-hydraulic analysis of the HDR test site Soultz-sous-Forêts. In *Proceedings World Geothermal Congress* (2000), pp. 2671–2676.

[56] KORSON, L., DROST-HANSEN, W., AND MILLERO, F. J. Viscosity of water at various temperatures. *The Journal of Physical Chemistry 73*, 1 (1969), 34–39.

[57] KÜHN, M., BARTELS, J., AND IFFLAND, J. Predicting reservoir property trends under heat exploitation: interaction between flow, heat transfer, transport, and chemical reactions in a deep aquifer at Stralsund, Germany. *Geothermics 31*, 6 (2002), 725–749.

[58] KUMAR, K., POP, I. S., AND RADU, F. A. Convergence analysis of mixed numerical schemes for reactive flow in a porous medium. *SIAM Journal on Numerical Analysis 51*, 4 (2013), 2283–2308.

[59] KUMAR, K., VAN NOORDEN, T. L., AND POP, I. S. Effective dispersion equations for reactive flows involving free boundaries at the microscale. *Multiscale Modeling & Simulation 9*, 1 (2011), 29–58.

[60] LAPWOOD, E. R. Convection of a fluid in a porous medium. In *Mathematical Proceedings of the Cambridge Philosophical Society* (1948), vol. 44, Cambridge Univ Press, pp. 508–521.

[61] LIE, K.-A., KROGSTAD, S., LIGAARDEN, I. S., NATVIG, J. R., NILSEN, H. M., AND SKAFLESTAD, B. Open-source MATLAB implementation of consistent discretisations on complex grids. *Computational Geosciences 16*, 2 (2012), 297–322.

[62] MARCINIAK-CZOCHRA, A., AND PTASHNYK, M. Derivation of a macroscopic receptor-based model using homogenization techniques. *SIAM Journal on Mathematical Analysis 40*, 1 (2008), 215–237.

[63] MATEK, B. Geothermal power: International market overview. *Geothermal Energy Association Reports [Internet]* (2013).

[64] MEIER, S. Global existence and uniqueness of solutions for a two-scale reaction–diffusion system with evolving pore geometry. *Nonlinear Analysis: Theory, Methods & Applications 71*, 1 (2009), 258–274.

[65] MIKELIĆ, A., DEVIGNE, V., AND VAN DUIJN, C. J. Rigorous upscaling of the reactive flow through a pore, under dominant Péclet and Damköhler numbers. *SIAM journal on mathematical analysis 38*, 4 (2006), 1262–1287.

[66] MIKELIĆ, A., AND ROSIER, C. Rigorous upscaling of the infinite adsorption rate reactive flow under dominant Péclet number through a pore. *ANNALI DELL'UNIVERSITA'DI FERRARA 53*, 2 (2007), 333–359.

[67] MROCZEK, E. K., WHITE, S. P., AND GRAHAM, D. J. Deposition of amorphous silica in porous packed beds - predicting the lifetime of reinjection aquifers. *Geothermics 29*, 6 (2000), 737–757.

[68] MUSUUZA, J. L., ATTINGER, S., AND RADU, F. A. An extended stability criterion for density-driven flows in homogeneous porous media. *Advances in water resources 32*, 6 (2009), 796–808.

[69] MUSUUZA, J. L., RADU, F. A., AND ATTINGER, S. Predicting predominant thermal convection in thermohaline flows in saturated porous media. *Advances in Water Resources 49* (2012), 23–36.

[70] NGUETSENG, G. A general convergence result for a functional related to the theory of homogenization. *SIAM Journal on Mathematical Analysis 20*, 3 (1989), 608–623.

[71] NIELD, D. A., AND BEJAN, A. *Convection in Porous Media*, 4 ed. Springer, 2013.

[72] OSHER, S., AND FEDKIW, R. *Level set methods and dynamic implicit surfaces*, vol. 153. Springer Science & Business Media, 2003.

[73] PAPE, H., CLAUSER, C., IFFLAND, J., KRUG, R., AND WAGNER, R. Anhydrite cementation and compaction in geothermal reservoirs: Interaction of porespace structure with flow, transport, P-T conditions, and chemical reactions. *International Journal of Rock Mechanics and Mining Sciences 42*, 7 (2005), 1056–1069.

[74] PATANKAR, S. *Numerical heat transfer and fluid flow*. McGraw-Hill, 1980.

[75] PETER, M. A. Coupled reaction–diffusion processes inducing an evolution of the microstructure: Analysis and homogenization. *Nonlinear Analysis: Theory, Methods & Applications 70*, 2 (2009), 806–821.

[76] PLUMMER, L. N., PARKHURST, D. L., FLEMMING, G. W., AND DUNKLE, S. A. A computer program incorporating Pitzer's equations for calculation of geochemical reactions in brines, 1988.

[77] PORTIER, S., VUATAZ, F. D., MARTINEZ, A. L. B., AND SIDDIQI, G. Preliminary modelling of the permeability reduction in the injection zone at Berlin geothermal field, El Salvador. In *Proceedings, World Geothermal Congress* (2010).

[78] QUINTARD, M., AND WHITAKER, S. One-and two-equation models for transient diffusion processes in two-phase systems. *Advances in heat transfer 23* (1993), 369–464.

[79] RADU, F. A., AND POP, I. S. Newton method for reactive solute transport with equilibrium sorption in porous media. *Journal of computational and applied mathematics 234*, 7 (2010), 2118–2127.

[80] RADU, F. A., AND POP, I. S. Mixed finite element discretization and Newton iteration for a reactive contaminant transport model with nonequilibrium sorption: convergence analysis and error estimates. *Computational Geosciences 15*, 3 (2011), 431–450.

[81] RAY, N., VAN NOORDEN, T., RADU, F. A., FRIESS, W., AND KNABNER, P. Drug release from collagen matrices including an evolving microstructure. *ZAMM-Journal of Applied Mathematics and Mechanics 93*, 10-11 (2013), 811–822.

[82] REDEKER, M., AND ECK, C. A fast and accurate adaptive solution strategy for two-scale models with continuous inter-scale dependencies. *Journal of Computational Physics 240* (2013), 268–283.

[83] REICHELT, M. W., AND SHAMPINE, L. F. The MATLAB ODE Suite. *SIAM Journal on Scientific Computing 18*, 1 (1997), 1–22.

[84] RYBACH, L. The geothermal conditions in the Rhine Graben - a summary. *Bull. angew. Geol. Vol 12* (2007), 29–32.

[85] SANDVE, T. H., BERRE, I., AND NORDBOTTEN, J. M. An efficient multi-point flux approximation method for discrete fracture–matrix simulations. *Journal of Computational Physics 231*, 9 (2012), 3784–3800.

[86] SONNENTHAL, E., ITO, A., SPYCHER, N., YUI, M., APPS, J., SUGITA, Y., CONRAD, M., AND KAWAKAMI, S. Approaches to modeling coupled thermal, hydrological, and chemical processes in the Drift Scale Heater Test at Yucca Mountain. *International Journal of Rock Mechanics and Mining Sciences 42*, 5 (2005), 698–719.

[87] TAYLOR, G. Dispersion of soluble matter in solvent flowing slowly through a tube. In *Proceedings of the Royal Society of London A: Mathematical, Physical and Engineering Sciences* (1953), vol. 219, The Royal Society, pp. 186–203.

[88] TESTER, J. W., ANDERSON, B., BATCHELOR, A., BLACKWELL, D., DIPIPPO, R., DRAKE, E., GARNISH, J., LIVESAY, B., MOORE, M. C., NICHOLS, K., ET AL. The future of geothermal energy: impact of Enhanced Geothermal Systems (EGS) on the United States in the 21st Century. *Final Report to the US Department of Energy Geothermal Technologies Program. Cambridge, MA.: Massachusetts Institute of Technology* (2006).

[89] TREFETHEN, L. N. *Spectral methods in MATLAB*. Society for Industrial Mathematics, 2000.

[90] UNION, PEAN. DIRECTIVE 2009/28/EC OF THE EUROPEAN PARLIAMENT AND OF THE COUNCIL of 23 April 2009 on the promotion of the use of energy from renewable sources and amending and subsequently repealing Directives 2001/77/EC and 2003&30/EC.

[91] VADASZ, P., BRAESTER, C., AND BEAR, J. The effect of perfectly conducting side walls on natural convection in porous media. *International journal of heat and mass transfer 36*, 5 (1993), 1159–1170.

[92] VAN DUIJN, C. J., AND POP, I. S. Crystal dissolution and precipitation in porous media: pore scale analysis. *Journal für die reine und angewandte Matematik 577* (2004), 171–211.

[93] VAN NOORDEN, T. L. Crystal precipitation and dissolution in a porous medium: effective equations and numerical experiments. *Multiscale Modeling & Simulation 7*, 3 (2009), 1220–1236.

[94] VAN NOORDEN, T. L. Crystal precipitation and dissolution in a thin strip. *European Journal of Applied Mathematics 20* (2009), 69–91.

[95] VAN NOORDEN, T. L., AND POP, I. S. A Stefan problem modelling crystal dissolution and precipitation. *IMA journal of applied mathematics 73*, 2 (2008), 393–411.

[96] VAN NOORDEN, T. L., POP, I. S., EBIGBO, A., AND HELMIG, R. An upscaled model for biofilm growth in a thin strip. *Water Resources Research 46*, 6 (2010).

[97] VAN NOORDEN, T. L., POP, I. S., AND RÖGER, M. Crystal dissolution and precipitation in porous media: L1-contraction and uniqueness. In *Discrete Contin. Dyn. Syst.,(Dynamical Systems and Differential Equations. Proceedings of the 6th AIMS International Conference, suppl.)* (2007), pp. 1013–1020.

[98] WAGNER, R., KÜHN, M., MEYN, V., PAPE, H., VATH, U., AND CLAUSER, C. Numerical simulation of pore space clogging in geothermal reservoirs by precipitation of anhydrite. *International Journal of Rock Mechanics and Mining Sciences 42*, 7 (2005), 1070–1081.

[99] WANG, C. Y. Onset of convection in a fluid-saturated rectangular box, bottom heated by constant flux. *Physics of Fluids 11*, 6 (1999), 1673–1675.

[100] WANG, C. Y. Thermo-convective stability of a fluid-saturated porous medium inside a cylindrical enclosure: Permeable top constant flux heating. *Mechanics research communications 26*, 5 (1999), 603–608.

[101] WELLER, F. F., NEUSS-RADU, M., AND JÄGER, W. Analysis of a free boundary problem modeling thrombus growth. *SIAM Journal on Mathematical Analysis 45*, 2 (2013), 809–833.

[102] WHITE, S. P., AND MROCZEK, E. K. Permeability changes during the evolution of a geothermal field due to the dissolution and precipitation of quartz. *Transport in porous media 33*, 1-2 (1998), 81–101.

[103] WITHERSPOON, P. A., WANG, J. S. Y., IWAI, K., AND GALE, J. E. Validity of cubic law for fluid flow in a deformable rock fracture. *Water resources research 16*, 6 (1980), 1016–1024.

[104] XU, T., AND PRUESS, K. Coupled modeling of non-isothermal multiphase flow, solute transport and reactive chemistry in porous and fractured media: 1. Model development and validation. *Lawrence Berkeley National Laboratory* (1998).

[105] XU, T., SPYCHER, N., SONNENTHAL, E., ZHENG, L., AND PRUESS, K. TOUGHREACT user's guide: A simulation program for non-isothermal multiphase reactive transport in variably saturated geologic media, version 2.0. *Earth Sciences Division, Lawrence Berkeley National Laboratory, Berkeley, USA* (2012).

[106] ZEBIB, A. Onset of natural convection in a cylinder of water saturated porous media. *Physics of Fluids 21*, 4 (1978), 699–700.

[107] ZHAO, J., WANG, H., LI, X., AND DAI, C. Experimental investigation and theoretical model of heat transfer of saturated soil around coaxial ground coupled heat exchanger. *Applied Thermal Engineering 28*, 2 (2008), 116–125.

Part II

Scientific results

Paper D

A model for non-isothermal flow and mineral precipitation and dissolution in a thin strip

C. Bringedal, I. Berre, I.S. Pop, F.A. Radu,

Journal of Computational and Applied Mathematics **289**, (2015)
http://dx.doi.org/10.1016/j.cam.2014.12.009

D

Journal of Computational and Applied Mathematics 289 (2015) 346–355

Contents lists available at ScienceDirect

Journal of Computational and Applied Mathematics

journal homepage: www.elsevier.com/locate/cam

A model for non-isothermal flow and mineral precipitation and dissolution in a thin strip

Carina Bringedal [a,*], Inga Berre [a,b], Iuliu Sorin Pop [a,c], Florin Adrian Radu [a]

[a] Department of Mathematics, University of Bergen, PO Box 7800, 5020 Bergen, Norway

[b] Christian Michelsen Research AS, PO Box 6031, 5892 Bergen, Norway

[c] Centre for Analysis, Scientific Computing, and Applications, Eindhoven University of Technology, PO Box 513, 5600 MB Eindhoven, Netherlands

ARTICLE INFO

Article history:
Received 29 August 2014
Received in revised form 3 December 2014

Keywords:
Geothermal energy
Homogenization
Mineral precipitation/dissolution
Porosity changes
Reactive transport
Free boundary

ABSTRACT

Motivated by porosity changes due to chemical reactions caused by injection of cold water in a geothermal reservoir, we propose a two-dimensional pore scale model of a thin strip. The pore scale model includes fluid flow, heat transport and reactive transport where changes in aperture is taken into account. The thin strip consists of void space and grains, where ions are transported in the fluid in the void space. At the interface between void and grain, ions are allowed to precipitate and become part of the grain, or conversely, minerals in the grain can dissolve and become part of the fluid flow, and we honor the possible change in aperture these two processes cause. We include temperature dependence and possible effects of the temperature in both fluid properties and in the mineral precipitation and dissolution reactions. For the pore scale model equations, we investigate the limit as the width of the thin strip approaches zero, deriving upscaled one-dimensional effective equations.

© 2014 Elsevier B.V. All rights reserved.

1. Introduction

Geochemistry has a substantial impact in exploiting geothermal systems. In a geothermal reservoir, the injected water and the in situ brine have different temperatures and chemical compositions. Also, the fluids flow through highly heterogeneous regions. Due to the varying chemical properties of the rocks, the temperature and the flow regimes can change significantly. As a consequence of flow and geochemical reactions, composition of reservoir fluids as well as reservoir rock properties will develop dynamically with time. Minerals dissolving and precipitating onto the reservoir matrix, can change the porosity and hence the permeability of the system substantially. Mineral solubility can change by the cooling of the rock, or by the different ion content in the in situ brine and in the injected water. The interaction between altering temperature, solute transport with mineral dissolution and precipitation and fluid flow is highly coupled and challenging to model appropriately as the relevant physical processes jointly affect each other [1]. The effect of changing porosity through the production period of the geothermal reservoir may have severe impact on operating conditions, as pores may close and block flow paths, or new pores may open to create enhanced flow conditions.

Injection of cold water into a geothermal reservoir can trigger the chemical reactions. The ion content of the injected water is normally different from the original groundwater, affecting the equilibrium state of the chemical system. Also,

* Corresponding author.
E-mail addresses: Carina.Bringedal@math.uib.no (C. Bringedal), Inga.Berre@math.uib.no (I. Berre), i.pop@TUE.nl (I.S. Pop), Florin.Radu@math.uib.no (F.A. Radu).

http://dx.doi.org/10.1016/j.cam.2014.12.009
0377-0427/© 2014 Elsevier B.V. All rights reserved.

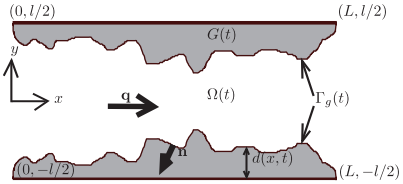

Fig. 1. Model of thin strip.

the solubility of several minerals are temperature dependent, hence the cooling of the porous medium can itself trigger chemical reactions. As reported from field studies and simulations, porosity and permeability changes due to precipitation and dissolution of minerals such as silica, quartz, anhydrite, gypsum and calcite have been observed [2–7]. Modeling of the mineral precipitation and dissolution is important in order to understand the processes and to better estimate to which extent the chemical reactions can affect the permeability of the porous medium.

When dealing with porosity changes, what happens at the pore scale is highly relevant. The pore geometry affects the reaction rates for the dissolution and precipitation process as the reactive surface area is changed, and the resulting permeability is affected by the pore geometry. To achieve expressions for both reaction rates and permeability that depend on the pore scale effects we start with a model at the pore scale, and derive the Darcy scale model by homogenization. We propose in this paper a pore scale model to investigate these matters. Pore scale models incorporating mineral precipitation and dissolution have been studied earlier in [8,9] and the corresponding Darcy scale models have been investigated further in [10,11]. These papers assume that the pore geometry is not changed by the chemical reactions, which is a valid assumption when the deposited or dissolved mineral layer is thin enough. Investigations honoring the porosity changes may be found in [12–14], where mineral precipitation and dissolution have been considered on either circular grains or in a thin strip. In these papers, the position of the interface between grain and void space is tracked, giving a problem with a free boundary. Similar models can also be obtained for biofilm growth [15], for drug release from collagen matrices [16], and on an evolving microstructure [17]. Recently, Kumar et al. [18] considered how to do numerical computations of a mineral precipitation and dissolution process in a thin strip with a free boundary.

In the spirit of [14], we consider mineral precipitation and dissolution in a thin strip and take into account the effect of temperature on the chemical reactions and on the fluid flow, giving a larger system of equations. Temperature changes can initiate or accelerate the rate of chemical reactions due to changes in solubility of the minerals. Also, the fluid flow is affected by the temperature changes due to changes in the fluid density and viscosity. For geothermal systems, the temperature dependence can be of high importance [19].

The structure of this paper is as follows. In Section 2 we discuss the pore scale model and the model equations describing the relevant processes on the pore scale. In Section 3 we perform formal homogenization on the model equations, obtaining upscaled equations valid when the width of the strip approaches zero. The paper ends with some concluding remarks on the resulting equations in Section 4.

2. Pore scale model

The pore model is represented by a two-dimensional thin strip with width l and length L, where L is much larger than l, and can be seen in Fig. 1.

We assume symmetry around the x-axis, hence the upper half of the strip is a reflection of the lower half. The width of the mineral part is $d(x, t)$ where $0 \leq d(x, t) < l/2$, as a greater width would clog the pore channel. The total domain Υ is the rectangle seen in the figure given by

$$\Upsilon = \{(x, y) \in R^2 | 0 \leq x \leq L, -l/2 \leq y \leq l/2\}.$$

The void space $\Omega(t)$ where fluid can flow is defined as

$$\Omega(t) = \{(x, y) \in R^2 | 0 \leq x \leq L, -(l/2 - d(x, t)) \leq y \leq (l/2 - d(x, t))\},$$

while the grain space $G(t)$ consisting of minerals is

$$G(t) = \{(x, y) \in R^2 | 0 \leq x \leq L, -l/2 \leq y \leq -(l/2 - d(x, t)) \vee (l/2 - d(x, t)) \leq y \leq l/2\}.$$

The void and grain spaces are separated by the interface $\Gamma_g(t)$ where mineral precipitation and dissolution can occur, and is given by

$$\Gamma_g(t) = \{(x, y) \in R^2 | 0 < x < L, y = \pm(l/2 - d(x, t))\}.$$

The inflow and outflow boundaries are

$$\Gamma_i(t) = \{(x, y) \in R^2 | x = 0, -(l/2 - d(x, t)) \leq y \leq (l/2 - d(x, t))\}$$

and

$$\Gamma_o(t) = \{(x, y) \in R^2 | x = L, -(l/2 - d(x, t)) \leq y \leq (l/2 - d(x, t))\},$$

respectively. The outward unit normal $\mathbf{n}$ of the interface is (for the lower part)

$$\mathbf{n} = (\partial_x d, -1)^T / \sqrt{1 + (\partial_x d)^2}.$$

As the mineral width $d(x, t)$ changes with time, a point located at the interface $\Gamma_g(t)$ has a certain velocity. A point at the interface has coordinates $\mathbf{s}(t) = (x(t), -(l/2 - d(x, t)))$ and velocity $\mathbf{s}'(t) = (x'(t), \partial_x d(x(t), t)x'(t) + \partial_t d(x(t), t))$. Hence, the normal velocity of the lower boundary is

$$v_n = \mathbf{n} \cdot \mathbf{s}'(t) = -\partial_t d / \sqrt{1 + (\partial_x d)^2}. \tag{1}$$

The Rankine–Hugoniot condition guarantees conservation of quantities across a moving boundary:

$$\mathbf{n} \cdot [\mathbf{j}] = v_n[u]. \tag{2}$$

Here, u is the preserved quantity (e.g. mass or energy) and $\mathbf{j}$ is the flux of this quantity. The use of square brackets means the *jump* of the quantities, and is the difference between the quantities at each side of the interface.

We assume conservation of ions, mass, momentum and energy to form a complete set of equations describing the relevant processes on the pore scale and refer readers to e.g. [20] for justification of the conservation equations. We will prescribe boundary conditions at the internal boundary $\Gamma_g(t)$ and otherwise at the external boundaries when these are necessary for the upscaling process.

For a complete model to be used for computer simulations, several boundary conditions at $\Gamma_i(t)$ and $\Gamma_o(t)$ will be necessary. Also, initial conditions are required. As these external boundary conditions and initial conditions are not necessary for the upscaling process, they will not be specified, but their presence will be briefly mentioned.

2.1. Conservation of ions

There are two active ions in the fluid, having molar concentrations u^1 and u^2. Both ions satisfy the convection–diffusion equation in the void space;

$$\partial_t u^i = \nabla \cdot (D\nabla u^i - \mathbf{q}u^i) \quad \text{for } (x, y) \in \Omega(t), \tag{3}$$

where D is the diffusion coefficient which is assumed constant and equal for both ions, and $\mathbf{q}$ is the fluid velocity. At the interface, one ion from each species can together form a mineral molecule, or conversely, one mineral can dissolve into two ions: $u^1 + u^2 \leftrightarrow C$. Hence the ions can appear on both sides of the interface $\Gamma_g(t)$; either as a free ion in the void space, or as part of a mineral in the grain space. The Rankine–Hugoniot condition (2) for conserving ions across the moving interface is

$$\mathbf{n} \cdot (D\nabla u^i - \mathbf{q}u^i) = v_n(\rho_C - u^i) \quad \text{on } \Gamma_g(t), \tag{4}$$

where ρ_C is the molar density of the formed solid. As the minerals do not move within the grain space $G(t)$, they have zero flux there. On the right-hand side, the difference $(\rho_C - u^i)$ appears as one mineral molecule contains one ion of u^i. We assume that our two ions have initially the same concentration, and that they are subject to the same external boundary conditions. Typical choices are Dirichlet conditions on $\Gamma_i(t)$ and Neumann conditions at $\Gamma_o(t)$. As the same number of ions disappear or are produced through the reaction, the two ions always have the same concentration. Hence, $u^1 = u^2 = u$.

2.2. Conservation of mass

The mass of the fluid is conserved when it flows through the pore. As the fluid consists mainly of water, the fluid molar density ρ_f depends on temperature and cannot be assumed constant as the temperature changes. Hence, the mass conservation equation is

$$\partial_t \rho_f + \nabla \cdot (\rho_f \mathbf{q}) = 0 \quad \text{for } (x, y) \in \Omega(t). \tag{5}$$

In a geothermal system, the fluid density is often assumed to also depend on pressure. As we are mainly interested in the effect from temperature, we neglect the pressure dependence. At the boundary, ions can leave the fluid and become part of the grain space instead. Hence, there is a mass flux through the boundary $\Gamma_g(t)$. Note that even though the ion concentration in the fluid varies, we assume that the variations are so small that we can assume the fluid density not to change due to the chemical reactions. The Rankine–Hugoniot boundary condition applied to mass is

$$\mathbf{n} \cdot (-\rho_f \mathbf{q}) = v_n(2\rho_C - \rho_f) \quad \text{on } \Gamma_g(t). \tag{6}$$

As one mineral molecule contains *two* ions; one of each kind, the term $2\rho_C$ appears. Note that if $\rho_f \equiv 2\rho_C$, the normal component of the velocity is zero at the interface, meaning that the chemical reactions do not cause volume change. This

simplifying assumption is made in some models, e.g. in [12], but would be inconsistent with our model having a varying fluid density and a constant grain density. Hence, we keep the original expression (6).

If Dirichlet boundary conditions are imposed for the velocity $\mathbf{q}$ at the inflow and outflow boundaries, they have to be consistent with mass being conserved. Hence, if $\mathbf{q} = \mathbf{q}_b$ on $\Gamma_i(t)$ and $\Gamma_o(t)$, then $\mathbf{q}_b$ has to satisfy

$$\int_{\Gamma_i(t)\cup\Gamma_o(t)} \rho_f \mathbf{q}_b \cdot \mathbf{n} d\mathbf{s} = \int_{\Gamma_g(t)} v_n(2\rho_C - \rho_f) ds - \int_{\Omega(t)} \partial_t \rho_f dV.$$

In practice, one would normally specify a Dirichlet condition for the velocity only on $\Gamma_i(t)$, and a condition for the pressure on $\Gamma_o(t)$.

2.3. Conservation of momentum

Momentum of the flowing fluid is also conserved. We assume that all body forces arise from viscous stress and that the fluid is Newtonian. Further we assume the stress tensor to be a linear function of the strain rates, that the fluid is isotropic and that the body forces are such that the fluid is at rest at hydrostatic pressure. Then conservation of momentum is expressed as

$$\partial_t(\rho_f \mathbf{q}) + \nabla \cdot (\rho_f \mathbf{q}\mathbf{q}) = -\nabla p + \nabla \cdot \left(\mu(\nabla \mathbf{q} + (\nabla \mathbf{q})^T)\right) - \frac{2}{3}\nabla(\mu \nabla \cdot \mathbf{q}) \quad \text{for } (x, y) \in \Omega(t), \tag{7}$$

where μ is fluid viscosity and p is pressure. No-slip conditions are assumed at the boundary which means that the velocity $\mathbf{q}$ does not have a tangential component at the internal boundary. Note that no-slip boundary conditions are normally associated with velocity $\mathbf{q}$ being zero at the boundary. This is however not the case when there is a *moving* boundary, where the no-slip condition reduces to $\mathbf{q}$ being normal to the movement of the boundary. Hence, $\mathbf{q}$ is parallel to $v_n\mathbf{n}$ at $\Gamma_g(t)$. Combining with the boundary condition (6), the new boundary condition becomes

$$\mathbf{q} = \frac{\rho_f - 2\rho_C}{\rho_f} v_n \mathbf{n} \quad \text{on } \Gamma_g(t). \tag{8}$$

2.4. Conservation of energy

For now, we separate between two temperatures: the temperature in the fluid T_f and temperature in the grain T_g. Fluid temperature only exists in the void space $\Omega(t)$ and grain temperature only exists in the grain space $G(t)$, and heat energy is transferred differently in the two domains. The separation between T_f and T_g is mainly to emphasize the difference between the energy in the void space and in the grain space and has no physical meaning.

We assume no viscous dissipation, hence energy transfer in $\Omega(t)$ can happen through diffusion and convection:

$$\partial_t(\rho_f c_f T_f) = \nabla \cdot (k_f \nabla T_f - \rho_f c_f \mathbf{q} T_f) \quad \text{in } \Omega(t). \tag{9}$$

In the grain space flow is not possible, hence

$$\partial_t(\rho_C c T_g) = \nabla \cdot (k_g \nabla T_g) \quad \text{in } G(t). \tag{10}$$

In the above equations, c_f and c are specific heats, and k_f and k_g are heat conductivities, of fluid and mineral respectively, and are all assumed constant. The Rankine–Hugoniot condition for conservation of energy across the interface is

$$\mathbf{n} \cdot (k_f \nabla T_f - \rho_f c_f \mathbf{q}\mathbf{T}_f - k_g \nabla T_g) = v_n(\rho_C c T_g - \rho_f c_f T_f) \quad \text{on } \Gamma_g(t), \tag{11}$$

and we also assume temperature continuity at the interface:

$$T_g = T_f \quad \text{on } \Gamma_g(t). \tag{12}$$

For the lower and upper parts of $G(t)$, we assume homogeneous Neumann boundary conditions:

$$\partial_y T_g = 0 \quad \text{for } 0 \le x \le L,\ y = \pm l/2. \tag{13}$$

To do simulations, boundary conditions for T_f should be specified at $\Gamma_i(t)$ and $\Gamma_o(t)$, while boundary conditions for T_g should be given at the vertical boundaries of the grain part; that is, at $\{(x, y) \in R^2 | x = 0,\ -l/2 \le y \le -(l/2 - d(x, t)) \vee (l/2 - d(x, t)) \le y \le l/2\}$ and similarly for $x = L$.

2.5. How reactions affect $d(x, t)$

At the boundary $\Gamma_g(t)$, minerals can precipitate and dissolve. When a mineral molecule dissolves and releases two ions into the fluid, the boundary change its position at the same time as the mineral molecule is no longer a part of the grain space $G(t)$. Oppositely, when two ions come together and form a mineral molecule, they attach themselves at the boundary between void and grain space and become a part of the grain space, hence changing the position of the interface at the same time.

As the position of the interface $\Gamma_g(t)$ changes with precipitation and dissolution, we can quantify this change using the width of $G(t)$; $d(x, t)$, and the normal velocity of the interface v_n. To quantify the extent of dissolution and precipitation

taking place, we introduce precipitation and dissolution rates. As we defined the normal vector $\mathbf{n}$ pointing into the grain space (out of the void space) as seen in Fig. 1, the normal velocity of the interface is positive when dissolution occurs, and negative when precipitation occurs. Hence, the normal velocity is proportional to the local difference between the dissolution and precipitation rates:

$$\rho_C v_n = -(f_p - f_d) \quad \text{on } \Gamma_g(t), \tag{14}$$

where f_p and f_d are the precipitation and dissolution rates for the reaction.

We assume the precipitation rate to increase with ion concentration and also with temperature. This is described by a kinetic rate with an Arrhenius factor:

$$f_p(T_f, u) = k_0 e^{-E/RT_f} \frac{(\gamma u)^2}{K_m(T_f)}, \tag{15}$$

where E is the activation energy, R is the gas constant, γ is the activity coefficient of the ions, $K_m(T_f)$ is the equilibrium constant for the mineral, and k_0 is a positive rate constant. The equilibrium constant is called a constant as it does not depend on ion or mineral concentrations, but it may however depend on fluid temperature. We assume dissolution to take place as long as there are minerals present; that is, as long as $d(x, t) > 0$. We further assume that the dissolution happens faster at higher temperatures, hence

$$f_d(T_f, d) = k_0 e^{-E/RT_f} w(d(x, t)), \tag{16}$$

where $w(d)$ is given by

$$w(d) = \begin{cases} 0 & \text{if } d < 0 \\ \min\left(\dfrac{(\gamma u)^2}{K_m(T_f)}, 1\right) & \text{if } d = 0 \\ 1 & \text{if } d > 0. \end{cases}$$

The reason for defining the rates this way is to incorporate equilibrium states of the reaction properly. At equilibrium, the ion concentration u does not change, meaning the precipitation and dissolution rates are equal. When there are minerals present, meaning $d(x, t) > 0$, then $f_p - f_d = k_0 \exp(-E/RT_f)((\gamma u)^2/K_m(T_f) - 1) = 0$ at equilibrium, resulting in $K_m(T_f) = (\gamma u_{eq})^2$, which is how the equilibrium constant is defined. At equilibrium, the precipitation rate and dissolution rate have the same magnitude, hence the position of the interface is not changed. When there are no minerals left, the dissolution rate can be either the same magnitude or smaller than the precipitation rate, corresponding to the system either being in equilibrium or supersaturated with ions.

Collecting Eqs. (14)–(16) and combining with Eq. (1) for v_n, yields

$$\rho_C \partial_t d(x, t) = k_0 e^{-E/RT_f} \left(\frac{(\gamma u)^2}{K_m(T_f)} - w(d(x, t)) \right) \sqrt{1 + (\partial_x d(x, t))^2} \quad \text{on } \Gamma_g(t), \tag{17}$$

which describes how the width $d(x, t)$ is changed by the reactions.

2.6. Non-dimensional equations

To achieve non-dimensional quantities, we introduce t_{ref}, $x_{ref} = L$, u_{ref}, $q_{ref} = L/t_{ref}$, $p_{ref} = L^3 u_{ref}/t_{ref}^2 l$, $\mu_{ref} = l^2 p_{ref}/Lq_{ref}$, T_{ref} and let $\epsilon = l/L$. Non-dimensional variables are denoted with a hat and are defined as

$$\hat{t} = t/t_{ref} \qquad \hat{x} = x/L \qquad \hat{y} = y/L \qquad \hat{u}^\epsilon = u/u_{ref} \qquad \hat{d}^\epsilon = d/l$$
$$\hat{\mathbf{q}}^\epsilon = \mathbf{q}/q_{ref} \qquad \hat{p}^\epsilon = p/p_{ref} \qquad \hat{\rho}_f = \rho_f/u_{ref} \qquad \hat{\rho} = \rho_C/u_{ref}$$
$$\hat{k} = k_0 t_{ref}/u_{ref} l \qquad \hat{D} = Dt_{ref}/L^2 \qquad \hat{\mu} = \mu/\mu_{ref} \qquad \hat{T}^\epsilon = T/T_{ref}.$$

We emphasize the dependence on the small variable ϵ by denoting our main variables with ϵ as a superscript. Since we will only use non-dimensional variables in the following, we skip the hat.

Using non-dimensional variables, the total domain is defined by

$$\Upsilon^\epsilon = \{(x, y) \in R^2 | 0 \le x \le 1, -\epsilon/2 \le y \le \epsilon/2\}.$$

The void space is now given by

$$\Omega^\epsilon(t) = \{(x, y) \in R^2 | 0 \le x \le 1, -\epsilon(1/2 - d^\epsilon(x, t)) \le y \le \epsilon(1/2 - d^\epsilon(x, t))\},$$

while the grain space is defined as

$$G^\epsilon(t) = \{(x, y) \in R^2 | 0 \le x \le 1, -\epsilon/2 \le y \le -\epsilon(1/2 - d^\epsilon) \vee \epsilon(1/2 - d^\epsilon) \le y \le \epsilon/2\}.$$

The interface between the void and the grain space is now

$$\Gamma^\epsilon(t) = \{(x, y) \in R^2 | 0 \le x \le 1, y = \pm\epsilon(1/2 - d^\epsilon(x, t))\},$$

while the outward unit normal for the lower part of the interface is given by

$$\mathbf{n}^\epsilon = (\epsilon\partial_x d^\epsilon, -1)^T / \sqrt{1 + (\epsilon\partial_x d^\epsilon)^2}. \tag{18}$$

Inserting the dimensionless variables into the model equations gives the following set of equations and boundary conditions. We insert the normal velocity v_n from Eq. (1), when necessary.

The convection–diffusion equation (3) describing the ion concentration, is now written

$$\partial_t u^\epsilon = \nabla \cdot (D\nabla u^\epsilon - \mathbf{q}^\epsilon u^\epsilon) \quad \text{in } \Omega^\epsilon(t), \tag{19}$$

while the boundary equation (4) becomes

$$\mathbf{n}^\epsilon \cdot (D\nabla u^\epsilon - \mathbf{q}^\epsilon u^\epsilon) = -\epsilon\partial_t d^\epsilon(\rho - u^\epsilon)/\sqrt{1 + (\epsilon\partial_x d^\epsilon)^2} \quad \text{on } \Gamma^\epsilon(t). \tag{20}$$

Note that a simplifying assumption is that the non-dimensional diffusion coefficient D is not depending on ϵ, hence diffusion and convection occur at the same time scale. Geothermal systems are often convection-dominated due to the injection of water, but our assumption is valid as long as the injection rate is not too large.

The mass conservation equation (5) transforms into

$$\partial_t \rho_f + \nabla \cdot (\rho_f \mathbf{q}^\epsilon) = 0 \quad \text{in } \Omega^\epsilon(t). \tag{21}$$

The corresponding Rankine–Hugoniot boundary equation (6) has the non-dimensional form

$$\mathbf{q}^\epsilon \cdot \mathbf{n}^\epsilon = -\epsilon \frac{\rho_f - 2\rho}{\rho_f} \partial_t d^\epsilon / \sqrt{1 + (\epsilon\partial_x d^\epsilon)^2} \quad \text{on } \Gamma^\epsilon(t). \tag{22}$$

The momentum balance equation (7) becomes

$$\epsilon\left(\partial_t(\rho_f \mathbf{q}^\epsilon) + \nabla \cdot (\rho_f \mathbf{q}^\epsilon \mathbf{q}^\epsilon)\right) = -\nabla p^\epsilon + \epsilon^2\left(\nabla \cdot \left(\mu(\nabla \mathbf{q}^\epsilon + (\nabla \mathbf{q}^\epsilon)^T)\right) - \frac{2}{3}\nabla(\mu\nabla \cdot \mathbf{q}^\epsilon)\right) \quad \text{in } \Omega^\epsilon(t), \tag{23}$$

while the boundary condition (8) is now written

$$\mathbf{q}^\epsilon = -\epsilon \frac{\rho_f - 2\rho}{\rho_f} \partial_t d^\epsilon \mathbf{n}^\epsilon / \sqrt{1 + (\epsilon\partial_x d^\epsilon)^2} \quad \text{on } \Gamma^\epsilon(t). \tag{24}$$

The non-dimensional form of the energy conservation equations (9) and (10) is

$$\partial_t(\rho_f T_f^\epsilon) + \nabla \cdot (\rho_f \mathbf{q}^\epsilon T_f^\epsilon) = \frac{1}{Pe}\nabla^2 T_f^\epsilon \quad \text{in } \Omega^\epsilon(t) \tag{25}$$

and

$$\partial_t(\varsigma\rho T_g^\epsilon) = \frac{1}{Pe}\kappa\nabla^2 T_g^\epsilon \quad \text{in } G^\epsilon(t), \tag{26}$$

where $Pe = L^2 u_{ref} c_f / k_f t_{ref}$ is the Péclet number, which we assume is not depending on ϵ. This means that we assume convection and diffusion to be on the same time scale. Further we have $\varsigma = c/c_f$ and $\kappa = k_g/k_f$, which are also assumed to be of order 1. The boundary condition (11) is written

$$\mathbf{n}^\epsilon \cdot \left(\frac{1}{Pe}\nabla T_f^\epsilon - \rho_f \mathbf{q}^\epsilon T_f^\epsilon - \frac{1}{Pe}\kappa\nabla T_g^\epsilon\right) = -\epsilon(\varsigma\rho T_g^\epsilon - \rho_f T_f^\epsilon)\partial_t d^\epsilon / \sqrt{1 + (\epsilon\partial_x d^\epsilon)^2} \quad \text{on } \Gamma^\epsilon(t), \tag{27}$$

and the continuity condition (12) is

$$T_g^\epsilon = T_f^\epsilon \quad \text{on } \Gamma^\epsilon(t). \tag{28}$$

The boundary condition (13) for T_g is now

$$\partial_y T_g^\epsilon = 0 \quad \text{for } 0 \le x \le 1, y = \pm\epsilon/2. \tag{29}$$

Finally, Eq. (17) describing how the width $d(x, t)$ is changed by chemical reactions is now written

$$\rho\partial_t d^\epsilon = (f_p(T_f^\epsilon, u^\epsilon) - f_d(T_f^\epsilon, d^\epsilon))\sqrt{1 + (\epsilon\partial_x d^\epsilon)^2} \quad \text{on } \Gamma^\epsilon(t). \tag{30}$$

Introducing the constant $\alpha = E/RT_{ref}$, the non-dimensional reaction rates are

$$f_p(T_f^\epsilon, u^\epsilon) = k e^{-\alpha/T_f^\epsilon} \frac{(\gamma u^\epsilon)^2}{K_m(T_f^\epsilon)} \quad \text{and} \quad f_d(T_f^\epsilon, d^\epsilon) = k e^{-\alpha/T_f^\epsilon} w(d^\epsilon(x, t)), \tag{31}$$

where the non-dimensional $K_m(T_f^\epsilon)$ has been scaled with u_{ref}^2.

3. Asymptotic expansion

We perform a formal asymptotic expansion for the variables depending on ϵ, namely u^ϵ, d^ϵ, $\mathbf{q}^\epsilon$, p^ϵ, T_f^ϵ and T_g^ϵ. For all excepting d^ϵ we assume

$$u^\epsilon(x,y,t) = u_0\left(x,\frac{y}{\epsilon},t\right) + \epsilon u_1\left(x,\frac{y}{\epsilon},t\right) + O(\epsilon^2).$$

Due to the scaling of the second variable, $u_i(x,z,t)$ is defined in the domain

$$\tilde{\Omega}(t) = \{(x,z)|0 \le x \le 1, -(1/2-d^\epsilon) \le z \le (1/2-d^\epsilon)\}.$$

The exception is T_{gi} which is defined in

$$\tilde{G}(t) = \{(x,z) \in R^2|0 \le x \le 1, -1/2 \le z \le -(1/2-d^\epsilon) \vee (1/2-d^\epsilon) \le z \le 1/2\}.$$

As the velocity $\mathbf{q}^\epsilon$ is a vector function, we assume the above expansion for both the horizontal component $q^{(1)}$ and vertical component $q^{(2)}$. The width of the grain space, d^ϵ, does not depend on y and has the expansion

$$d^\epsilon(x,t) = d_0(x,t) + \epsilon d_1(x,t) + O(\epsilon^2).$$

The components d_i are defined for $0 \le x \le 1$.

We assume the fluid density ρ_f and viscosity μ to depend linearly on fluid temperature T_f^ϵ:

$$\rho_f(T_f^\epsilon) = \rho_0 - \beta_{\rho_f} T_f^\epsilon = \rho_0 - \beta_{\rho_f}(T_{f0} + \epsilon T_{f1} + O(\epsilon^2)); \tag{32}$$

$$\mu(T_f^\epsilon) = \mu_0 - \beta_\mu T_f^\epsilon = \mu_0 - \beta_\mu(T_{f0} + \epsilon T_{f1} + O(\epsilon^2)), \tag{33}$$

where β_{ρ_f} and β_μ are positive constants. Other forms can be considered straightforwardly.

Below we follow the ideas in [14], details can be found in [21]. The goal is to derive an upscaled effective model describing the thin strip with vanishing width, obtaining a one-dimensional model still honoring the changes in aperture.

Inserting the asymptotic expansion for u^ϵ into (19) and (20), and collecting the lowest order terms yield

$$\partial_{zz}u_0 = 0 \quad \text{in } \tilde{\Omega}(t) \quad \text{and} \quad \partial_z u_0 = 0 \quad \text{on } \tilde{\Gamma}(t),$$

implying $u_0 = u_0(x,t)$. Integrating equation (19) over y, interchanging integration and differentiation, recalling the symmetry in y, give

$$\partial_t\left(\frac{1}{\epsilon}\int_{-\epsilon(1/2-d^\epsilon)}^{\epsilon(1/2-d^\epsilon)} u^\epsilon dy\right) + 2\partial_t d^\epsilon u^\epsilon|_{y=-\epsilon(1/2-d^\epsilon)} = \partial_x\left(\frac{1}{\epsilon}\int_{-\epsilon(1/2-d^\epsilon)}^{\epsilon(1/2-d^\epsilon)} (D\partial_x u^\epsilon - q^{\epsilon(1)}u^\epsilon)dy\right)$$
$$+ 2\partial_x d^\epsilon (D\partial_x u^\epsilon - q^{\epsilon(1)}u^\epsilon)|_{y=-\epsilon(1/2-d^\epsilon)} - \frac{2}{\epsilon}(D\partial_y u^\epsilon - q^{\epsilon(2)}u^\epsilon)|_{y=-\epsilon(1/2-d^\epsilon)}.$$

For the last two terms we use (20). Inserting the asymptotic expansion for u^ϵ and substituting $z = y/\epsilon$ give the lowest order terms

$$\partial_t((1-2d_0)u_0 + 2\rho d_0) = \partial_x(D(1-2d_0)\partial_x u_0 - \bar{q}u_0) \quad \text{for } 0 \le x \le 1,$$

where we have used the fact that u_0 does not depend on z, and where we have defined the transmissivity $\bar{q}(x,t) = \int_{-(1/2-d_0)}^{1/2-d_0} q_0^{(1)}(x,z,t)dz$.

As for the concentration, the lowest order terms of the temperatures, T_{f0} and T_{g0} do not depend on z. Inserting the expansions for T_f^ϵ and T_g^ϵ into their energy equations (25) and (26) and collecting the lowest order terms give

$$\partial_{zz}T_{f0} = 0 \quad \text{in } \tilde{\Omega}(t) \quad \text{and} \quad \partial_{zz}T_{g0} = 0 \quad \text{in } \tilde{G}(t).$$

The lowest order terms arising from inserting the expansions into the boundary conditions (27)–(29) are

$$\partial_z T_{f0} - \kappa\partial_z T_{g0} = 0 \quad \text{and} \quad T_{f0} = T_{g0} \quad \text{on } \tilde{\Gamma}(t), \qquad \partial_z T_{g0} = 0 \quad \text{at } z = \pm 1/2.$$

The only possible solution of the above equations with these boundary conditions is that T_{f0} and T_{g0} do not depend on z, hence

$$T_{f0} = T_{f0}(x,t) \quad \text{and} \quad T_{g0} = T_{g0}(x,t).$$

Since the continuity condition assures that T_{g0} and T_{f0} are equal for all x, we introduce $T_0 = T_{g0} = T_{f0}$.

To find the upscaled equation for the velocity, we integrate equation (21) across a thin section of the void space with width δx; the integration area is given by $Y = \{(x,y) \in R^2|x_1 \le x \le x_1 + \delta x, -\epsilon(1/2-d^\epsilon) \le y \le \epsilon(1/2-d^\epsilon)\}$. Applying Gauss Theorem to the integral of the flux term and dividing the equation by δx provide

$$0 = \frac{1}{\delta x}\int_Y \partial_t \rho_f dV + \frac{1}{\delta x}\int_{\partial Y} \rho_f \mathbf{q}^\epsilon \cdot \mathbf{n} ds,$$

where $\mathbf{n}$ is the outward unit normal field of the boundary ∂Y. Due to the symmetry around the x-axis, the integrals of the upper and lower parts of the boundary of ∂Y are equal, hence

$$0 = \frac{1}{\delta x}\int_{x_1}^{x_1+\delta x}\int_{-\epsilon(1/2-d^\epsilon)}^{\epsilon(1/2-d^\epsilon)} \partial_t \rho_f \, dy dx + \frac{1}{\delta x}\int_{-\epsilon(1/2-d^\epsilon)}^{\epsilon(1/2-d^\epsilon)} \rho_f q^{\epsilon(1)} dy|_{x=x_1+\delta x} - \frac{1}{\delta x}\int_{-\epsilon(1/2-d^\epsilon)}^{\epsilon(1/2-d^\epsilon)} \rho_f q^{\epsilon(1)} dy|_{x=x_1} + \frac{2}{\delta x}\int_{x_1}^{x_1+\delta x} \rho_f \mathbf{q}^\epsilon \cdot \mathbf{n}^\epsilon \sqrt{1+(\epsilon \partial_x d^\epsilon)^2} dx|_{y=-\epsilon(1/2-d^\epsilon)}.$$

For the last term, we use (22). We insert the expression for the density (32) together with asymptotic expansions for $\mathbf{q}^\epsilon$ and T_f^ϵ. We make a change in variables, using $z = y/\epsilon$, and collect the lowest order terms:

$$0 = \frac{1}{\delta x}\int_{x_1}^{x_1+\delta x}\int_{-(1/2-d_0)}^{1/2-d_0} \partial_t \rho_{f0} \, dz dx + \frac{1}{\delta x}\int_{-(1/2-d_0)}^{1/2-d_0} \rho_{f0} q_0^{(1)} dz|_{x=x_1+\delta x} - \frac{1}{\delta x}\int_{-(1/2-d_0)}^{1/2-d_0} \rho_{f0} q_0^{(1)} dz|_{x=x_1} - \frac{2}{\delta x}\int_{x_1}^{x_1+\delta x} (\rho_{f0} - 2\rho)\partial_t d_0 dx.$$

In the above equation, $\rho_{f0} = \rho_0 - \beta_{T_f} T_{f0}$. Since T_{f0} does not depend on z, integral evaluation in z is straight forward. Letting δx approach zero results in

$$0 = (1-2d_0)\partial_t \rho_{f0} + \partial_x(\rho_{f0}\bar{q}) - 2(\rho_{f0} - 2\rho)\partial_t d_0,$$

which can be rewritten as

$$\partial_t\Big((1-2d_0)\rho_{f0} + 2d_0 2\rho\Big) + \partial_x(\rho_{f0}\bar{q}) = 0 \quad \text{for } 0 \le x \le 1.$$

This is the upscaled mass conservation equation with varying fluid density.

Inserting the asymptotic expansions directly into the mass conservation equation (21) gives

$$\partial_t\Big(\rho_0 - \beta_{\rho_f}(T_{f0} + \epsilon T_{f1})\Big) + \Big(\partial_x \mathbf{i} + \frac{1}{\epsilon}\partial_z \mathbf{j}\Big) \cdot \Big((\rho_0 - \beta_{\rho_f}(T_{f0} + \epsilon T_{f1}))(\mathbf{q}_0 + \epsilon \mathbf{q}_1)\Big) = 0.$$

The lowest order term is

$$\partial_z(\rho_{f0} q_0^{(2)}) = 0.$$

As ρ_{f0} does not depend on z, this implies $\partial_z q_0^{(2)} = 0$. The lowest order term of (22) gives $q_0^{(2)} = 0$ at $z = \pm(1/2 - d_0)$, hence

$$q_0^{(2)} \equiv 0 \quad \text{in } \tilde{\Omega}(t).$$

Further, the asymptotic expansions in (23) leads to

$$\partial_z p_0 = 0,$$

hence $p_0 = p_0(x, t)$. The horizontal component of the second-lowest order terms is

$$-\partial_x p_0 + \partial_z(\mu_{f0}\partial_z q_0^{(1)}) = 0.$$

As $\mu_{f0} = \mu_0 - \beta_\mu T_{f0}$ does not depend on z, this results in

$$\mu_{f0}\partial_{zz} q_0^{(1)} = \partial_x p_0. \tag{34}$$

The lowest order terms of (24) is

$$q_0^{(1)} = 0 \quad \text{at } z = \pm(1/2 - d_0).$$

Integrating (34) twice with respect to z and applying this boundary condition, give

$$q_0^{(1)} = \frac{1}{2\mu_{f0}}\partial_x p_0 (z^2 - (1/2 - d_0)^2).$$

We then integrate this equation from $z = -(1/2 - d_0)$ to $z = 1/2 - d_0$ to obtain $\bar{q}$:

$$\bar{q} = -\frac{(1-2d_0)^3}{12\mu_{f0}}\partial_x p_0 \quad \text{for } 0 \le x \le 1.$$

For the energy equations (25) and (26), we seek one upscaled equation containing information from both. We integrate both equations over their respective domains in y and sum the integrals. Changing the order of integration and

differentiation, and making use of (27) and (29) along with symmetry in y results in

$$\partial_t\Big(\frac{1}{\epsilon}\int_{-\epsilon(1/2-d^\epsilon)}^{\epsilon(1/2-d^\epsilon)}\rho_f T_f^\epsilon\,dy+\frac{2}{\epsilon}\int_{-\epsilon/2}^{-\epsilon(1/2-d^\epsilon)}\varsigma\rho T_g^\epsilon\,dy\Big)+\partial_x\Big(\frac{1}{\epsilon}\int_{-\epsilon(1/2-d^\epsilon)}^{\epsilon(1/2-d^\epsilon)}\rho_f q^{\epsilon(1)}T_f^\epsilon\,dy\Big)$$
$$=\partial_x\Big(\frac{1}{\epsilon}\int_{-\epsilon(1/2-d^\epsilon)}^{\epsilon(1/2-d^\epsilon)}\frac{1}{Pe}\partial_x T_f^\epsilon\,dy+\frac{2}{\epsilon}\int_{-\epsilon/2}^{-\epsilon(1/2-d^\epsilon)}\frac{1}{Pe}\kappa\partial_x T_g^\epsilon\,dy\Big).$$

Inserting the expansion for T_f^ϵ and T_g^ϵ, collecting lowest order terms and integrating, give

$$\partial_t\Big((1-2d_0)\rho_{f0}T_0+2d_0\varsigma\rho T_0\Big)+\partial_x(\rho_{f0}\bar{q}T_0)=\frac{1}{Pe}\partial_x\Big((1-2d_0)\partial_x T_0+2d_0\kappa\partial_x T_0\Big)\quad\text{for } 0\le x\le 1.$$

In order to derive an effective equation for how the width d^ϵ is affected by the reactions, we need to regularize the dissolution rate to ensure a Lipschitz continuous function. We define $w_\delta(d^\epsilon)$ such that

$$w_\delta(d^\epsilon)=\begin{cases}0 & \text{if } d^\epsilon<0\\ d^\epsilon/\delta & \text{if } 0\le d^\epsilon\le\delta\\ 1 & \text{if } d^\epsilon>\delta.\end{cases}$$

We insert the asymptotic expansions for d^ϵ, u^ϵ and T_f^ϵ into (30), obtaining

$$\rho\partial_t(d_0+\epsilon d_1)=(f_p(T_{f0}+\epsilon T_{f1},u_0+\epsilon u_1)-f_d(T_{f0}+\epsilon T_{f1},d_0+\epsilon d_1))\sqrt{1+(\epsilon\partial_x(d_0+\epsilon d_1))^2},$$

where $w(d^\epsilon)$ in Eq. (31) is to be replaced with the regularized function defined here. Since f_p and f_d are both Lipschitz, the lowest order expansion is

$$\rho\partial_t d_0=f_p(T_{f0},u_0)-f_d(T_{f0},d_0)\quad\text{for } 0\le x\le 1.$$

If we now let the δ approach zero, we obtain our original expression for $w(d_0)$.

4. Summary and discussion

To summarize, we have derived an upscaled model for mineral precipitation and dissolution in a thin strip honoring changes in aperture, with fluid flow and heat transport. The model includes five unknowns: ion concentration $u_0(x,t)$, mineral width $d_0(x,t)$, fluid transmissivity $\bar{q}(x,t)$, pressure $p_0(x,t)$ and temperature $T_0(x,t)$. Recall that the fluid density ρ_{f0} and viscosity μ_{f0} are not constant, but depend linearly on the temperature T_0. We can note that all our main variables only depend on x and t, hence the thin strip problem has reduced to a one-dimensional problem which is as expected. We have five equations to describe our main variables:

$$\partial_t\Big((1-2d_0)u_0+2d_0\rho\Big)=\partial_x\Big((1-2d_0)D\partial_x u_0-\bar{q}u_0\Big),$$
$$\partial_t\Big((1-2d_0)\rho_{f0}+2d_0 2\rho\Big)+\partial_x(\rho_{f0}\bar{q})=0,$$
$$\bar{q}=-\frac{(1-2d_0)^3}{12\mu_{f0}}\partial_x p_0,$$
$$\partial_t\Big((1-2d_0)\rho_{f0}T_0+2d_0\varsigma\rho T_0\Big)+\partial_x(\rho_{f0}\bar{q}T_0)=\frac{1}{Pe}\partial_x\Big((1-2d_0)\partial_x T_0+2d_0\kappa\partial_x T_0\Big),$$
$$\rho\partial_t d_0=f_p(T_0,u_0)-f_d(T_0,d_0).$$

All equations are valid for $0\le x\le 1$. When the system of equations is used for modeling purposes, the equations should be accompanied with boundary conditions at $x=0$ and $x=1$, and with initial conditions for $t=0$.

The equations follow a certain pattern; terms associated with the void space appear in combination with the factor $(1-2d_0)$, which is the width of the void space. Terms associated with the grains have the factor $2d_0$, which is the width of the grain space. This means we obtain upscaled equations taking into account the changing aperture through the derivatives of d_0. We can also note that the middle equation is similar to Darcy's law. In a fracture, the permeability is known to be proportional to the aperture width squared, and we obtain a cubic relationship as we integrated the velocity across the height of the aperture. Our findings are consistent with the findings of van Noorden [14], where our results include the effect from temperature dependence through fluid properties ρ_{f0} and μ_{f0} and the reaction rates.

The thin strip problem is relevant for a geothermal setting as our thin strip may represent a fracture. In geothermal reservoirs where the rock is highly fractured and has otherwise low permeability; such as in e.g. granite reservoirs, the fluid flow is mainly through the fractures. The model presented here can describe how the efficient equations for flow, heat transport and solute transport are affected as minerals precipitate and dissolve inside the fractures through the production period of the geothermal reservoir.

Acknowledgments

The authors are members of the International Research Training Group NUPUS funded by the German Research Foundation DFG (GRK 1398), the Netherlands Organisation for Scientific Research NWO (DN 81-754) and by the Norway Research Council NRC (215627). F.A. Radu and I.S. Pop acknowledge the support of Statoil through the Akademia agreement. C. Bringedal and I. Berre acknowledge the support from the Norway Research Council (grant number 228832).

References

[1] C. Bringedal, I. Berre, F.A. Radu, An approach for investigation of geochemical rock–fluid interactions, in: Proceedings, Thirty-Ninth Workshop on Geothermal Reservoir Engineering, Stanford University, 2014.
[2] K.S. McLin, K.M. Kovac, J.N. Moore, M.C. Adams, T. Xu, Modeling the geochemical effects of injection at Coso geothermal field, CA; comparison with field observations, in: Proceedings, Thirty-first Workshop on Geothermal Reservoir Engineering, Stanford University, 2006.
[3] E.K. Mroczek, S.P. White, D.J. Graham, Deposition of amorphous silica in porous packed beds—predicting the lifetime of reinjection aquifers, Geothermics 29 (6) (2000) 737–757.
[4] H. Pape, C. Clauser, J. Iffland, R. Krug, R. Wagner, Anhydrite cementation and compaction in geothermal reservoirs: interaction of pore-space structure with flow, transport, p-t conditions, and chemical reactions, Int. J. Rock Mech. Min. Sci. 42 (7) (2005) 1056–1069.
[5] E. Sonnenthal, A. Ito, N. Spycher, M. Yui, J. Apps, Y. Sugita, M. Conrad, S. Kawakami, Approaches to modeling coupled thermal, hydrological, and chemical processes in the drift scale heater test at yucca mountain, Int. J. Rock Mech. Min. Sci. 42 (5) (2005) 698–719.
[6] R. Wagner, M. Kühn, V. Meyn, H. Pape, U. Vath, C. Clauser, Numerical simulation of pore space clogging in geothermal reservoirs by precipitation of anhydrite, Int. J. Rock Mech. Min. Sci. 42 (7) (2005) 1070–1081.
[7] S.P. White, E.K. Mroczek, Permeability changes during the evolution of a geothermal field due to the dissolution and precipitation of quartz, Transp. Porous Media 33 (1–2) (1998) 81–101.
[8] C.J. van Duijn, I.S. Pop, Crystal dissolution and precipitation in porous media: pore scale analysis, J. Reine Angew. Math. 577 (2004) 171–211.
[9] T.L. van Noorden, I.S. Pop, M. Röger, Crystal dissolution and precipitation in porous media: L1-contraction and uniqueness, in: Discrete Contin. Dyn. Syst. (Dynamical Systems and Differential Equations. Proceedings of the 6th AIMS International Conference, suppl.), 2007, pp. 1013–1020.
[10] P. Knabner, C.J. van Duijn, S. Hengst, An analysis of crystal dissolution fronts in flows through porous media. Part 1: compatible boundary conditions, Adv. Water Resour. 18 (3) (1995) 171–185.
[11] C.J. van Duijn, P. Knabner, Travelling wave behavior of crystal dissolution in porous media flow, European J. Appl. Math. 8 (1997) 49–72.
[12] K. Kumar, T.L. Van Noorden, I.S. Pop, Effective dispersion equations for reactive flows involving free boundaries at the microscale, Multiscale Model. Simul. 9 (1) (2011) 29–58.
[13] T.L. van Noorden, Crystal precipitation and dissolution in a porous medium: effective equations and numerical experiments, Multiscale Model. Simul. 7 (3) (2009) 1220–1236.
[14] T.L. van Noorden, Crystal precipitation and dissolution in a thin strip, European J. Appl. Math. 20 (2009) 69–91.
[15] T.L. van Noorden, I.S. Pop, A. Ebigbo, R. Helmig, An upscaled model for biofilm growth in a thin strip, Water Resour. Res. 46 (6) (2010).
[16] N. Ray, T. van Noorden, F.A. Radu, W. Friess, P. Knabner, Drug release from collagen matrices including an evolving microstructure, ZAMM Z. Angew. Math. Mech. 93 (10–11) (2013) 811–822.
[17] M.A. Peter, Coupled reaction–diffusion processes inducing an evolution of the microstructure: analysis and homogenization, Nonlinear Anal. TMA 70 (2) (2009) 806–821.
[18] K. Kumar, M.F. Wheeler, T. Wick, Reactive flow and reaction-induced boundary movement in a thin channel, SIAM J. Sci. Comput. 35 (6) (2013) B1235–B1266.
[19] C. Bringedal, I. Berre, J.M. Nordbotten, Influence of natural convection in a porous medium when producing from borehole heat exchangers, Water Resour. Res. 49 (8) (2013) 4927–4938.
[20] S. Patankar, Numerical Heat Transfer and Fluid Flow, McGraw-Hill, 1980.
[21] C. Bringedal, I. Berre, F.A. Radu, I.S. Pop, Pore scale model for non-isothermal flow and mineral precipitation and dissolution in a thin strip. CASA Report 14-24, 2014.